STAMPING CHARACTERISTICS OF TWO COPPER ALLOY SPRING MATERIALS

A THESIS

Presented to

The Faculty of the Division

of Graduate Studies

By

Dennis C. Kent

In Partial Fulfillment

of the Requirements for the Degree

Master of Science in Mechanical Engineering

Georgia Institute of Technology

June, 1976

STAMPING CHARACTERISTICS OF TWO COPPER ALLOY SPRING MATERIALS

Approved:

John T. Berry, Co-Chairman

David Kalish, Co-Chairman

Pieter Muije

Date approved by Chairman: 7th July 1978

ACKNOWLEDGMENTS

I am most grateful to Charles McGonigal and Chris Scholly, both at Western Electric, Norcross, Georgia, for their support of this work, and to Jim Elling of the Bell Laboratories, Norcross, Georgia, for his help in material testing. I am especially indebted to Andy Lyon at Western Electric for the photomicrographs included here and for the patient metallography instruction that enabled me to perform this work.

I am grateful to Dr. J. T. Berry of Georgia Tech for his help in establishing the background for this investigation, influence in the direction of industrial applicability, and constructive criticism of the work, and to Dr. P. Muije of Georgia Tech for his careful review of the work and constructive comments in the areas of metallography and presentation.

This research is an outgrowth of courses in the fabrication of metals taught by Dr. D. Kalish of Georgia Tech and Bell Laboratories. His help setting up and guiding the experimental plan; many helpful, thought-provoking discussions through the experiment; thorough review of the work; and general inspiration were invaluable.

TABLE OF CONTENTS

LIST OF TABLES

LIST OF ILLUSTRATIONS

SUMMARY

The objective of this investigation is to compare the stamping behavior of two copper alloy spring materials. Specifically, the effects of the material work-hardening capacity, ultimate tensile strength, and tensile fracture ductility on the width of the stamping shear deformation zone, peak stamping force requirements, and punch penetration at slug separation were investigated. Phosphor bronze and spinodal Cu-4Ni-4Sn, both processed by solution heat treating and cold rolling to different strength levels, were punched to varying depths using different die clearances. Samples were sectioned and characterized by metallography and micro-hardness testing; empirically developed micro-hardness versus tensile plastic strain relationships were used for analysis.

Results showed the stamping shear deformation zone to be related to die clearance but unrelated to the work-hardening exponent of the material and unrelated to punch penetration. Punch penetration at slug separation is proportional to tensile fracture ductility. Peak stamping forces are related to the ultimate tensile strength and hardness of the workpiece material but not die clearance.

CHAPTER I

INTRODUCTION

1.1. Introduction

The relationship between a material's mechanical properties, as determined by heat treatment and cold work, and manufacturing parameters in stamping* is generally unknown. Some empirical rules as to thickness of stock, type of workpiece material, and die clearance** are currently applied in stamping, but a materials engineering basis for selecting workpiece condition or die clearance has not been established. As a result, the engineering of a stamped product in both the product design and manufacture must usually rely heavily on the engineer's intuition or previous experience with a given workpiece material.

Phosphor Bronze (Copper Alloy 510, 94.8Cu-5Sn-0.2P) is commonly used for spring connector devices [1]. This alloy

---

*The term "stamping" used here broadly includes the operations commonly referred to as punching or piercing, in which the material removed from the sheet or strip is scrap, and blanking, in which the material removed is the product.

**Die clearance commonly refers to either the clearance per side, i.e. the difference in radii for a round punch and die, or the overall clearance, i.e. the difference in diameters for a round punch and die. Die clearance as used here always refers to the clearance per side unless stated otherwise. Clearance is expressed as a percent of the workpiece material thickness.

is strengthened by coldworking (rolling) to the desired reduction and is used at 0.2% offset yield strengths in the range of 65-100 ksi. Gohn, Guerard, and Freynik [2] have characterized the mechanical properties and behavior of the phosphor bronzes. A relatively new type of copper alloy with nickel and tin alloying elements has been recommended for application as a spring material [3]. Alloys containing 4-20% nickel and 4-10% tin can provide very high strengths by appropriate combinations of cold work and heat treatment. The strengthening in these alloys occurs by spinodal decomposition [4,5,6]. Piece parts properly designed could be stamped out from such a material in the as-rolled (soft) condition and subsequently aged to the hard condition. 0.01% offset yield strengths in the range of 100-200 ksi have been achieved with these spinodal copper alloys. However, the mechanical properties of the full range of compositions of this alloy have not been published.

1.2. Objectives

The broad objective of this investigation was to compare the stamping behavior of the two types of copper alloys which strengthen by quite different metallurgical mechanisms. The particular spinodal alloy chosen was 92Cu-4Ni-4Sn. Both alloys, CA 510 and Cu-Ni-Sn were obtained in two different conditions, representing different levels of cold-rolling: the CA 510 was obtained in the half hard and

spring tempers and the Cu-Ni-Sn alloy was in the hard and spring tempers. These are qualitative terms commonly used in copper alloy technology to describe degrees of cold work [7]; the specific properties will be described later.

The specific objectives of the investigation were:

(a) To establish relationships between readily obtained material properties, from tensile and hardness tests, and the level of punch penetration at slug separation and the peak punch loads for various punch-to-die clearances.

(b) To investigate the strain-hardening patterns developed in these workpiece materials as a stamping punch penetrates them with various die clearances.

(c) To investigate the utility of microhardness profiles for experimental analysis of the stamping process.

The strain hardening behavior of these materials in tension was characterized and then the strain hardening behavior in static shearing was analyzed in terms of punch penetration into the workpiece and punch-to-die clearance. Tensile properties are related to behavior in dry quasi-static shearing with a typical stamping die.

1.3. Discussion of the Problem

Figure 1 shows a typical geometry for a stamping punch and die. The die clearance is based on workpiece thickness, the desired appearance of the sheared edge, tool wear considerations, and to some extent the mechanical properties

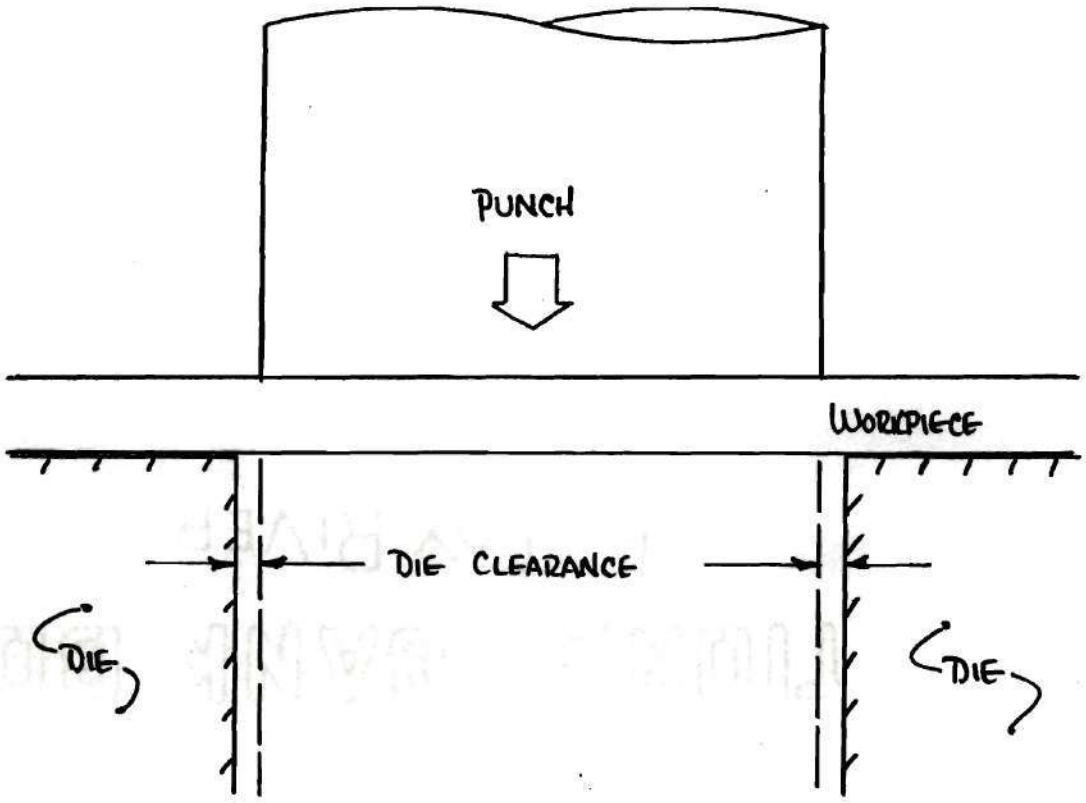

Fig. 1. Typical Stamping Die Geometry

of the workpiece material. This clearance has the effect of adding a bending moment to the shear load imposed on the workpiece by the punch and die (see Appendix 4). Increased die clearance gives an increased bending moment which causes slug separation at an earlier punch penetration and a consequent narrowing of the shiny burnished zone typical of the sheared surface on a conventional stamped part, Figure 2. Die design handbooks offer guidelines for the determination of optimum clearances [8-12]. However, such guidelines typically group the workpiece materials into broad compositional categories (i.e. aluminum alloys, brasses, etc.) without regard to specific material properties and are frequently contradictory. Materials exhibiting different strength or ductility properties require different die clearances to achieve similar sheared edge characteristics in stamping. The die designer must thus rely on previous experience with a given material, his intuition, or a proven means of evaluation to establish die clearance within the broad guidelines offered by handbooks.

Stamping forces are also of prime interest to die designers. The maximum force on the punch is given [10] by:

$$P = L\ T\ S \qquad (1)$$

where P is the maximum punch force, L is the length of the perimeter of the punch, T is the workpiece thickness, and S

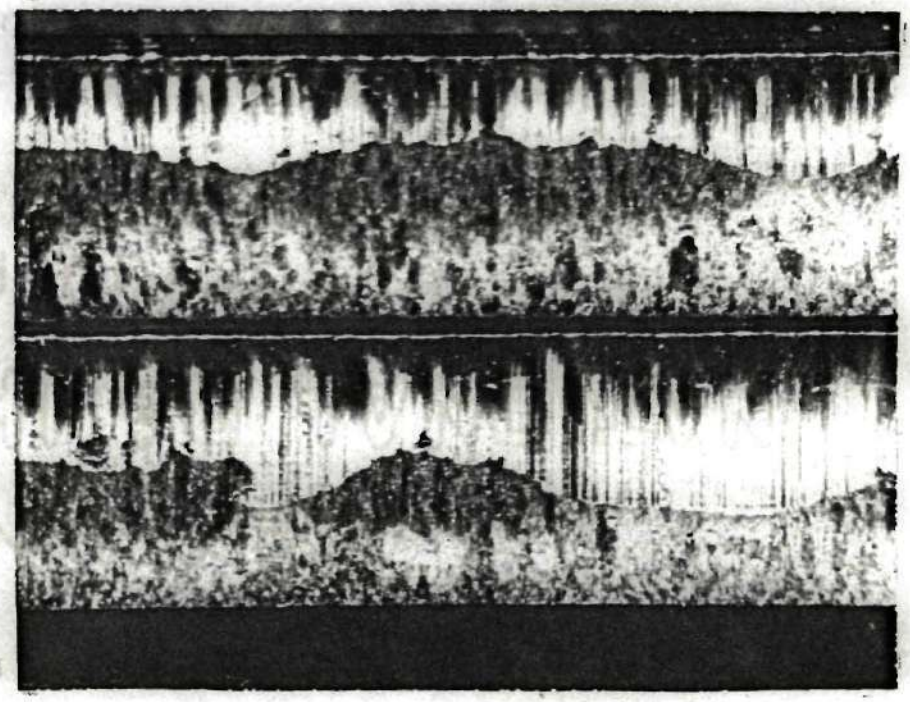

Fig. 2. Shear Surfaces of Half Hard Phosphor Bronze Stamped with 3% (Top) and 9% Die Clearance (10X)

is the shear strength of the workpiece material. While there is general agreement in the literature on this relationship, there is some question as to whether or not die clearance affects the maximum stamping force. Several sources suggest increased maximum stamping load with decreased die clearance, while others report the opposite or no variation at all in maximum force with changing die clearance.

1.4. Review of the Literature

The literature on experimental and analytical investigations of the stamping process describes the effects of process variables (workpiece material, stock thickness, blank diameter, die clearance, punch rake angle, and punch penetration) on the plastic deformation pattern, crack initiation and propagation to slug separation, punch load, edge appearance of the blank, blank curvature, and in-process horizontal loading on the blank. Considerable attention has been given to tool wear and life as well. The work most relevant to the present investigation is that in the areas of workpiece plastic deformation patterns, crack initiation and propagation, punch loads and punch penetration at slug separation.

Chang and Swift [13] etched square grids on the edges of metal bars and described the grid deformation as the punch penetrated the bars in quasi-static shearing. Peak punch loads were found to drop very slightly with increasing die clearance from nil to 15% for both soft copper and mild

steel. In shearing, soft copper and soft aluminum, lead, and tin deform by sliding in shear to complete slug separation, while hard copper and hard aluminum formed cracks in the deformation zone which propagated away from one another leaving tongue-like facets on the sheared surfaces.

Chang [14] later attributed some of the results of the above study to edge effects. He made through-thickness sections of mild steel and aluminum workpiece materials and etched grids on the section planes, fitted the two halves of the workpieces back together, then stamped out circular blanks. Deformation of these grids were studied at various punch penetrations, die clearances, and in the two different workpiece materials. Aluminum again plastically sheared to slug separation but the tongue-like facets which previously [13] developed in mild steel disappeared at die clearances over 10% of the material thickness. Chang also monitored punch loads versus workpiece material, die clearance, blank diameter, and punch rake angle. His results indicated a lowering of the maximum punch load with increasing die clearance from nil through 10% of stock thickness for both mild steel and aluminum.

The Production Engineering Research Association (PERA) of Great Britain conducted an extensive metallographic investigation into the stamping process [15]. One feature of this research was the use of microhardness surveys on sectioned 3/8 inch thick workpiece samples of annealed 0.1%

carbon steel penetrated to various depths by punches with different edge configurations. The Vickers diamond pyramid indenter was used with a 1kg load to form microhardness profiles with 0.2 mm horizontal spacings and 0.5 mm vertical spacings. The resultant detailed microhardness profiles showed maximum work hardening near the punch and die corners. It was concluded that, for conventional stamping, cracks formed at the edge of the severely deformed region and that crack propagation followed the contours of the steepest hardness gradients. Also, a single line of hardness measurements across the deformation zone would discern variations in the workpiece due to differing punch and die edge configurations. This approach was applied to soft and hard copper, soft brass, and soft and half hard aluminum alloy workpiece materials. The investigators [15] concluded:

(a) Crack propagation follows the boundary of the zone of intense work hardening in the soft materials, except in soft brass where it follows the shear line.

(b) Only in annealed materials does the total width of the work hardened zone vary with material thickness and to a lesser extent with die clearance.

(c) The position of the maximum hardness gradient varies with stock thickness.

(d) Distinct differences between annealed and work hardened materials can be seen in the strain hardening developed in the piercing operation.

Several investigators studied punch load as a function of workpiece material, die clearance and punch penetration. There is disagreement as to the effect of die clearance on the maximum punch load. As noted above, Chang [14] found a decrease in maximum punch load with an increase in die clearance for aluminum and steel.

Tilsly and Howard [16] studied the forces required for the blanking of copper and mild steel as a function of die clearance. Using a dynamometer they showed that maximum punching load increases linearly with die clearances up to about 19% of material thickness.

Biegel [17] used a dynamometer to assess stamping forces for steel as a function of die clearance, and showed that the maximum punch force was unaffected by die clearance. The punch load reached a maximum at more shallow punch penetrations as the die clearance increased, corresponding to the more narrow burnished land on the sheared surface when larger die clearances are used [18,19]. This also leads to a decrease in the total amount of energy required for stamping [17].

Two groups of researchers developed analytical models of the stamping process. Masuda and Jimma [20] divided the punch penetration into four parts, assumed a plastic-rigid workpiece material, and used limit analysis and slip line fields to analyze the workpiece deformation process. Their four-part model shows a linearly decreasing punch load as

the punch penetrates with zero die clearance. With increasing die clearance, a constant peak punch load is predicted. Moreover, a delayed slug separation is predicted with increasing die clearance in contrast with observed stamping behavior. Maeda, et al. [21] analyzed the forces imposed on the blank as it is being formed in order to develop an analytical expression for the "dishing" curvature of circular blanks based on die clearance, punch and die deflections, punch penetration, and tool-workpiece friction. Among their empirical data is a plot of shearing resistance versus die clearance, showing only a slight dip in force at about 25% clearance.

In summary, studies to date of maximum punch load as a function of die clearance have had conflicting results. Chang and Swift [13] and Chang [14] predict a decreasing maximum load with increasing clearance. Tilsey and Howard [16] found an increasing maximum load with increasing clearance. Biegel [17] and Maeda et al. [21] experimentally showed the peak load unaffected by clearance, in agreement with the analytical model developed by Masuda and Jimma [20]. From these experimental results, the effect of die clearance on punch loads is unclear.

The metallographic work of PERA [15] presents an analytical tool for investigating the strain hardening patterns in the stamping workpiece.

CHAPTER II

EXPERIMENTAL PROCEDURE

2.1. Experimental Plan

The experiments consisted of three parts. The first part was the development of a relationship between microhardness and true plastic strain in tension; the plastic strain was based on the reduction in cross-sectional area of tensile test samples and calculated as:

$$\varepsilon_i = \ln A_o/A_i \qquad (2)$$

The tensile properties of the alloys and tempers were established. The second part of the experiment consisted of a series of dry quasistatic stamping tests on the four materials with varying levels of punch penetration and nominal die clearances of 3%, 6%, and 9%. Selected samples were metallographically sectioned for determination of microhardness profiles across the shear deformation zones. These microhardness profiles are related to the microhardness versus tensile plastic strain relationships generated in the first part of the experiment. Data from the shearing tests are also related to tensile test data collected in the first part of the experiment. The third part of the experiment

consisted of tensile tests conducted over a range of strain rates to determine if any of the properties of these materials was strain-rate sensitive.

All hardness tests in the experiment were performed on a vertical/longitudinal plane near the center of the strip as shown in Figure 3.

2.2. Test Equipment

The twelve tensile tests for the microhardness versus plastic strain correlation were performed on an Instron Model TTD tensile tester. The twenty tensile tests for the strain-rate sensitivity investigation were performed on an Instron Model 1251 tensile tester. The 88 quasistatic stamping tests made were performed on a Baldwin Model 60-H Universal Testing Machine using a Baldwin Type POIM strain follower and a Baldwin Microformer stress-strain recorder; this arrangement gave a 50:1 amplification of the punch displacement. All microhardness tests (approximately 2270) were done on a Leitz Miniload hardness tester.

The stamping tool used in this experiment consisted of a Danly all-steel precision two-post die set in which were mounted a standard Di-Acro Houdaille punch and one of three interchangeable dies giving three different die clearances. The dimensions of the punch and dies used are shown in Figure 4. The punch face was flat and the punch and die edges were sharp. No spring-loaded stripper was

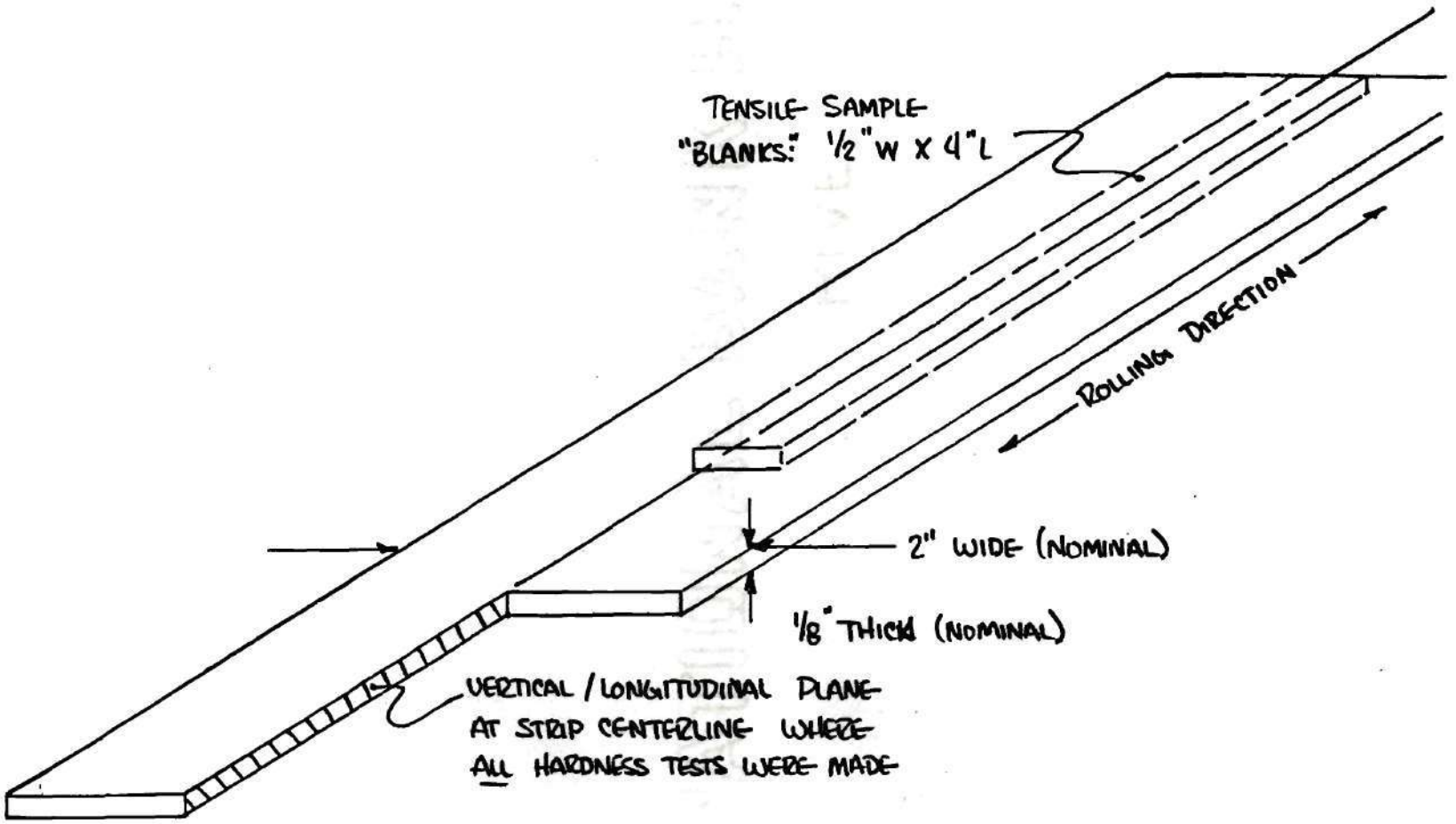

Fig. 3. Nominal Strip Dimemsions and Location of Hardness Measurement Plane

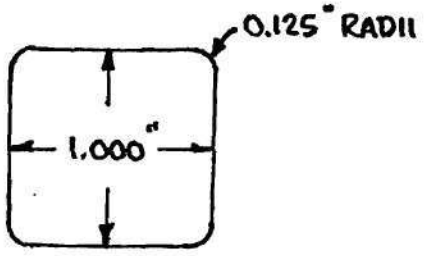

A. PUNCH DIMENSIONS

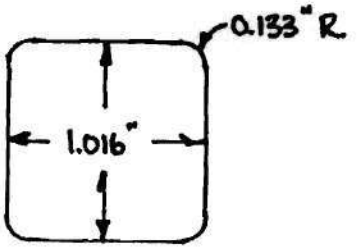

B. DIE DIMENSIONS FOR NOMINAL CLEARANCE OF 6% OF METAL THICKNESS PER SIDE

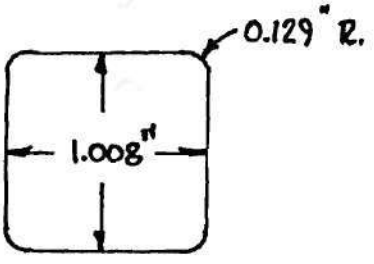

C. DIE DIMENSIONS FOR NOMINAL CLEARANCE OF 3% OF METAL THICKNESS PER SIDE

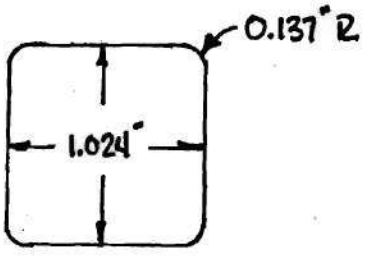

D. DIE DIMENSIONS FOR NOMINAL CLEARANCE OF 9% OF METAL THICKNESS PER SIDE

Fig. 4. Punch and Die Dimensions

provided, however a hold-down plate was used to locate the sample and keep it relatively flat during the stamping operation.

2.3. Materials Tested

The materials tested are described in Table 1. The tempers were chosen to represent a range which is of commercial interest in the manufacture of spring connector devices.

2.4. Experimental Procedure: Microhardness Versus Plastic Strain

Three tensile test specimen blanks, 4 inches long and one-half inch wide, were cut from the centers of adjacent one-foot lengths of the strip samples of each of the four materials listed in Table 1, and numbered. The thickness of each blank was measured at its longitudinal center and one-half inch either side of the center and the three thickness measurements averaged. The measurements were made to the nearest 0.0001 inch with a vernier micrometer.

Tensile test specimens were then fabricated from the blanks in accordance with ASTM Standard E8, using a Tensilkut router. The twelve subsize specimens (1 inch gage length and one-fourth inch gage width) were fabricated in random order. The width of each specimen was measured to the nearest 0.0001 inch with a vernier micrometer at the center of the gage section and one half inch either side of the center, and the three width measurements were averaged.

Table 1. Materials Tested

Temper, Material	Nominal Composition, weight %	Nominal Reduction After Final Anneal	Casting Size, Reduction Schedule	Average Thickness, in.	Source
Half hard, Phosphor Bronze (CA 510) HHPB	94.8Cu-5Sn-0.2P	20%	13¾X2-1/8X78 in. 0.156-0.125	0.1295	Western Electric Co., Hawthorn Station, Chicago, Ill.
Spring, Phosphor Bronze (CA 5510) STPB	94.8Cu-5Sn-0.2P	60%	(Not Available)	0.1253	Saunders Brass & Copper Supply Chamblee, Ga.
Hard, Copper-Nickel-Tin HCNS	92Cu-4Ni-4Sn	37½%	13¾X2-1/8X78 in. 0.200-0.162-0.125	0.1251	Western Electric Co., Hawthorn Station, Chicago, Ill.
Spring, Copper-Nickel-Tin	92Cu-4Ni-4Sn	60%	13¾X2-1/8X78 in. 0.290-0.225-0.180-0.150-0.116		Western Electric Co., Hawthorn Station, Chicago, Ill.

In random order, the twelve specimens were loaded to failure in an Instron Model TTD tensile tester, with a cross-head speed of 0.2 ipm, a chart speed of 10 ipm and a full-scale chart deflection of 10,000 lb. From the force-elongation print-outs the loads at 0.2% offset yield, the ultimate, and fracture were noted. An average original cross-sectional area (A_o) was calculated for each specimen using the average thickness and average width as described above. The A_o was then divided into the 0.2% offset yield load and into the ultimate load for each specimen to obtain the engineering 0.2% offset yield strength and ultimate tensile strength (UTS). These data are given in Table A3-1, Appendix 3.

The fracture area of each half of each failed specimen was measured by observing the area end-on at 40X in a microscope, thus measuring the projected area normal to the specimen axis. The two measured areas from each specimen were averaged and the average fracture area, A_f, was recorded. These average fracture areas were divided into the fracture loads for the respective specimens and the true stress at failure was recorded for all 12 specimens. The true strain at failure, given by

$$\varepsilon_f = \ln A_o/A_f \qquad (3)$$

was also calculated for each specimen. The local radius of curvature of the necked region near the fracture was estimated for both sides of each specimen using radius gages. The radii from each side were averaged for each specimen and recorded along with the thickness at the fracture. The Bridgman correction factor [22] for rectangular cross-section tensile samples, given by

$$C.F. = (1 + 2R/a)^{\frac{1}{2}} \log[1 + a/R + (2a/R)^{\frac{1}{2}}(1 + a/2R)^{\frac{1}{2}}] - 1 \quad (4)$$

where a is half the specimen thickness at the fracture and R is the local radius of curvature at the neck, was calculated for each sample and multiplied by the true stress at failure to correct for the effect of the hydrostatic stress state developed in the tensile sample neck. These fracture strain and fracture stress data are given in Table A3-1, Appendix 3.

The longer half of each fractured tensile sample was viewed at 40X in a microscope and the intersection of the longitudinal axis of the sample with its fracture surface was selected as a reference point. The width of the test specimen piece was measured to the nearest 0.0001 inch at distance increments of 0.005 inch from the reference point in the specimen axial direction. For each test specimen piece, a plot was made of width versus distance from the reference point. A sample of these plots is given in Appendix 3.

The longer half of each specimen was then metallographically mounted for observation of the vertical/longitudinal plane, and the specimen ground off and polished to its widthwise center (see Figure 3). This polished plane thus included the reference point described in the above paragraph.

In random order, the twelve mounted specimens were selected for microhardness indentation tests using the Vickers 136° diamond pyramid indenter, Figure 5, with a 200 gm load, according to ASTM Standard E384-73. In these tests, as in all subsequent tests in the experiment, the load was applied for 25 seconds and the indentations were located using a vernier micrometer adjustment to move the platform with the test specimen firmly attached. The first indentation was made 0.36 mm from the through-thickness center of the fracture surface. Successive indentations were made at 0.18 mm increments (see Appendix 2) of distance from the fracture surface, to the region of uniform strain as indicated by the tensile specimen width measurements described above. The indentations were measured and the hardness readings were listed in columns in ascending order of distance from the fracture surface. The mounted specimens were then viewed at 40X on a microscope and the specimen thickness at each hardness indentation was measured to the nearest 0.0001 inch and recorded.

The distance from the reference point at the fracture surface to the first hardness indentation was measured

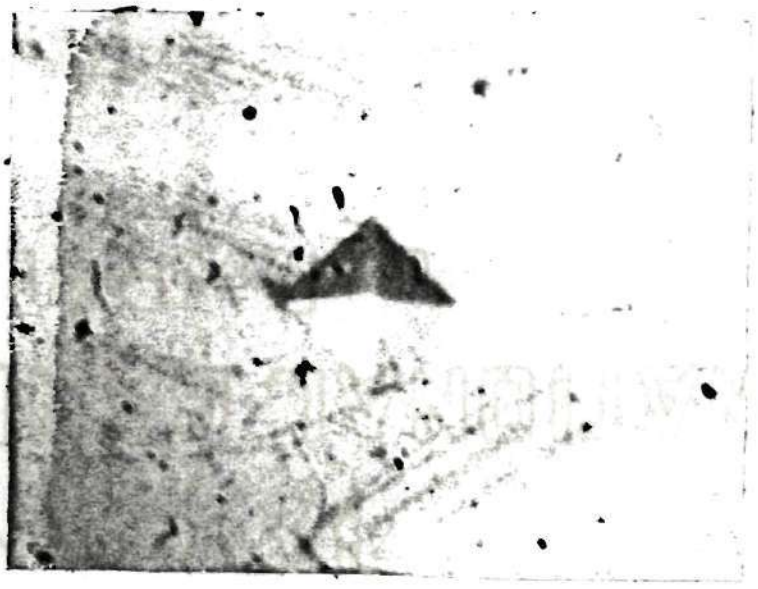

Fig. 5. Photomicrograph of Vickers Hardness Indentation in Hard Temper Cu-4Ni-4Sn (500X)

parallel to the specimen axis. From this measurement, the first indentation was located on the width versus distance plot described above.

From the location of the first indentation on the width versus distance plot, the widths at 0.18 mm increments on each plot were noted and recorded along with the respective microhardness and thickness values from the above paragraph. Thus, for each microhardness reading, a cross-sectional area was calculated, and finally, the true strain was calculated using A_o. A sample of these data are given in Appendix 3.

Two 3/4 inch long samples were taken from each material and metallographically mounted and ground and polished to the width-wise center of the strip. After etching these samples, they were selected in random order for microhardness indentation. Five indentations were made in each sample and the indentations were measured and hardness values recorded. Then the ten hardness values for each material were averaged together to give a zero-strain hardness value. These data are given in Appendix 3.

A plot of VHN versus true strain was made for each of the four materials, each plot being a combination of data points from three tensile samples. The VHN versus true strain data points for each material were fitted to a curve of the form*

*This is the form of the Holloman logarithmic stress-strain relationship [23].

$$VHN = a\varepsilon^{b} + VHN\Big|_{\varepsilon=0} \qquad (5)$$

using a least squares fit program provided by Hewlett-Packard** and run on a Hewlett-Packard model 9100B calculator.

2.5. Experimental Procedure: Stamping Tests

Seventeen two-inch squares were cut from adjacent six-inch lengths of the strips of both HHPB and HCNS (see Table 1) and seven squares were cut from adjacent lengths of both the STPB and the STCNS strips. The squares were numbered and the thickness of each was measured to the nearest 0.0001 inch near its center using a vernier micrometer. The numbered squares were randomized for the following series of tests, which are outlined in Table 2.

Two samples of each material were punched through to slug separation using the 1.015 inch square die (for approximately 6% die clearance) and an approximate punch travel speed of 0.050 ipm; the strip rolling direction was oriented the same in all cases. The point of slug separation and consequent load drop-off was noted on the force-penetration profile generated with each test. A sample profile for each material is given in Appendix 3. For each material, the average (of two samples) punch penetration at slug separation was computed, as a percent of the sample thickness. Next,

** Taken from the Hewlett-Packard Calculator Model 9100B Program Library; Program No. 70811, Least Squares Fit-Power Curve; Part No. 09100-70812; November 15, 1968.

Table 2. Stamping Test Experiment*

Material	Die Clearance					
	3%		6%		9%	
	punch pen.	matrix size	punch pen.	matrix size	punch pen.	matrix size
HHPB			11%	5X35		
	25%	1X15	22%	5X35	22%	1X15
	(49%)	1X10	33%	5X35	(43%)	1X10
			(43%)	5X17		
STPB			13%	1X15		
			(25%)	1X10		
HCNS			11%	5X35		
	23%	1X15	22%	5X35	20%	1X15
	(47%)	1X8	32%	5X35	(40%)	1X10
			(43%)	5X17		
STCNS			17%	1X15		
			(33%)	1X10		

*This table gives the die clearances and punch penetrations for each material for which metallographically sectioned samples were prepared and the size of the hardness indentation matrix which was established on each sample to establish microhardness profiles in and near the deformation zone on that sample.

one sample of each material was punched to 1/4-, one sample to 1/2-, and one sample to 3/4 of the percent penetration required for slug separation for that material. Penetrations in all cases were based on the force-penetration profiles and made as a percentage of material thickness. Peak loads were read from a direct-readout gage on the universal testing machine used.

The samples of HHPB and HCNS at 1/4, 1/2, and 3/4 of slug separation penetration and one of the separated samples for each of these two materials were metallographically sectioned, mounted, polished, and etched for observation of a vertical/longitudinal plane near the center of the strip (see Figure 3). Microhardness grids were made on each of these samples according to Figures 6a and 6b, using the Vickers indenter with the 200-gm load. The samples of STPB and STCNS at 1/2 of slug separation penetration and one of the separated samples for each of these two materials were prepared as above for observation of a vertical/longitudinal plane near the center of the strip. Microhardness grids were made on each of these samples according to Figures 6c and 6d. Photomicrographs of examples of these grids are shown in Figure 7.

Two samples each of HHPB and HCNS were punched through to slug separation using the 1.008 inch square die (for approximately 3% die clearance) and an approximate punch travel speed of 0.050 ipm. Again, the punch penetration at

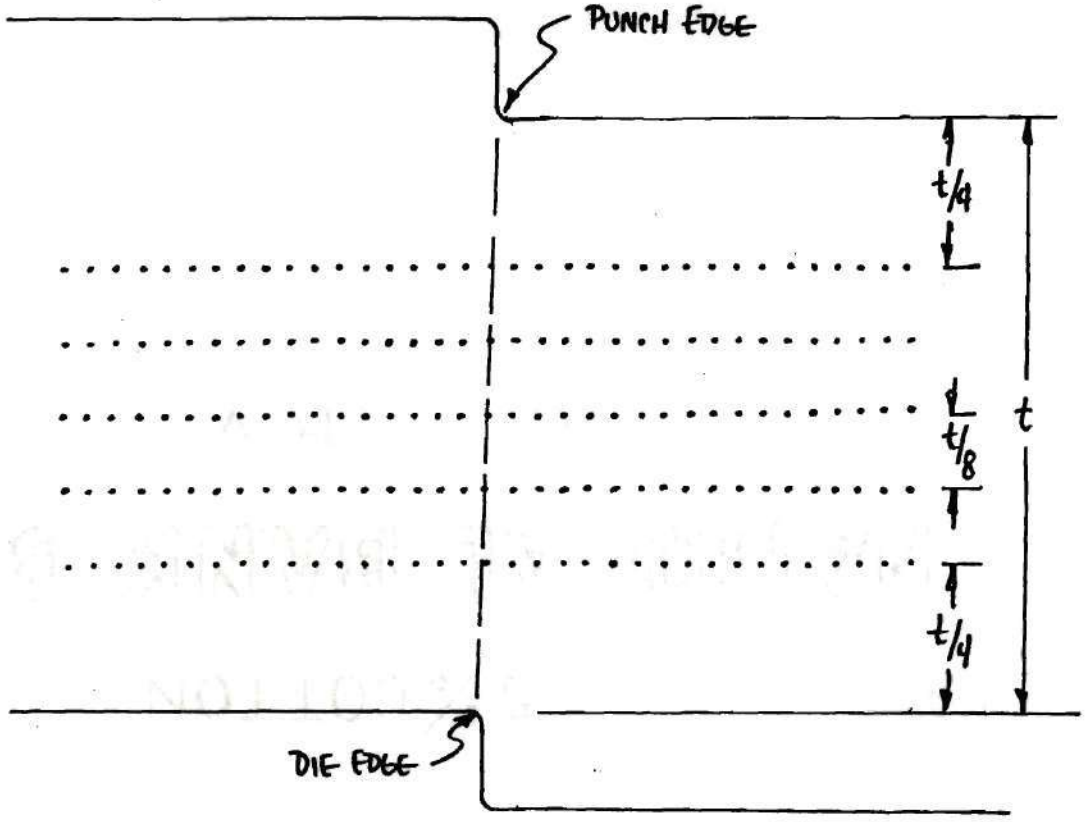

FIVE ROWS OF 35 HARDNESS INDENTATIONS EACH
HORIZONTAL SPACING: 0.18 mm (0.007 IN.)

Fig. 6a. Hardness Test Matrix Dimensions

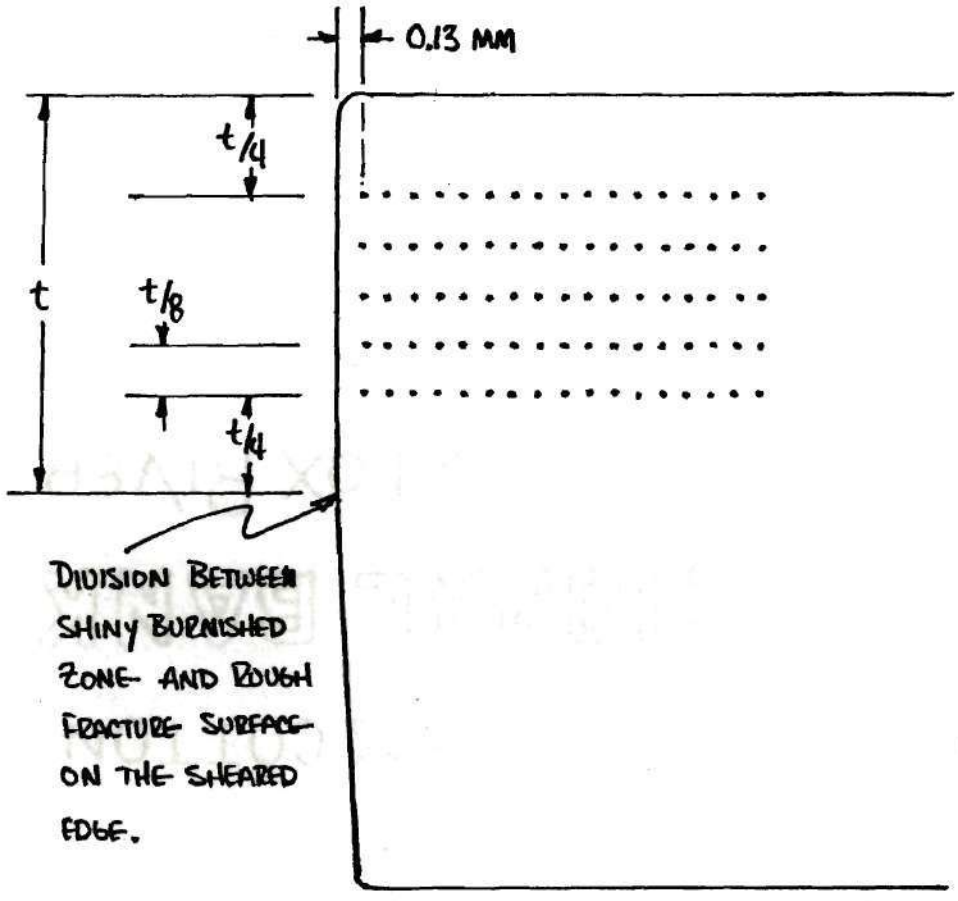

FIVE ROWS OF 17 HARDNESS INDENTATIONS EACH
HORIZONTAL SPACING: 0.18 MM (0.007 IN.)

Fig. 6b. Hardness Test Matrix Dimensions

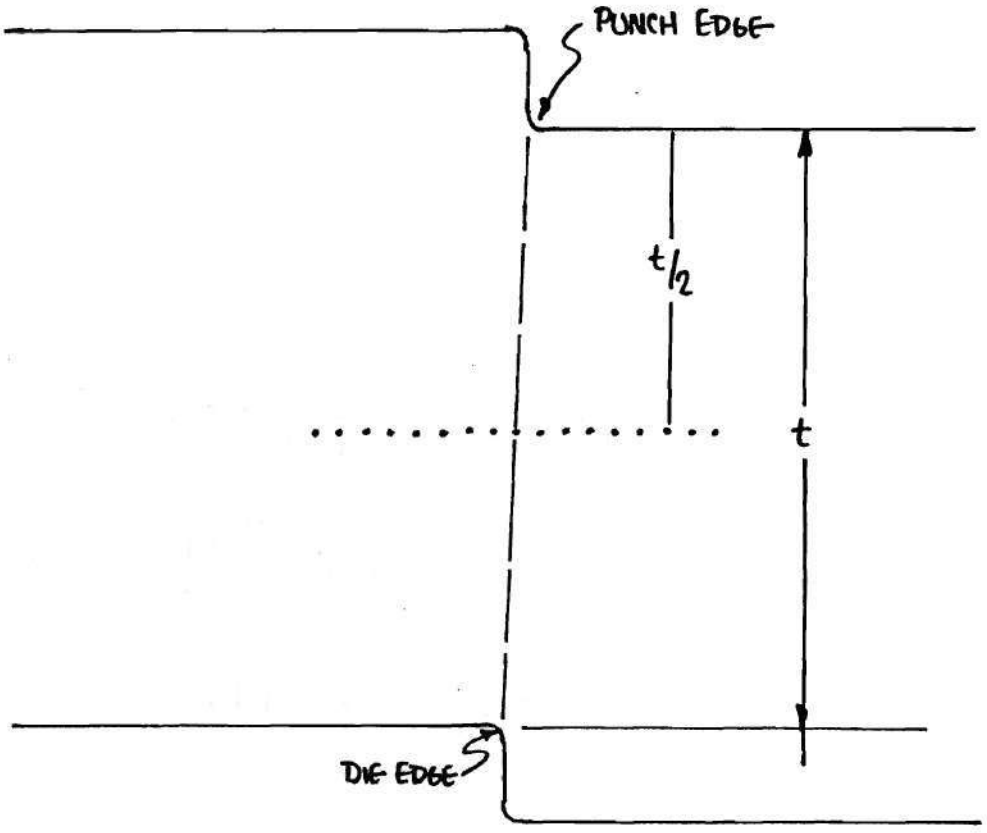

ONE ROW OF FIFTEEN HARDNESS INDENTATIONS
HORIZONTAL SPACING: 0.18 MM

Fig. 6c. Hardness Test Matrix Dimensions

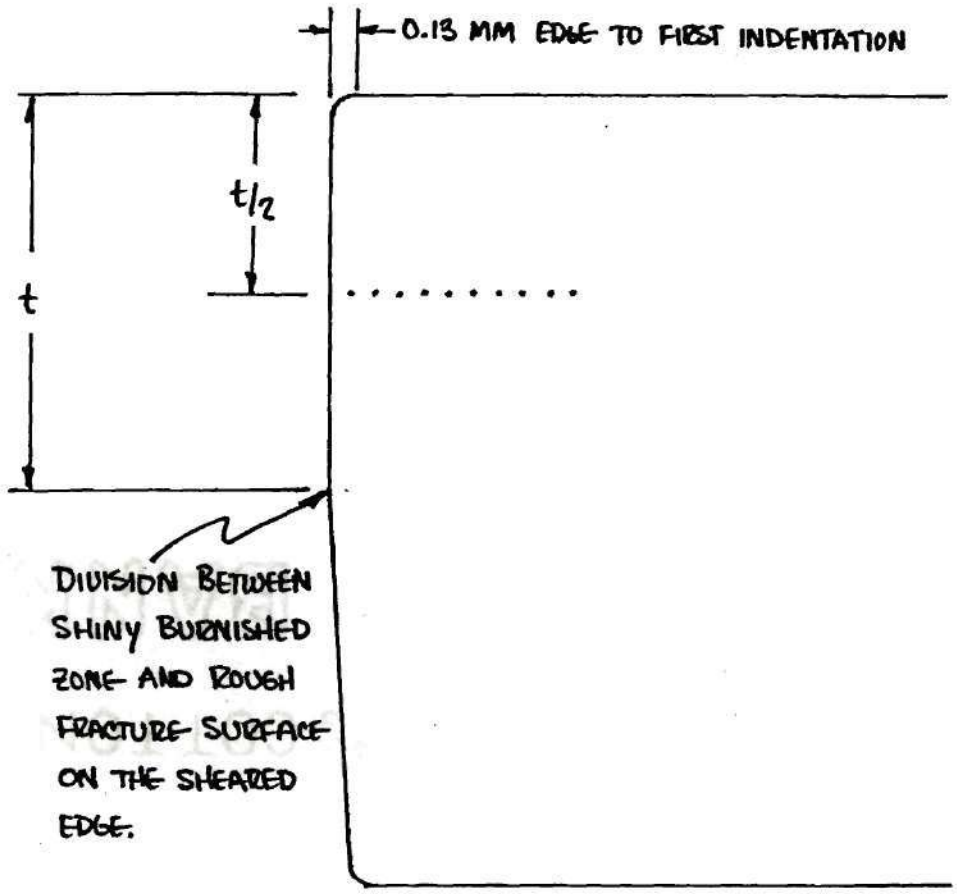

Fig. 6d. Hardness Test Matrix Dimensions

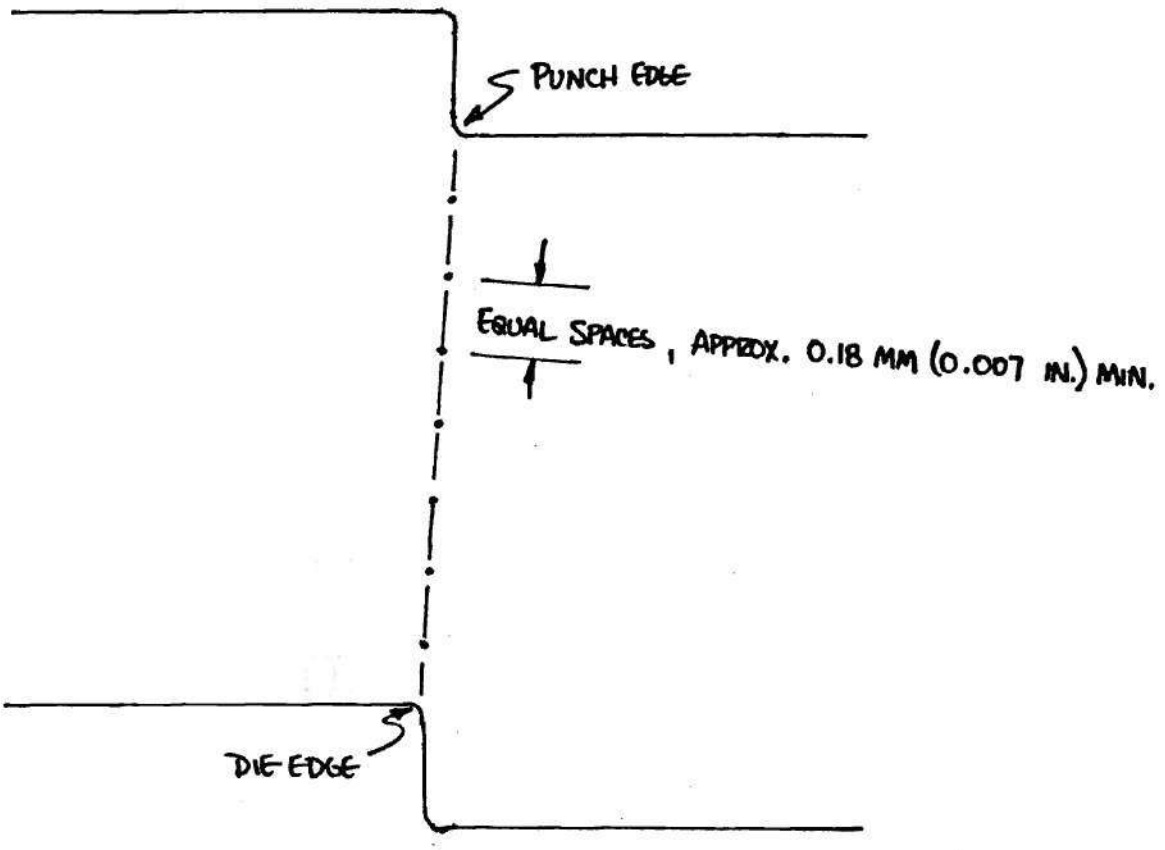

ONE ROW OF HARDNESS INDENTATIONS
ALONG THE DEFORMATION LINE

Fig. 6e. Hardness Test Matrix Dimensions

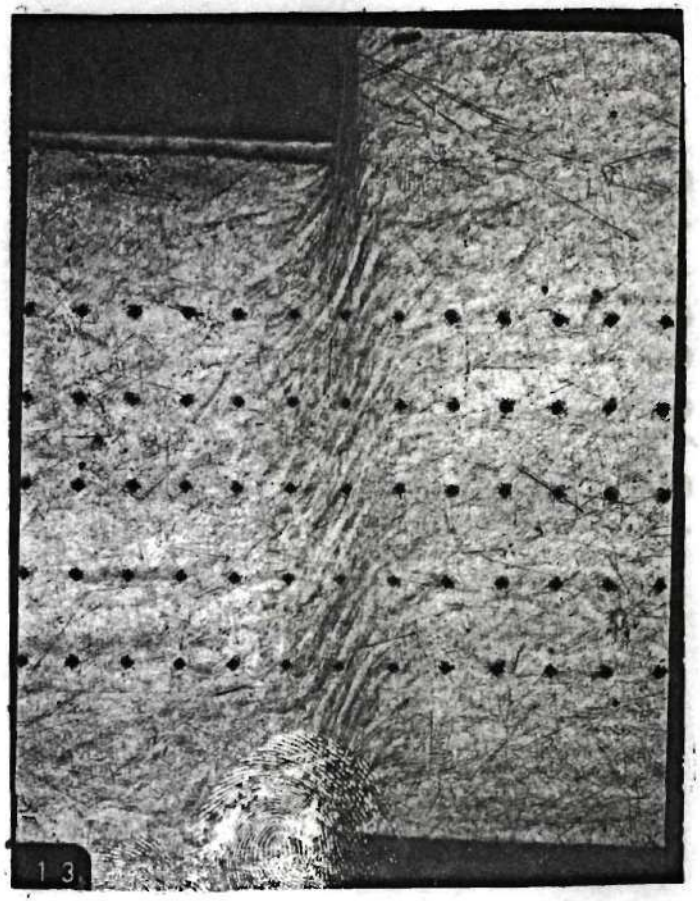

HHPB, 6% D.C., 32.2% PUNCH PEN.

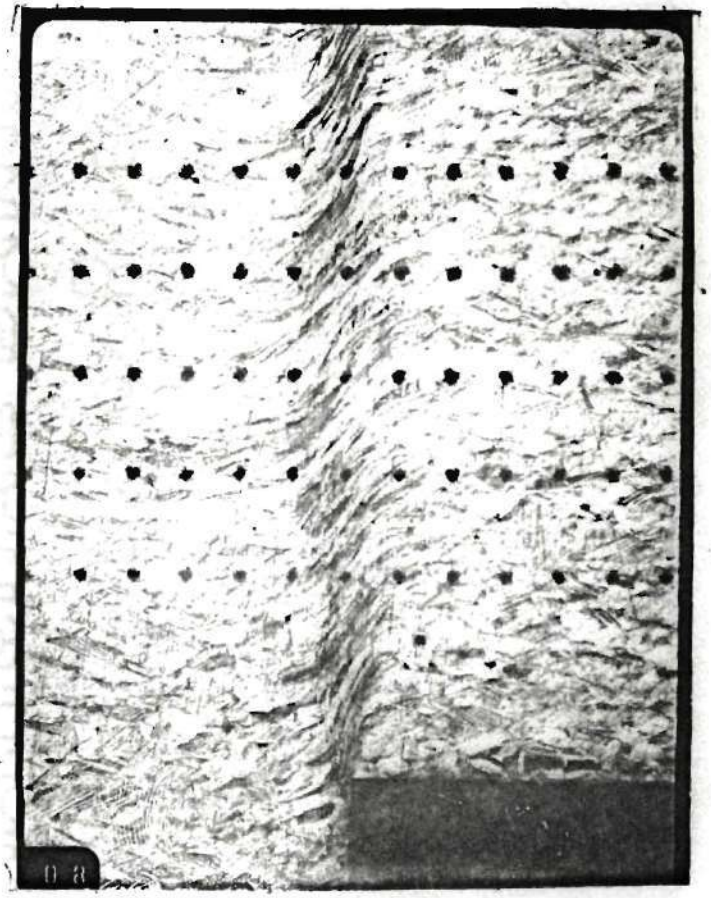

HCNS, 6% D.C., 21.3 % PUNCH PEN.

Fig. 7. Photomicrographs of Hardness Test Matrices (40X)

slug separation was computed as above, based on an average of two tests for each material. One sample of each of these two materials was then punched to 1/4, one sample to 1/2, and one sample to 3/4 of that material's slug separation penetration for the 1,008 inch die. This procedure was repeated for HHPB and HCNS using the 1.024 inch die for approximately 9% die clearance.

The samples of HHPB and HCNS punched to half their separation penetration with the 1.008 inch die and with the 1.024 inch die and the side of one of the separated samples of each of those two materials with each of those two dies, were also metallographically sectioned, mounted, polished, and etched for observation of a vertical/longitudinal plane of the strip. Microhardness grids were made on each of these samples according to Figures 6c and 6d.

Twelve additional two-inch squares of each of the four materials were then cut from adjacent 6-inch lengths of the material strips. These samples were punched to near slug separation, using the 1.016 inch square die. Samples of each of the materials were selected from this group and metallographically sectioned, mounted, polished, and etched for observation by light microscopy to check for crack formation in the deformation. For each material, one of these mounted samples which did <u>not</u> show crack formation was selected for hardness tests down the deformation line according to Figure 6e.

2.6. Experimental Procedure: Strain Rate Sensitivity Tests

Five tensile test specimens of each material were fabricated as detailed in the first two paragraphs of Section 2.4. The samples were made in random order, and were randomized for the following tests.

Two tensile samples of each material were strained to failure at a crosshead speed of 0.1 mm/min. Next, two samples of each material were strained to failure at a crosshead speed of 10 mm/min. Finally, one sample of each was strained to failure using a crosshead speed of 100 mm/min. In all of these tests, a one-inch extensometer was used to monitor the strain. Thus, based on a one-inch gage length, strain rates of $7X10^{-5}$, $7X10^{-3}$, and $7X10^{-2}$ sec^{-1} were obtained.

The 0.2% offset yield strength, ultimate tensile strength, and true strain at failure according to Eq. 3 were recorded for each test. These data are given in Appendix 3.

2.7. Metallographic Sample Preparation

Fractured ends of tensile samples to be mounted were cut off with a shear. Stamping samples were sectioned with a Buehler cut-off wheel, making the section near the longitudinal centerline of the strip. All samples were mounted in Diallyl Phthalate (Blue) in a Buehler press. The initial thicknesses of the mounted samples of the tensile specimens

were measured to the nearest 0.0005 inch with dial calipers. In the first two steps these samples were ground to within a few thousandths of the tensile sample (and original strip-) centerline.

All samples were ground on 150-grit and 300-grit size papers on a wet belt sander. Next, the samples were ground on a wet grinding wheel with discs of 240-grit, 400-grit, and finally 600-grit size paper. Samples were polished in a vibratory polisher for 1-2 hours in a suspension of 0.05 micron alumina powder in a 50 vol% mixture of water and ethylene glycol. This suspension medium increased the polishing time approximately twofold, but helped avoid pitting of the samples during polishing.

A ferric chloride etchant was applied with a cotton-tipped swab, followed quickly by a water rinse. After rinsing, the samples were dried with a warm-air blower before applying additional etchant. The phosphor bronze tended to etch darker than the Cu-Ni-Sn alloy.

This metallographic sample preparation procedure is in accordance with the guidelines set forth in ASTM Standard E3-62.

CHAPTER III

RESULTS AND DISCUSSION OF RESULTS

3.1. Results

Experimental data relating microhardness with true plastic tensile strain are plotted in Figures 8a-8d. Also plotted in Figure 8 are the respective plots of Eq. 5.

Microhardness plots from grids made as in Figure 6a across the shear deformation zones of HHPB at 10, 20, and 30 percent punch penetration with 6% die clearance are given in Figures 9a-9c. Microhardness plots from a grid made according to Figure 6b on a HHPB sample punched through to slug separation with 6% die clearance are shown in Figure 9d. A similar series of plots for HCNS with 6% die clearance for 10, 20, and 30 percent punch penetration and post-slug separation are given in Figure 9e-9h.

Figures 9i and 9j show microhardness profiles for STPB with 6% die clearance obtained from grids made according to Figures 6c and 6d with 13% punch penetration (half that required for slug separation) and post-slug separation. Similar profiles for STCNS with 6% die clearance at 17 percent punch penetration (half that required for slug separation) and post-slug separation are shown in Figures 9k and 9l.

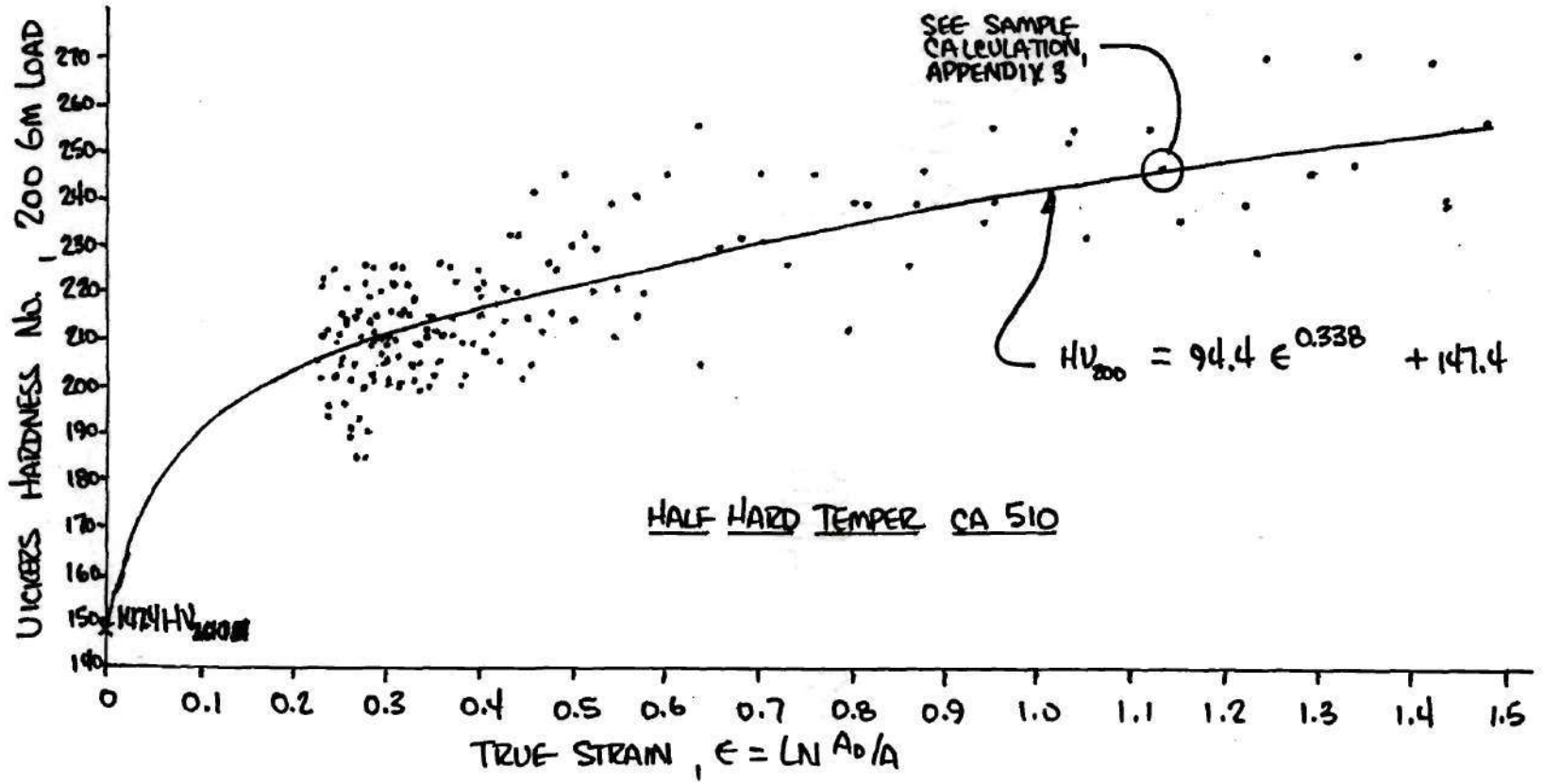

Fig. 8a. VHN Versus True Strain: HHPB

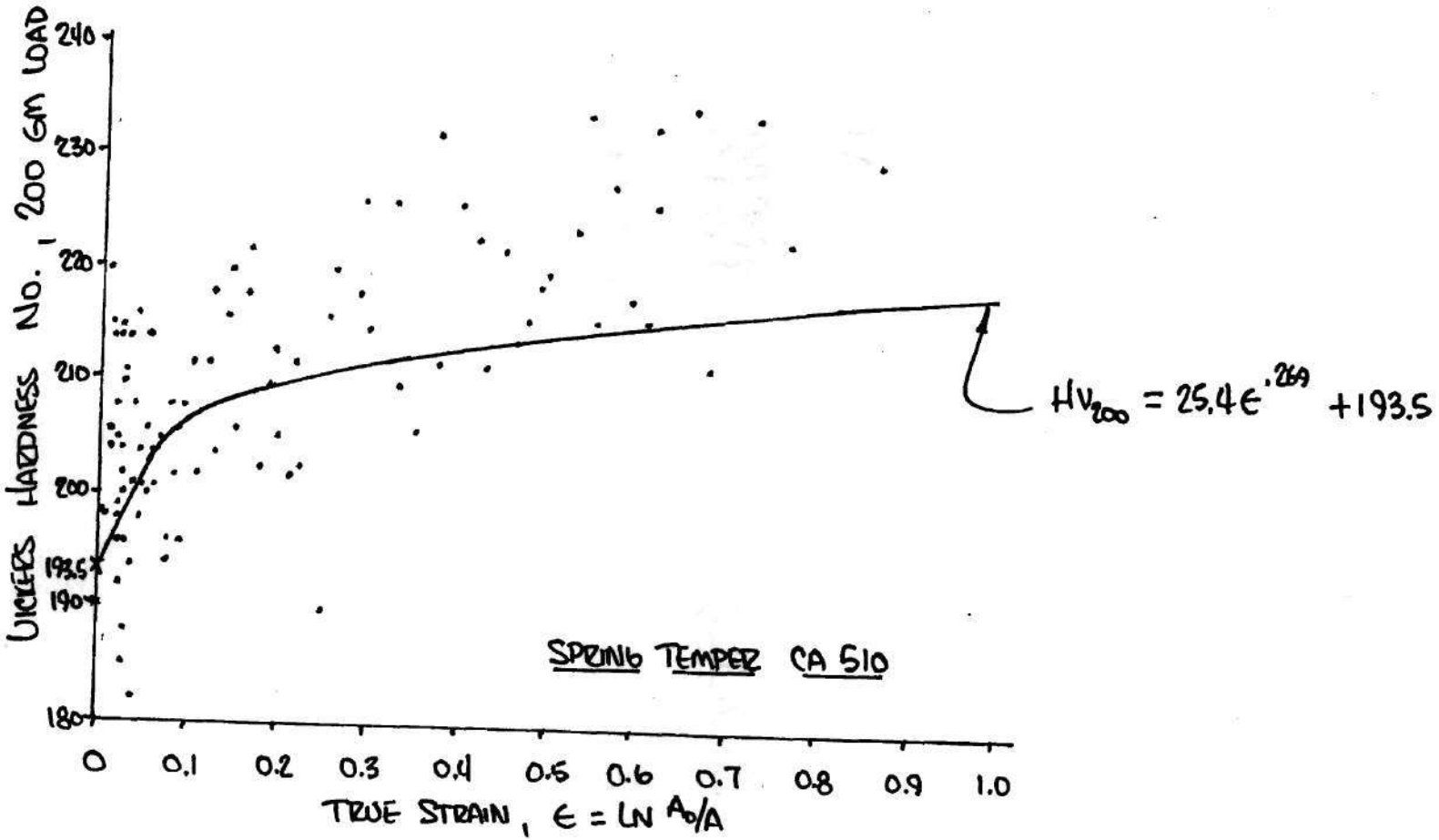

Fig. 8b. VHN Versus True Strain: STPB

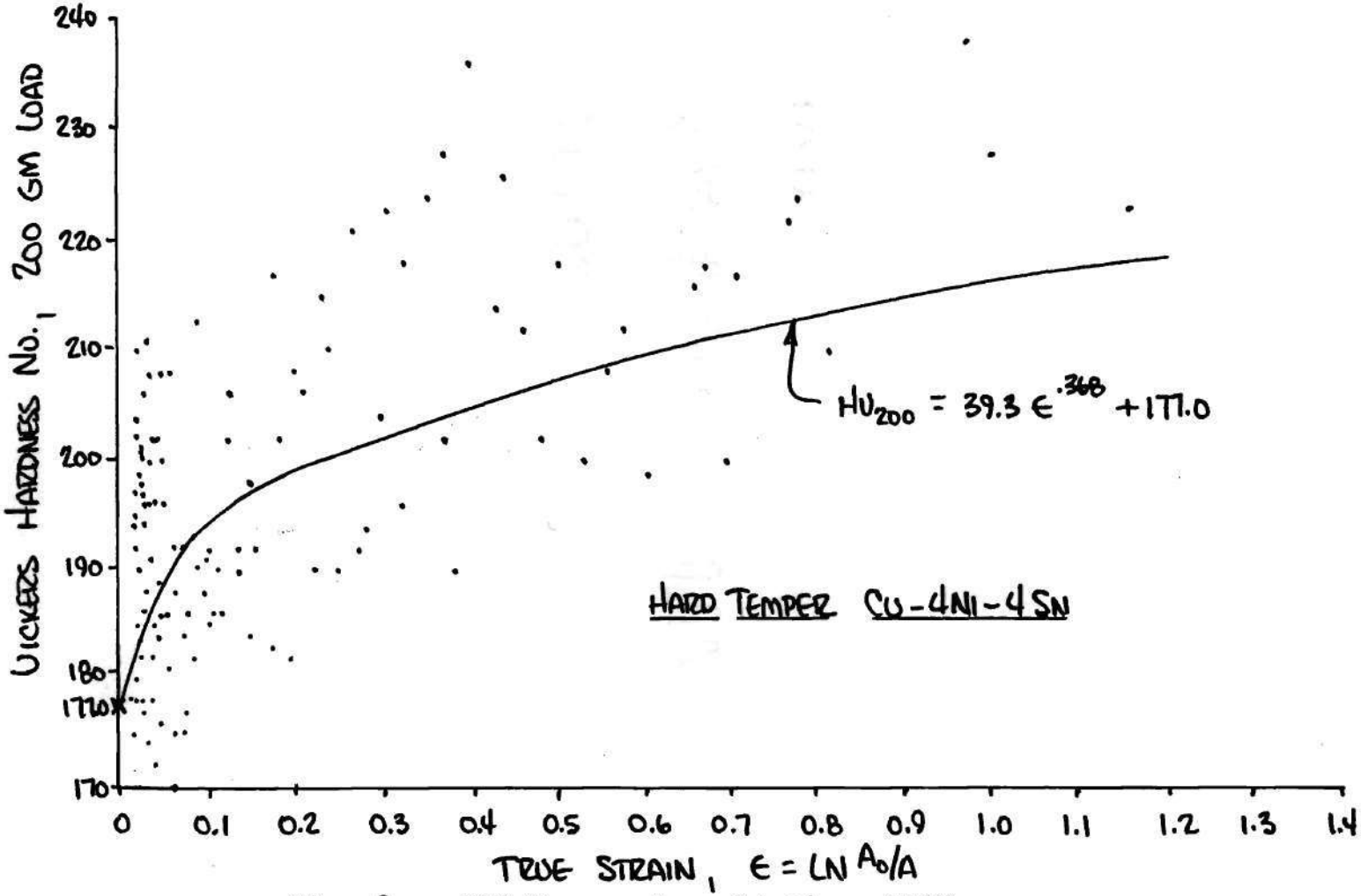

Fig. 8c. VHN Versus True Strain: HCNS

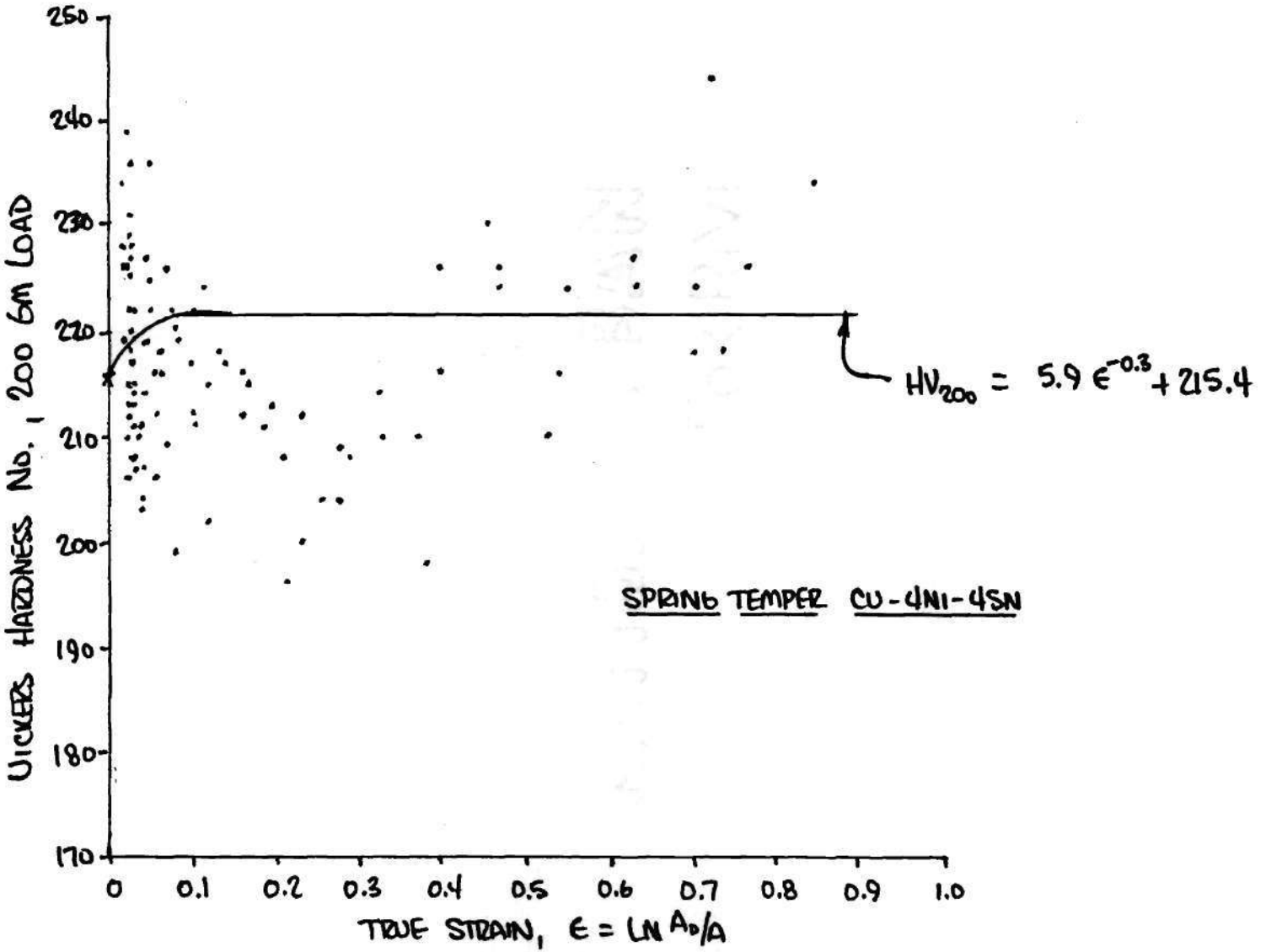

Fig. 8d. VHN Versus True Strain: STCNS

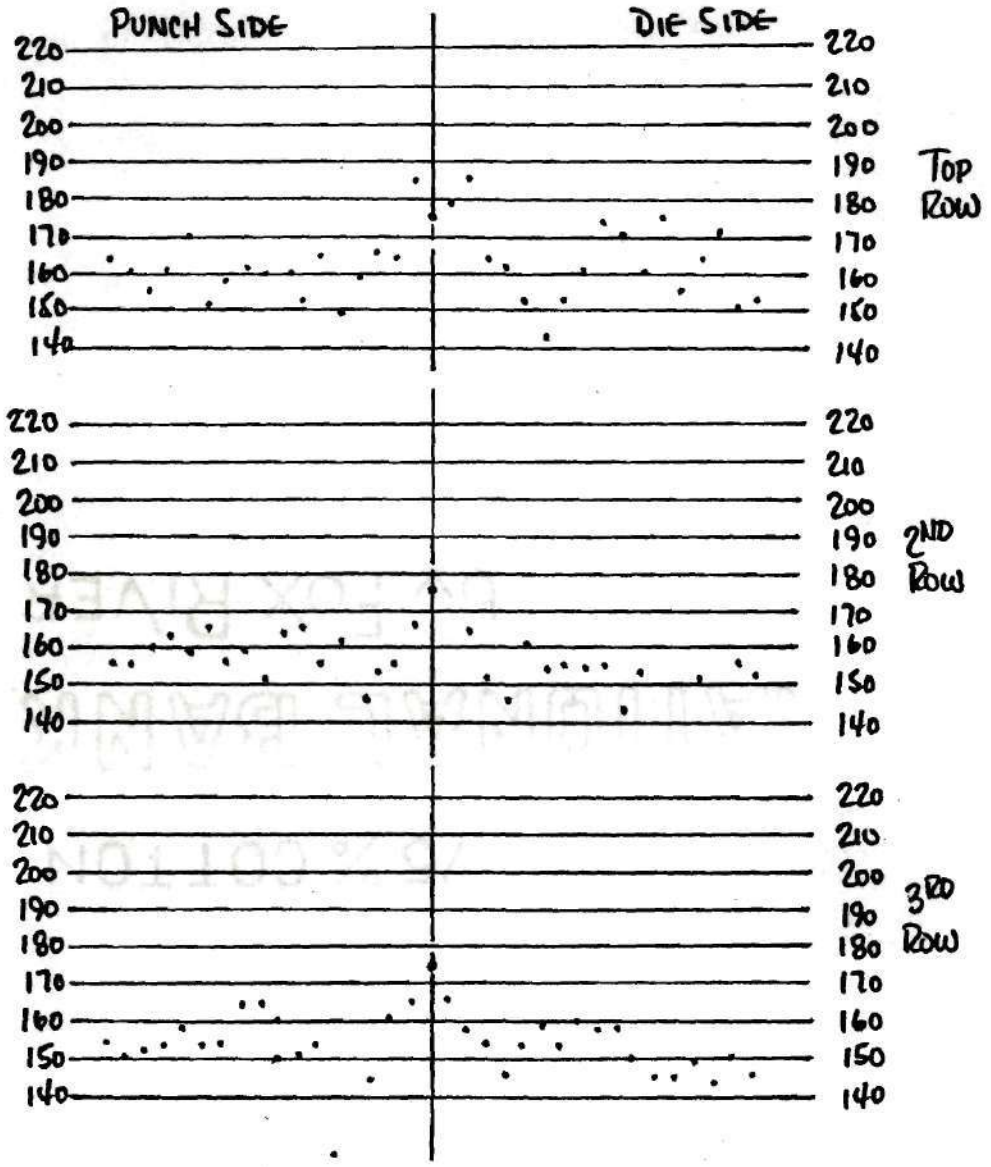

Fig. 9a. Microhardness Profiles on Sectioned Stamping Samples: HHPB, 6% Die Clear., 11% Punch Pen.

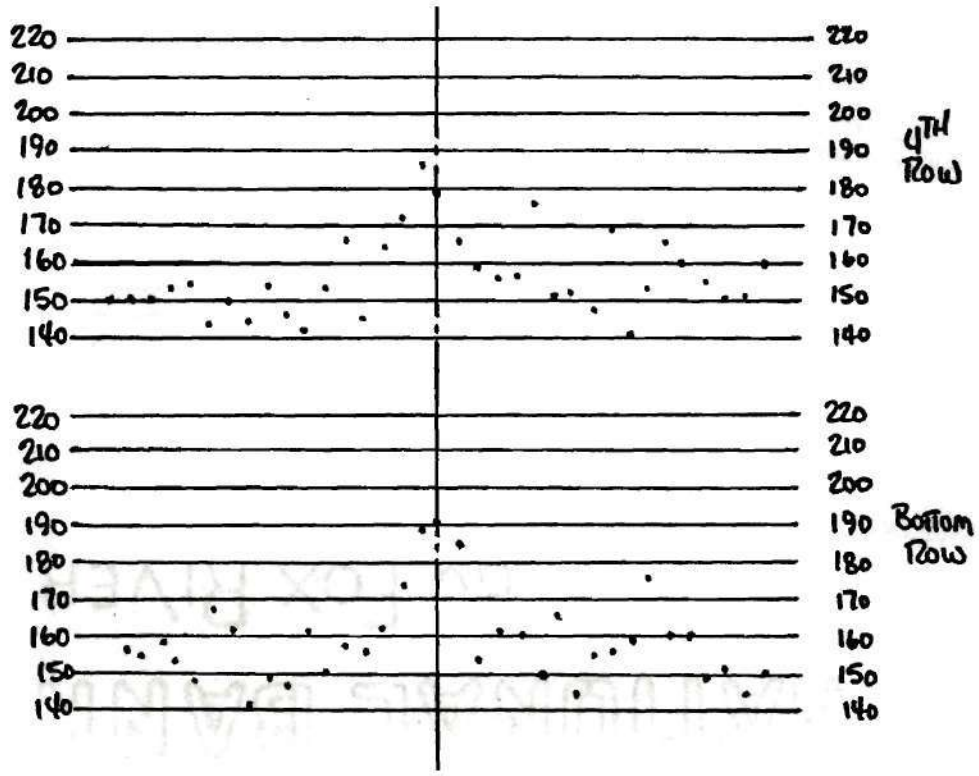

Fig. 9a, Continued: HHPB, 6% Die Clear., 11% Punch Pen.

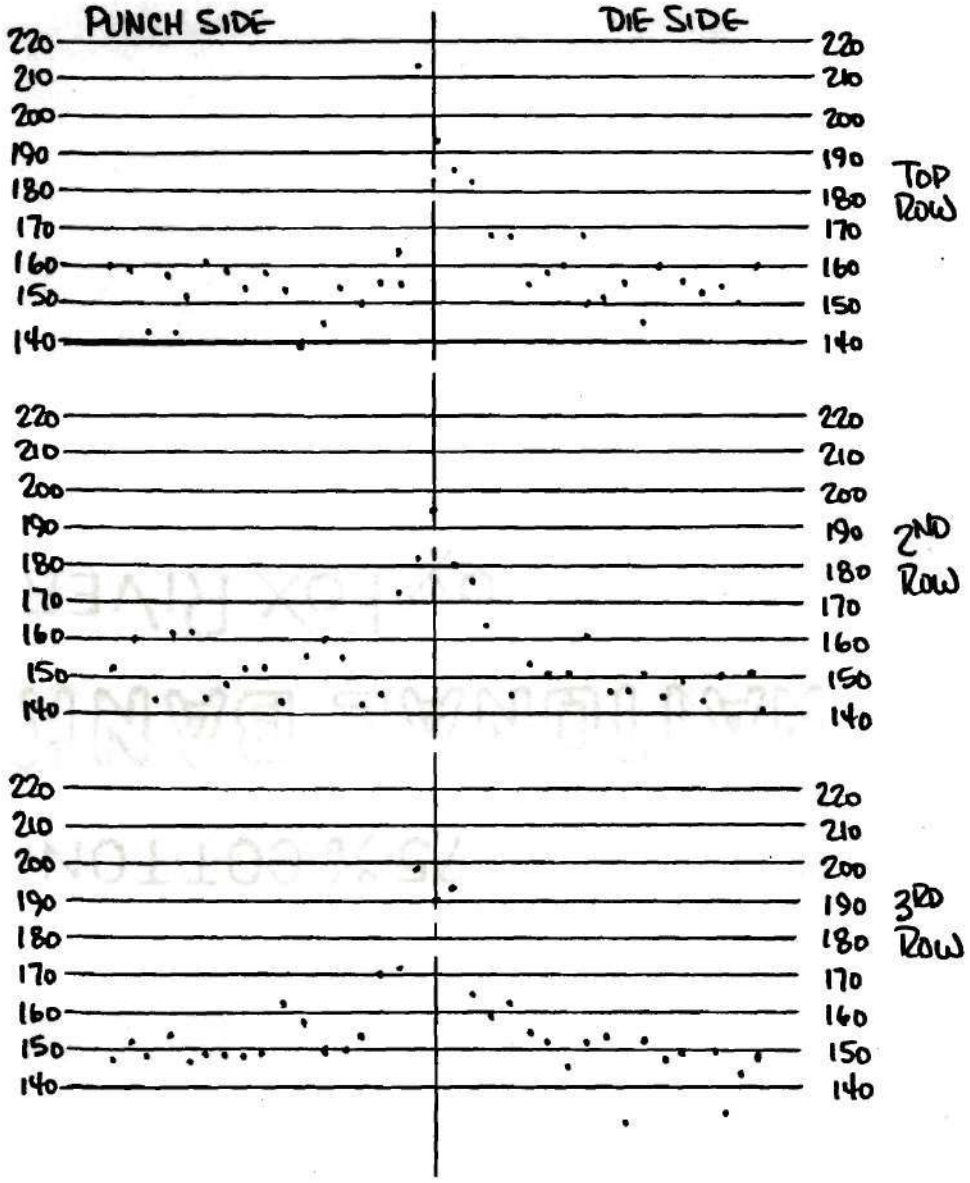

Fig. 9b. Microhardness Profiles on Sectioned Stamping Samples: HHPB, 6% Die Clear., 22% Punch Pen.

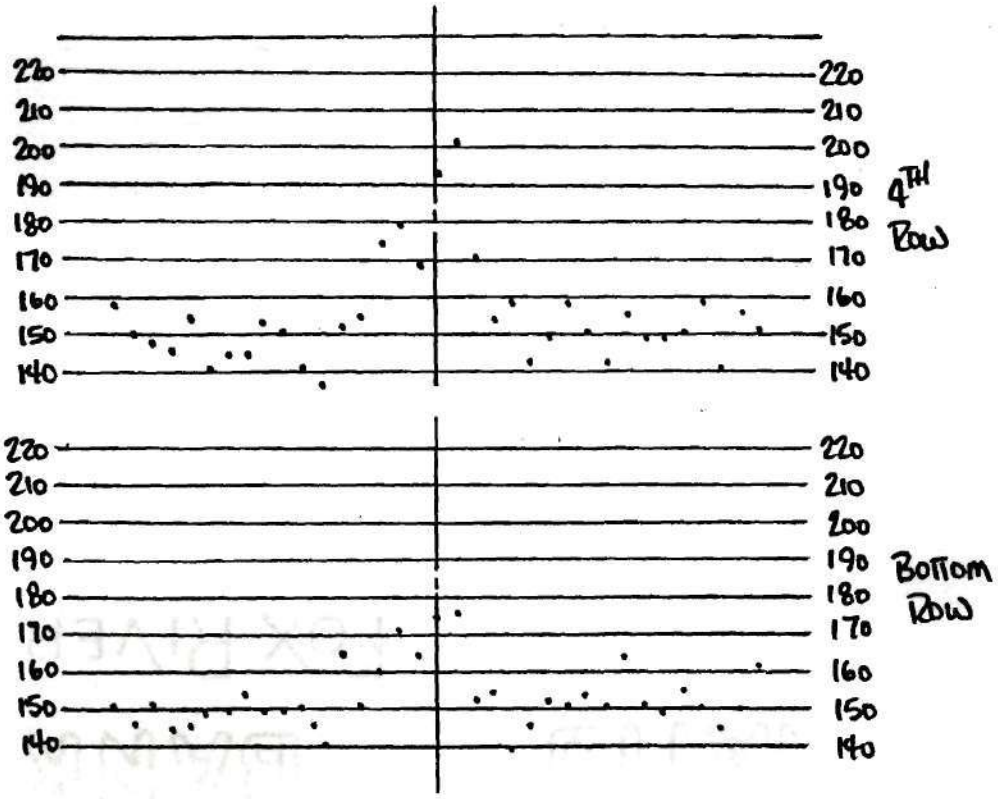

Fig. 9b., Continued: HHPB, 6% Die Clear., 22% Punch Pen.

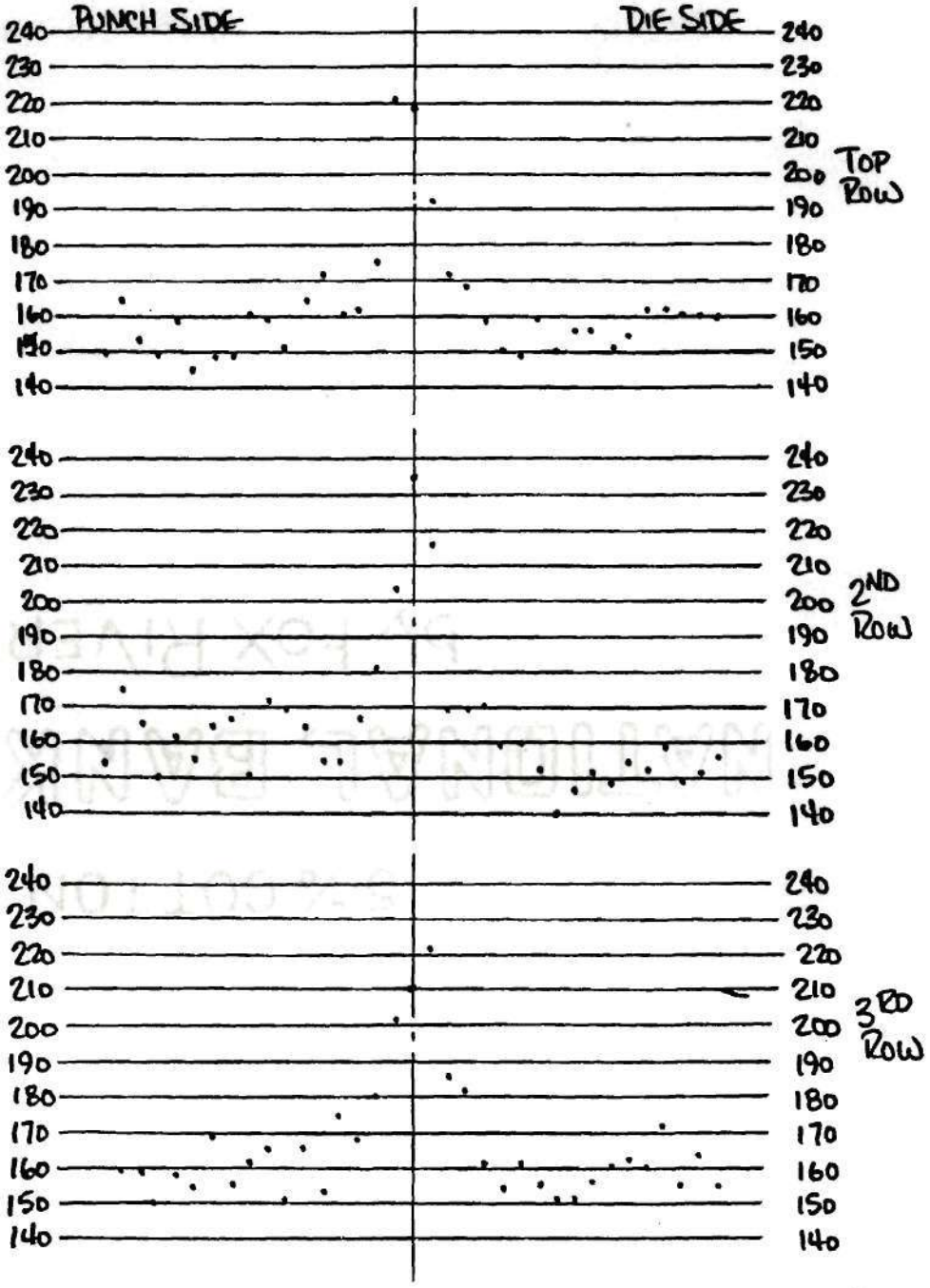

Fig. 9c. Microhardness Profiles on Sectioned Stamping Samples: HHPB, 6% Die Clear., 33% Punch Pen.

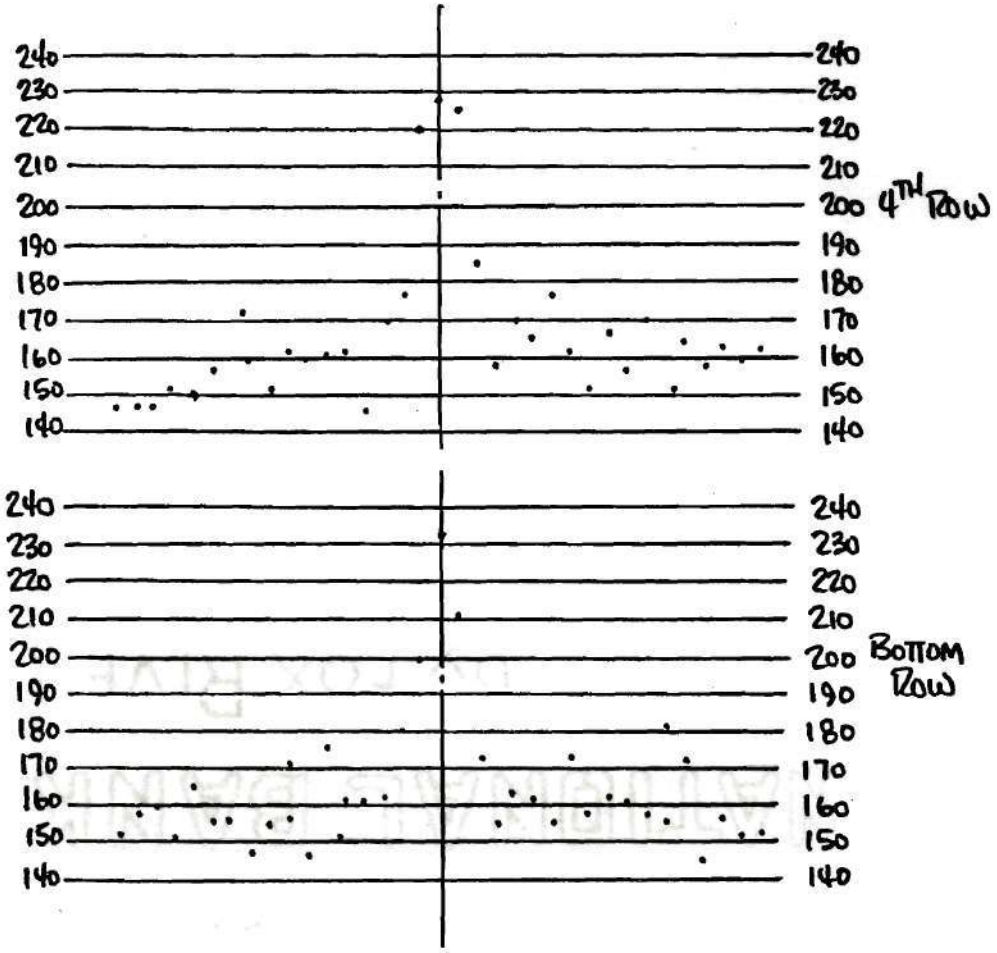

Fig. 9c., Continued: HHPB, 6% Die Clear., 33% Punch Pen.

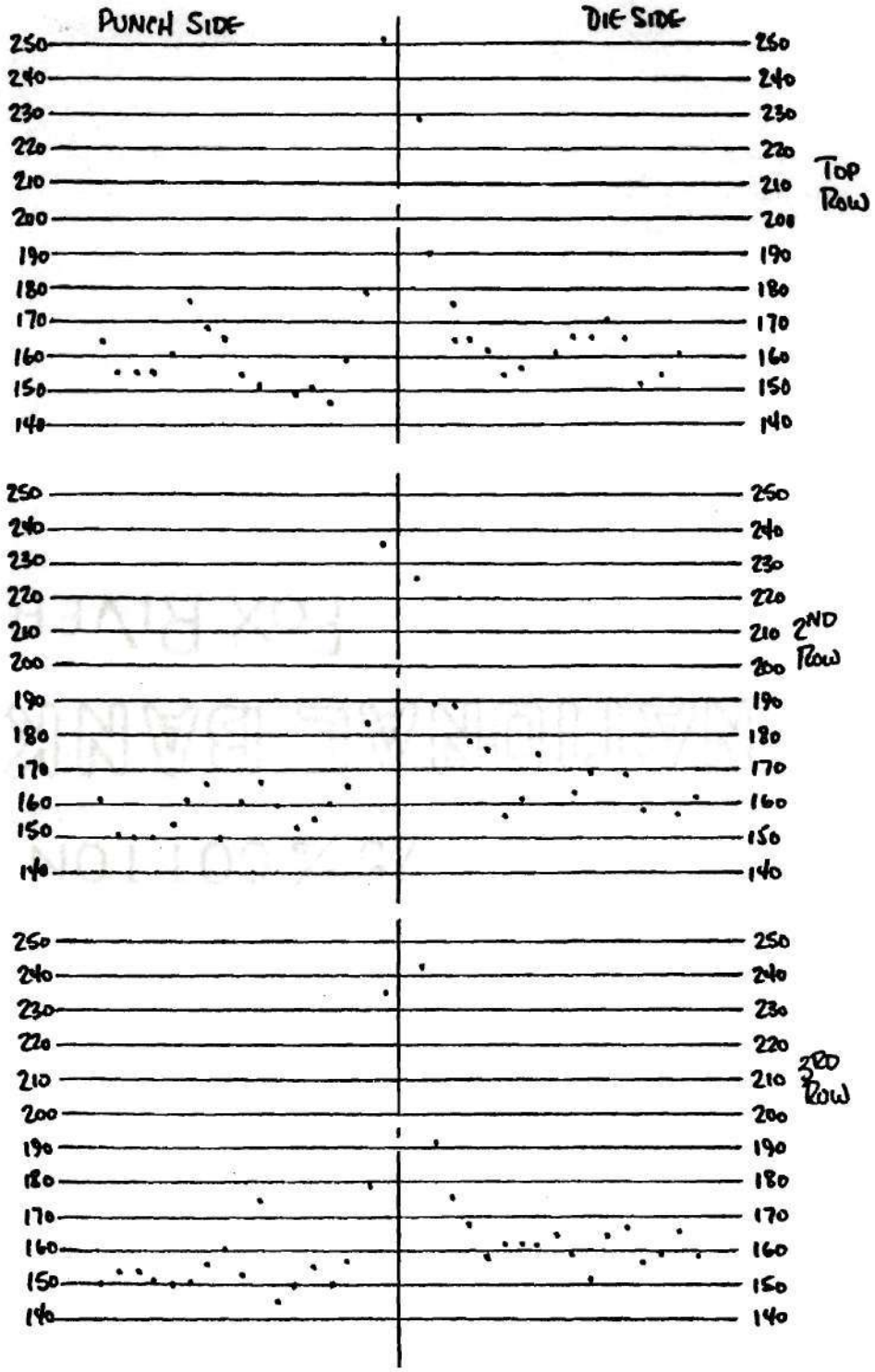

Fig. 9d. Microhardness Profiles on Sectioned Stamping Samples: HHPB, 6% Die Clear., Post-Slug Separation

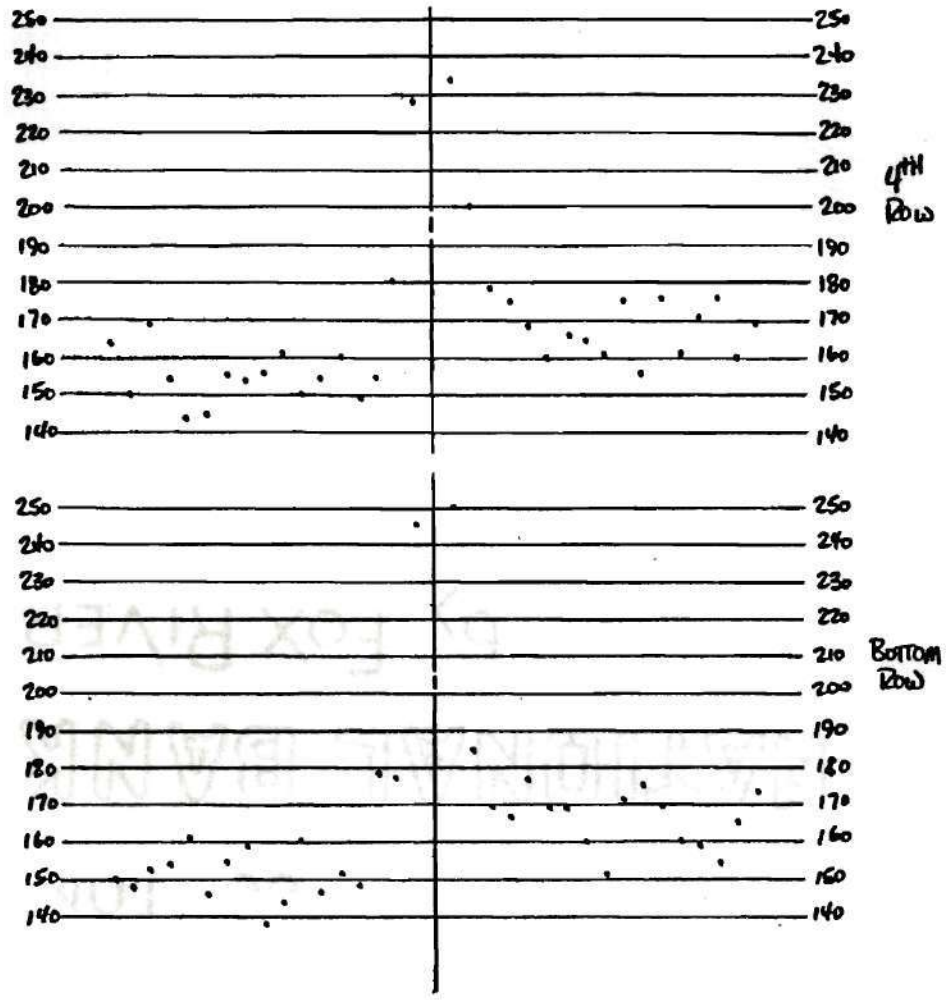

Fig. 9d., Continued: HHPB, 6% Die Clear., Post-Slug Separation

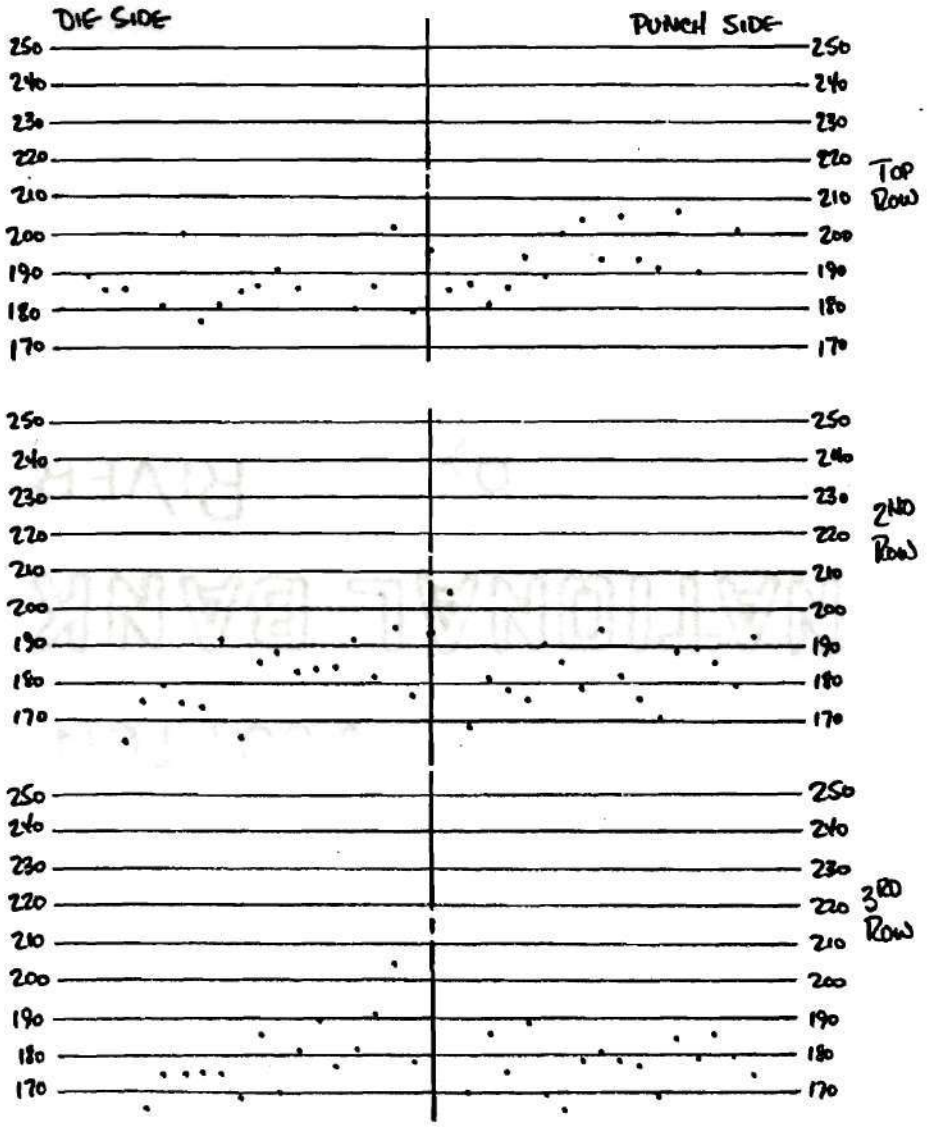

Fig. 9e. Microhardness Profiles on Sectioned Stamping Samples: HCNS, 6% Die Clear., 11% Punch Pen.

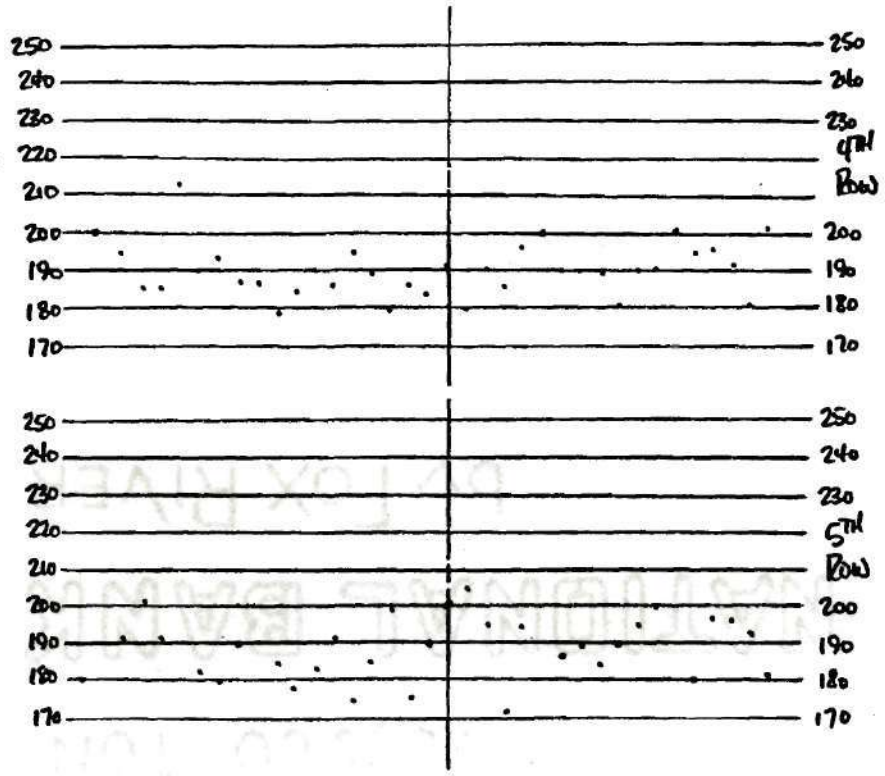

Fig. 9e., Continued: HCNS, 6% Die Clear., 11% Punch Pen.

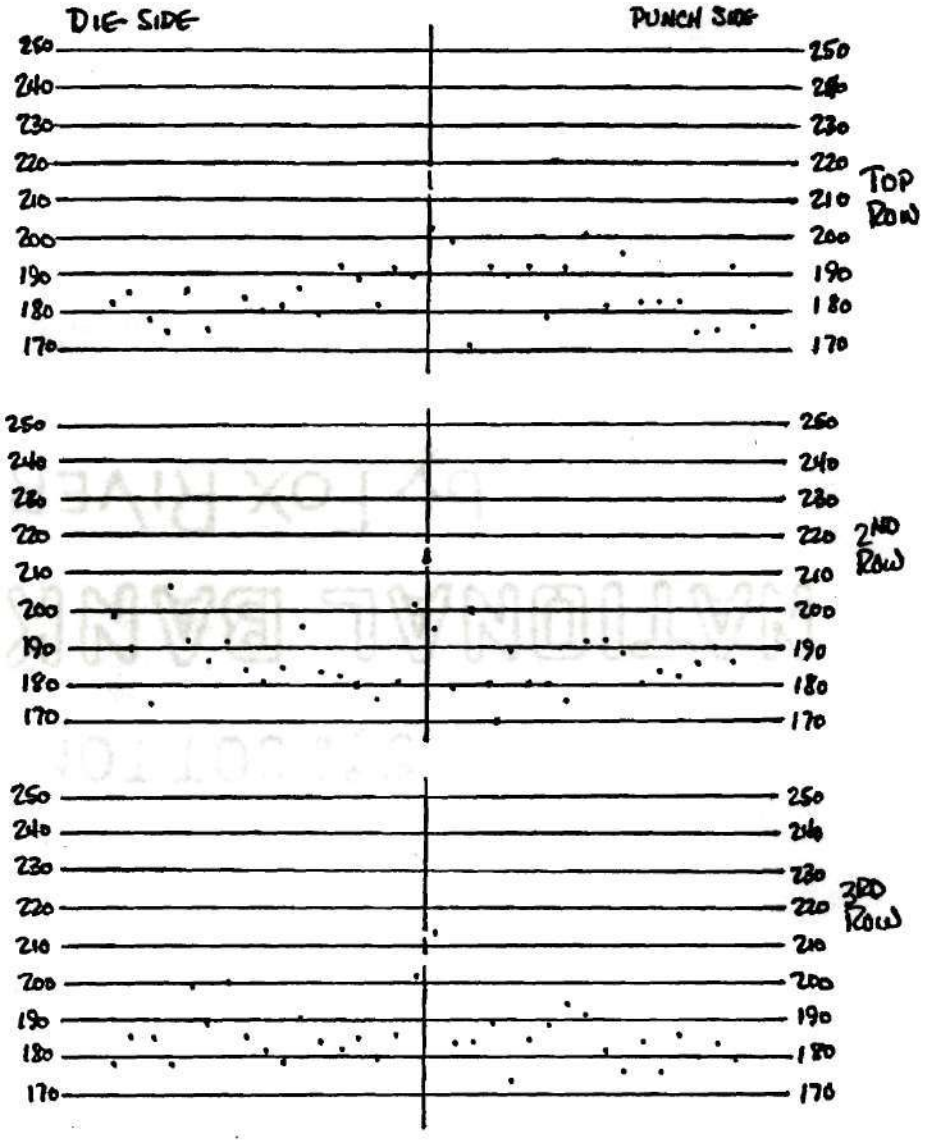

Fig. 9f. Microhardness Profiles on Sectioned Stamping Samples: HCNS, 6% Die Clear., 22% Punch Pen.

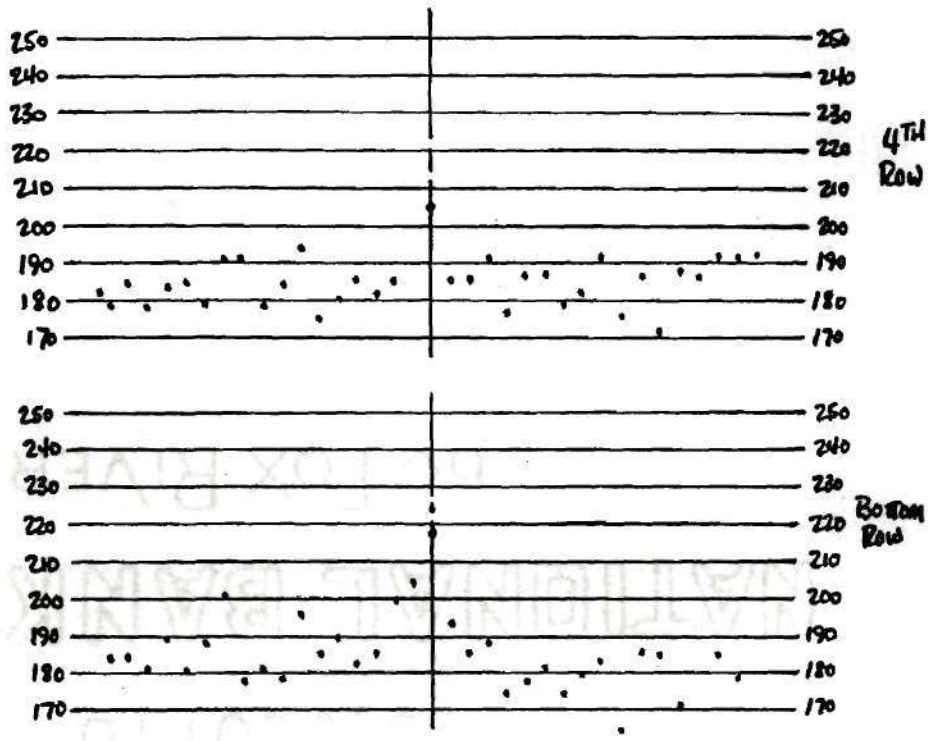

Fig. 9f., Continued: HCNS, 6% Die Clear., 22% Punch Pen.

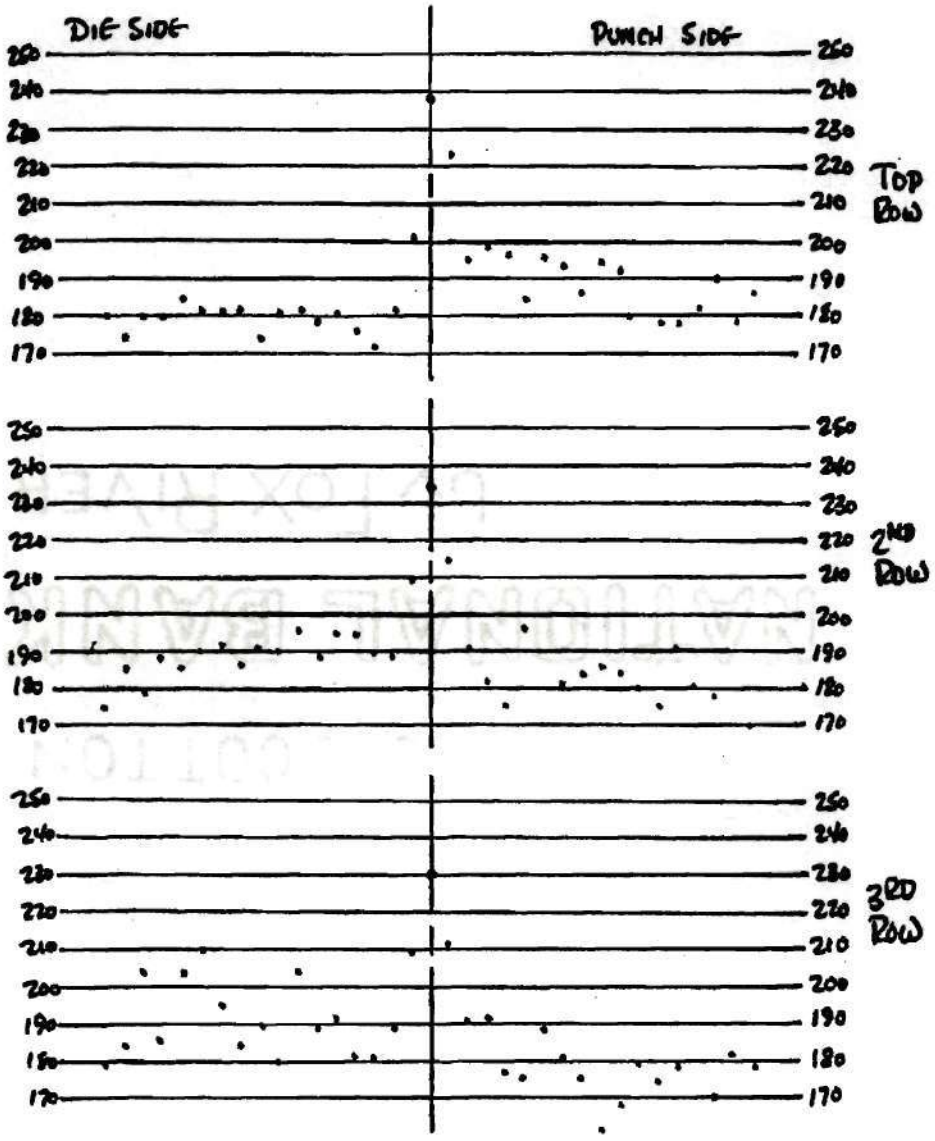

Fig. 9g. Microhardness Profiles on Sectioned Stamping Samples: HCNS, 6% Die Clear., 32% Punch Pen.

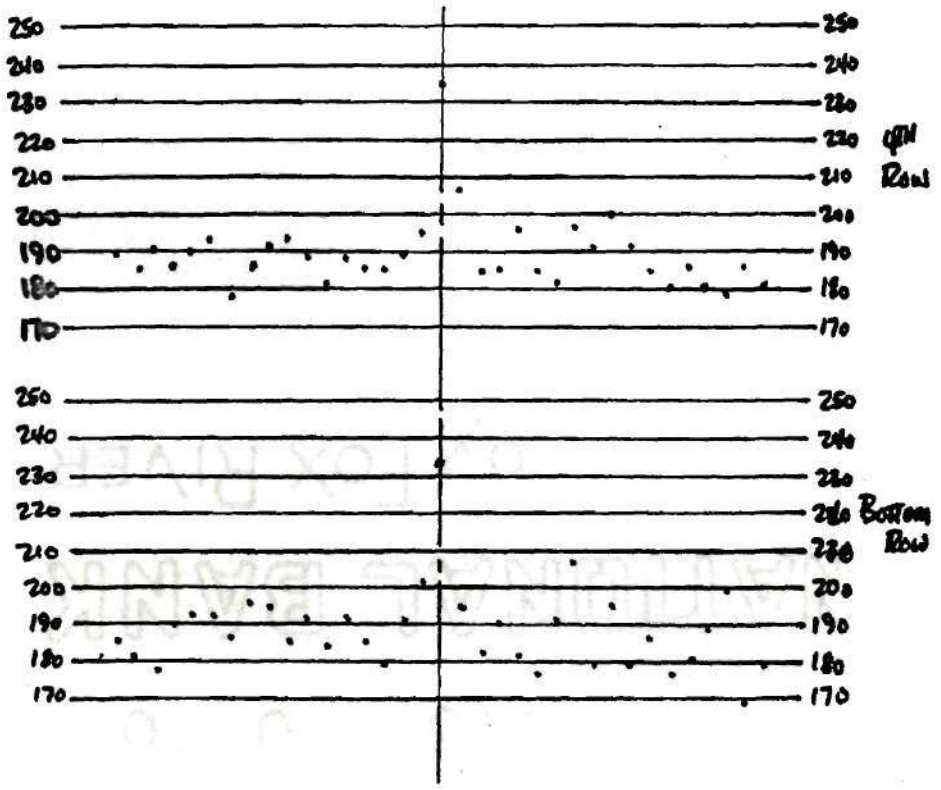

Fig. 9g., Continued: HCNS, 6% Die Clear., 32% Punch Pen.

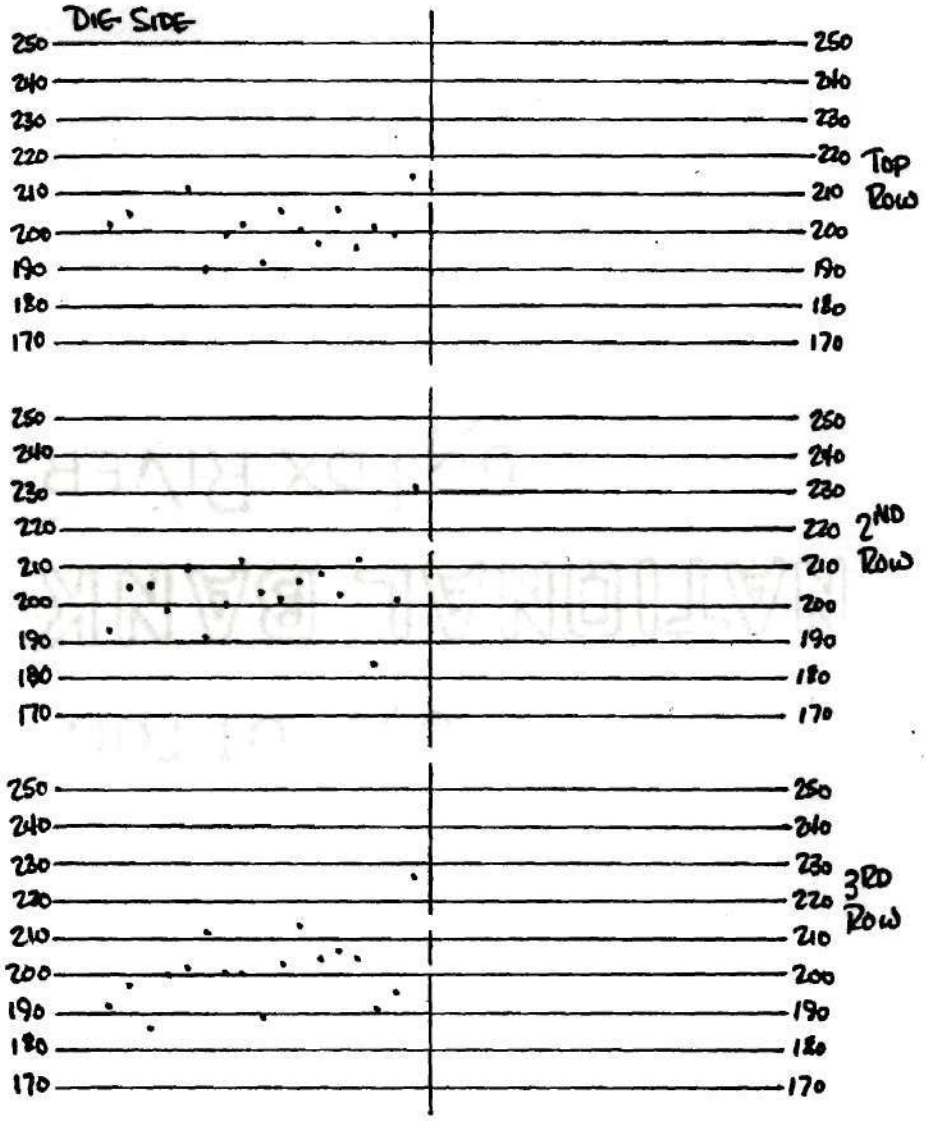

Fig. 9h. Microhardness Profiles on Sectioned Stamping Samples: HCNS, 6% Die Clear., Post-Slug Separation

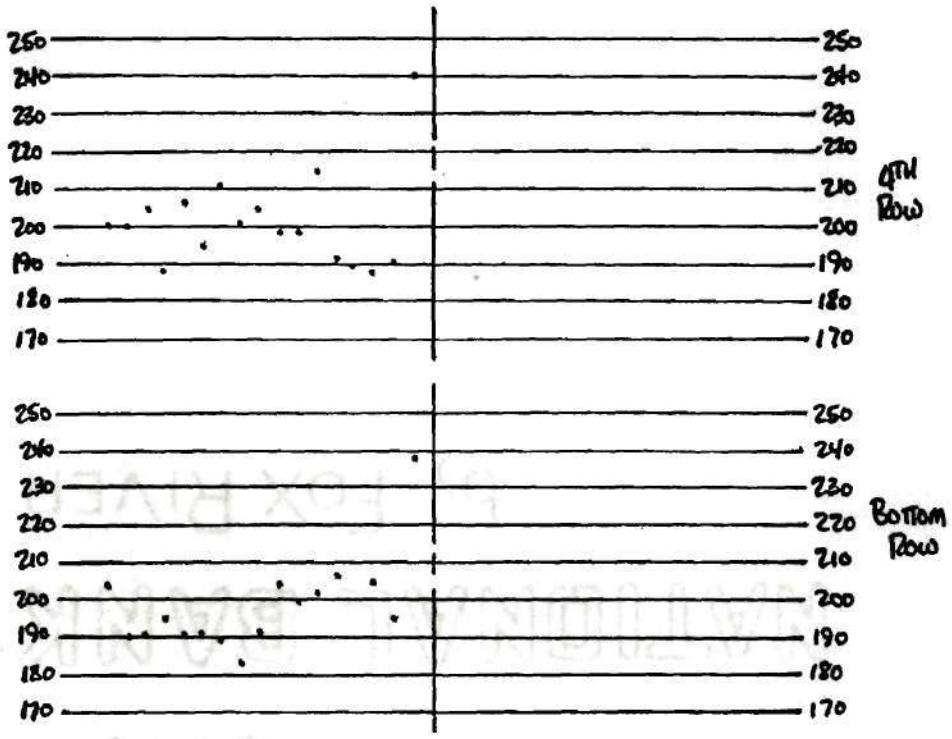

Fig. 9h., Continued: HCNS, 6% Die Clear., Post-Slug Separation

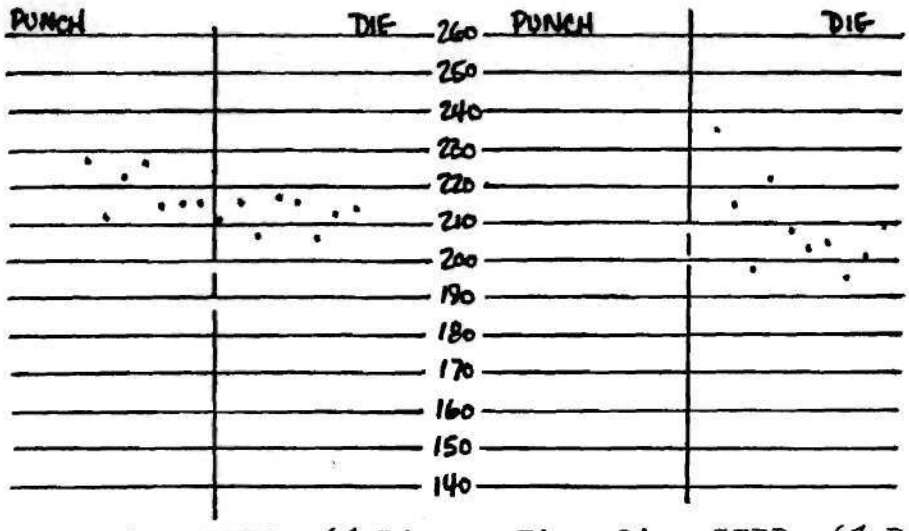

Fig. 9i. STPB, 6% Die Clear., 13% Punch Pen.

Fig. 9j. STPB, 6% Die Clear., Post-Slug Sep.

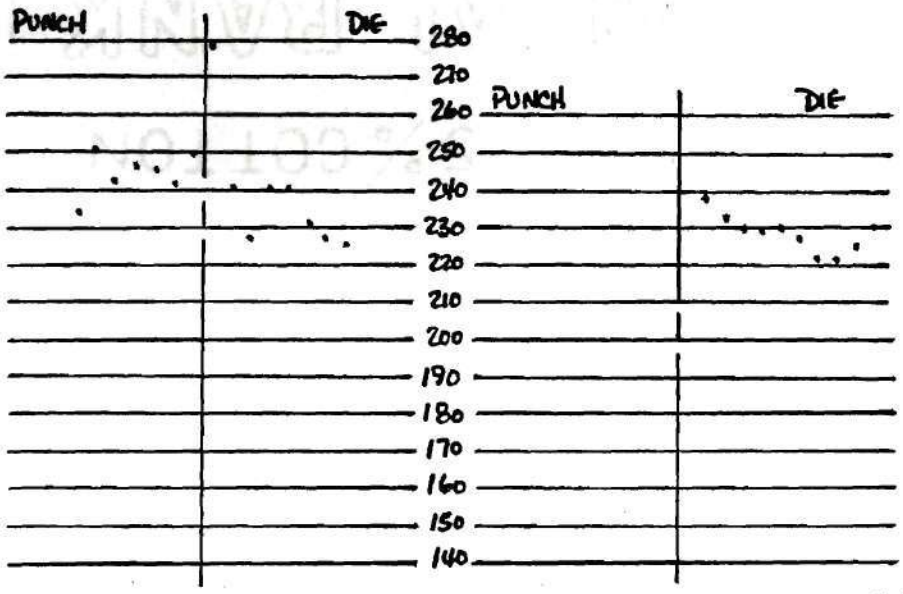

Fig. 9k. STCNS, 6% Die Clear., 17% Punch Pen.

Fig. 9l. STCNS, 6% Die Clear., Post-Slug Sep.

Fig. 9: Microhardness Profiles on Sectioned Stamping Samples

In Figures 10a and 10b microhardness profiles for HHPB are given for 3% die clearance at 25 percent punch penetration (half that required for slug separation) and post slug separation from grids made according to Figure 6c and 6d. Figure 10c and 10d give the microhardness profiles for HHPB with 9% die clearance at 22% punch penetration (half that required for slug separation) and post-slug separation from grids made according to Figures 6c and 6d. Figures 10e and 10f show hardness profiles for HCNS with 3% die clearance at 23% punch penetration (half that required for slug separation) and post-slug separation from grids laid out according to Figures 6c and 6d. The same hardness indentation grids for HCNS with 9% die clearance at 19.5% punch penetration (half that required for slug separation) and post-slug separation yielded the hardness profiles shown in Figures 10g and 10h.

Hardness measurements made according to Figure 6e along the shear deformation lines of samples of all four materials just prior to slug separation with 6% die clearance are plotted in Figure 11.

Crack formation at incipient slug separation with 6% die clearance is shown for HHPB, STPB, and HCNS in photomicrographs in Figures 12a through 12c, respectively. Such crack formation was not found in any of several STCNS samples checked.

Table 3 summarizes tensile test data, strain hardening

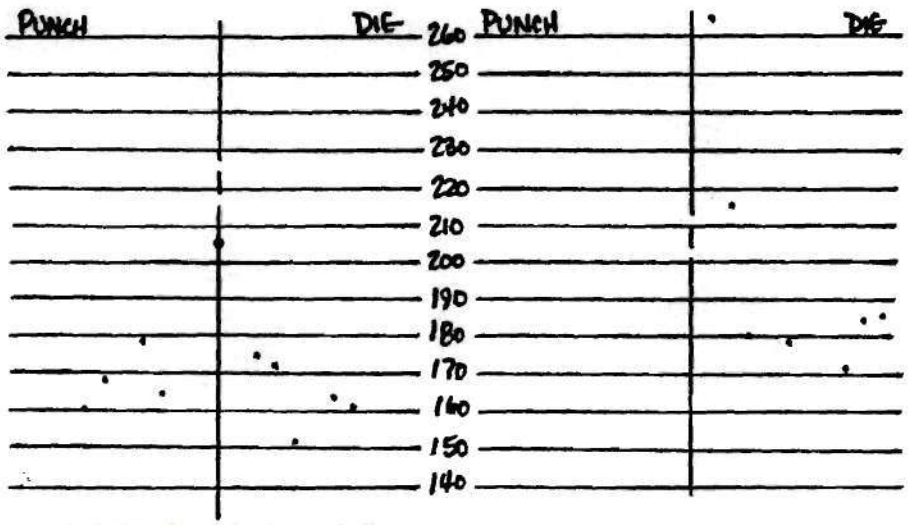

Fig. 10a. HHPB, 3% Die Clear., 25% Punch Pen.

Fig. 10b. HHPB, 3% Die Clear., Post-Slug Sep.

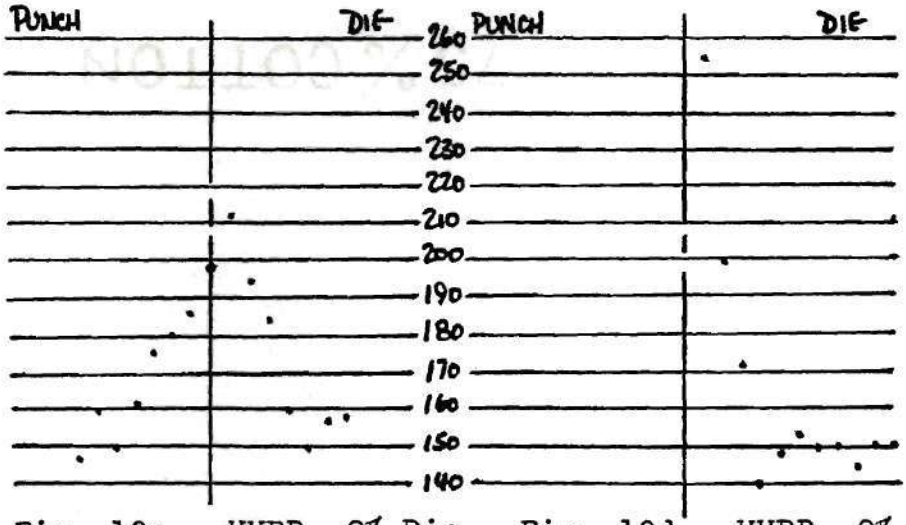

Fig. 10c. HHPB, 9% Die Clear., 22% Punch Pen.

Fig. 10d. HHPB, 9% Die Clear., Post-Slug Sep.

Fig. 10: Microhardness Profiles on Sectioned Stamping Samples with Varying Die Clearance

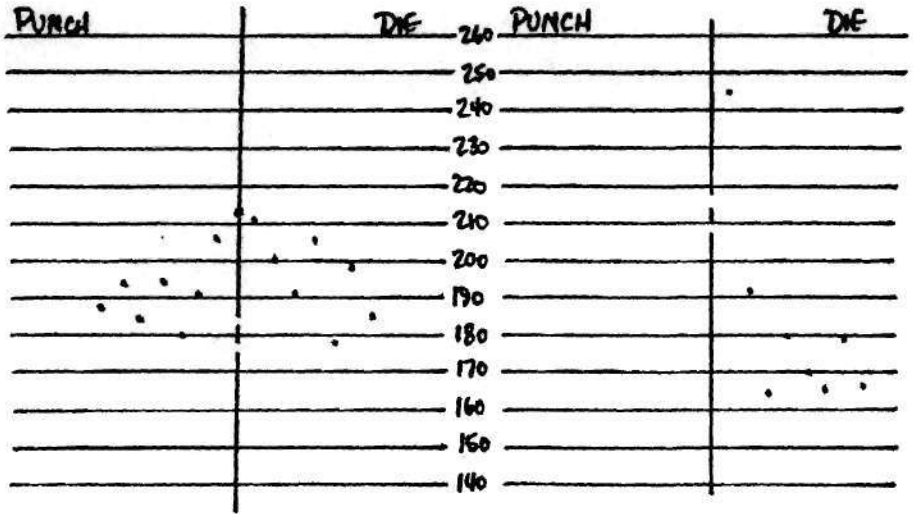

Fig. 10e. HCNS, 3% Die Clear., 23% Punch Pen.

Fig. 10f. HCNS, 3% Die Clear., Post-Slug Sep.

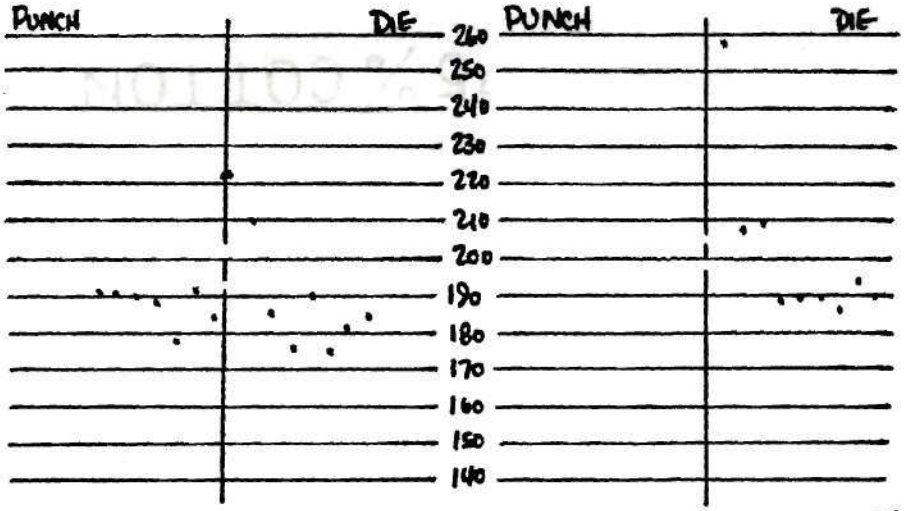

Fig. 10g. HCNS, 9% Die Clear., 19.5% Punch Pen.

Fig. 10h. HCNS, 9% Die Clear., Post-Slug Sep.

Fig. 10, Continued: HCNS

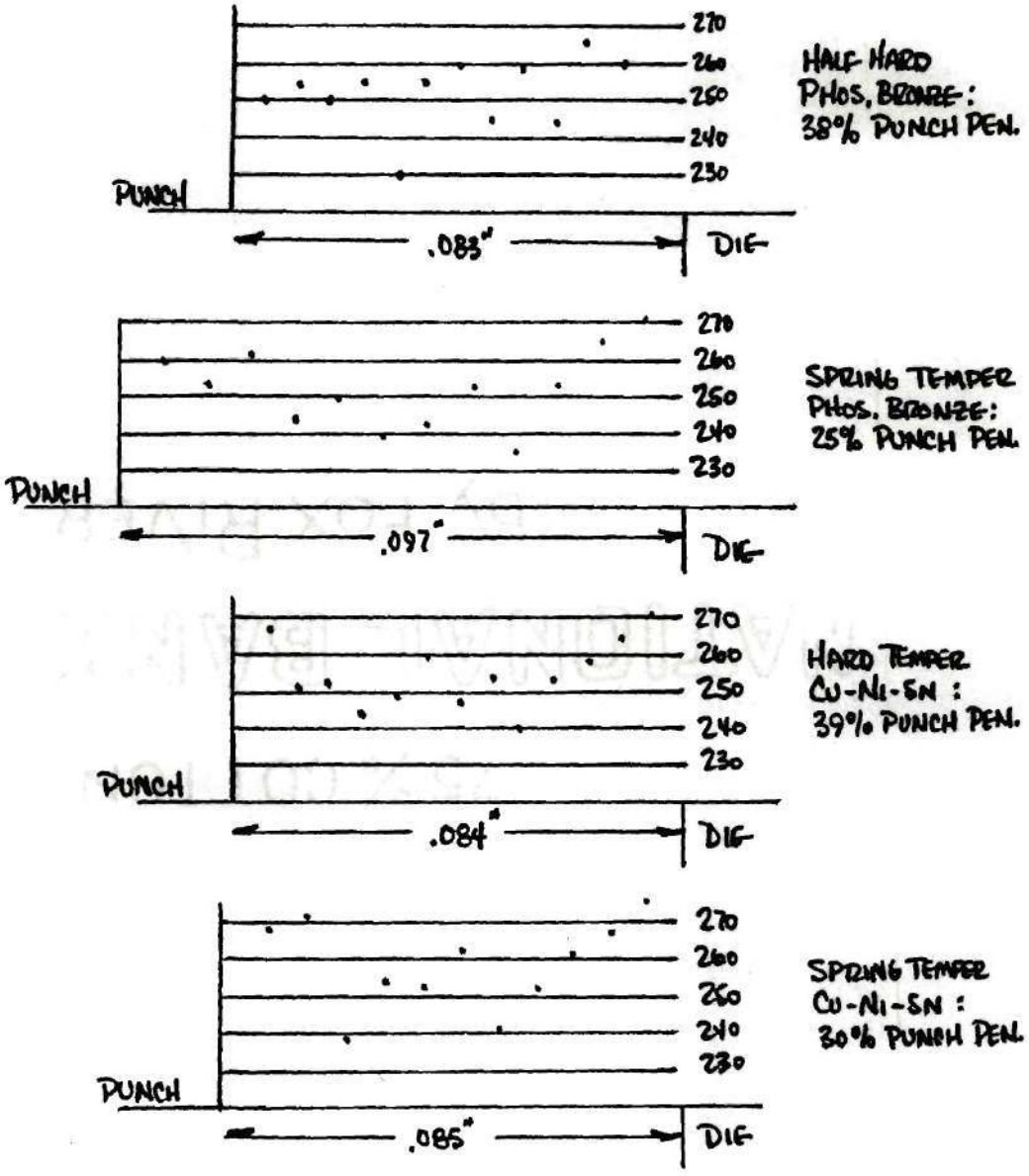

Fig. 11: Microhardness Gradients Along Deformation Lines

Fig. 12a. HHPB Cracking at the Punch Edge (40X) 6% Die Clearance, 40.1% Punch Pen.

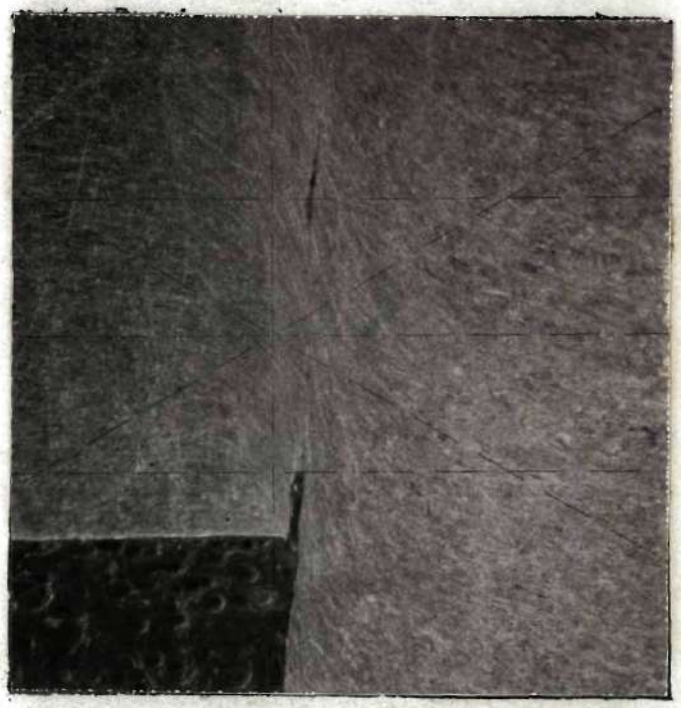

Fig. 12b. STPB Cracking at the Die Edge (100X) 6% Die Clear., 23.2% Punch Pen.

Fig. 12; Crack Formation in the Workpiece at the Punch and Die Edges Initiating Slug Separation

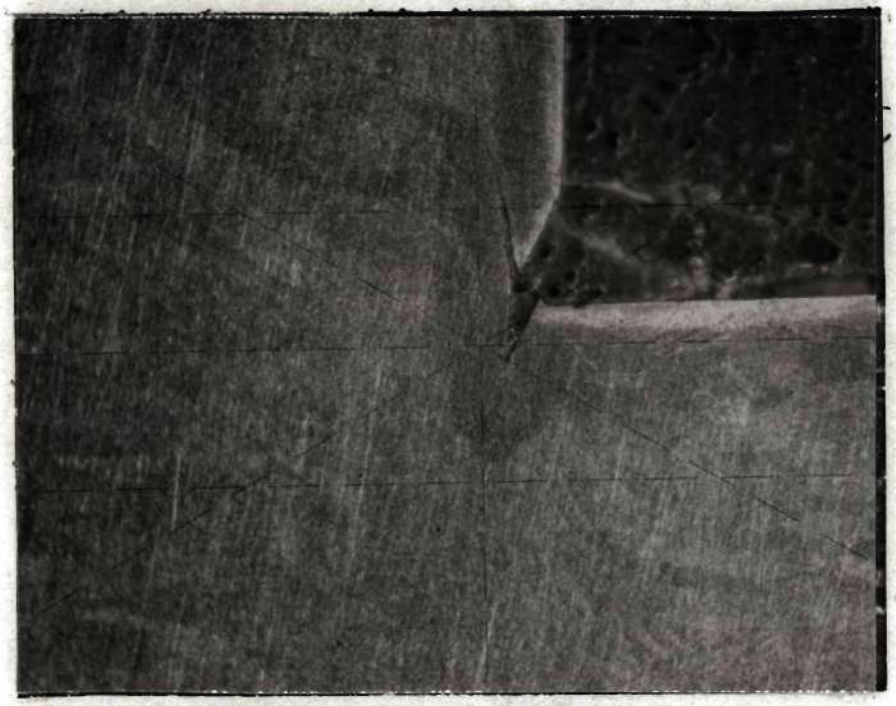

Fig. 12c. HCNS Cracking at the Punch Edge (40X)
6% Die Clearance, 38.1% Punch Pen.

Fig. 12: Crack Formation in the Workpiece at the Punch and Die Edges Initiating Slug Separation

Table 3. Summary of Data from Hardness, Tensile, and Stamping Tests

Material	HHPB	STPB	HCNS	STCNS
0.2% yield strength, ksi	58.5	83.1	78.8	97.3
UTS, ksi	66	87	81	99
$\varepsilon_f = \ln A_o/A_f$	1.4	0.7	1.0	0.8
%RA at failure	75	48	65	54
"Corrected" fracture stress, ksi	161	126	131	136
VHN, $\varepsilon = 0$*	150	190	180	215
Proportionality constant, K*	94	25	39	6
Strain-hardening exponent, n*	.34	.27	.37	0
% penetration at slug separation				
3% die clearance	49		47	
6%	43	26	43	31.5
9%	43		40	
Max. nominal shear stress, ksi				
3% die clearance	37		37	
6%	36	40	37	44
9%	37		37	

*These values are from the least squares fits of VHN vs. true strain data to equations of the form:

$$VHN = K\varepsilon^n + VHN\Big|_{\varepsilon=0}$$

equation constants, and data obtained from the quasistatic stamping tests. In Figure 13, the UTS and zero-strain Vickers hardness numbers of the materials are plotted against the maximum nominal shear stress obtained from the stamping tests with 6% die clearance. In Figure 14, the true strain at failure and the percent reduction in area for all the materials are plotted against the percent penetration at slug separation from the stamping tests with 6% die clearance.

Table 4 gives the results of the tensile strain rate sensitivity tests.

3.2. Discussion of Results: Tensile Tests

The tensile test data in Table 3 show tensile strengths ranging from 66 ksi for HHPB to 99 ksi for STCNS. Available manufacturers published data typically advertise a tensile strength of about 100 ksi for CA 510 in the spring temper, which is 13 ski higher than the results of these tests indicate; the half hard CA 510 tensile strength is well within advertised ranges. The spinodal Cu-Ni-Sn has a markedly higher tensile strength in the spring temper than does the CA 510 (99 ksi versus 87 ksi); the spring temper CA 510 is only slightly stronger then the hard temper spinodal. The logarithmic true strain at failure, a measure of fracture ductility, ranges from 0.7 for STPB to 1.4 for HHPB. In the spring temper, the STCNS shows slightly higher fracture ductility than the STPB. The HHPB exhibited a much higher

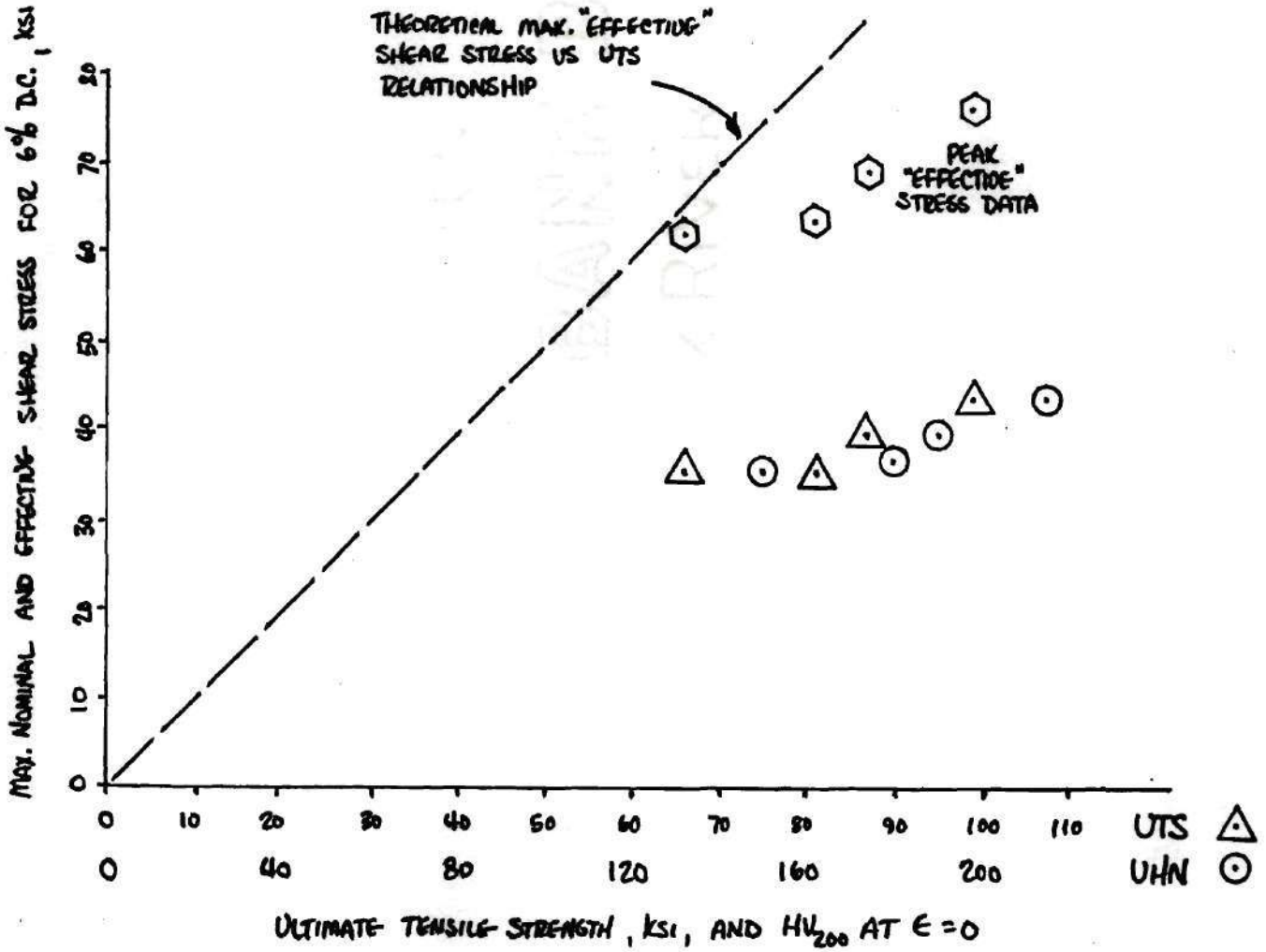

Fig. 13. Stamping Peak Shear Stress Versus Tensile Strength and $VHN_{\epsilon=0}$

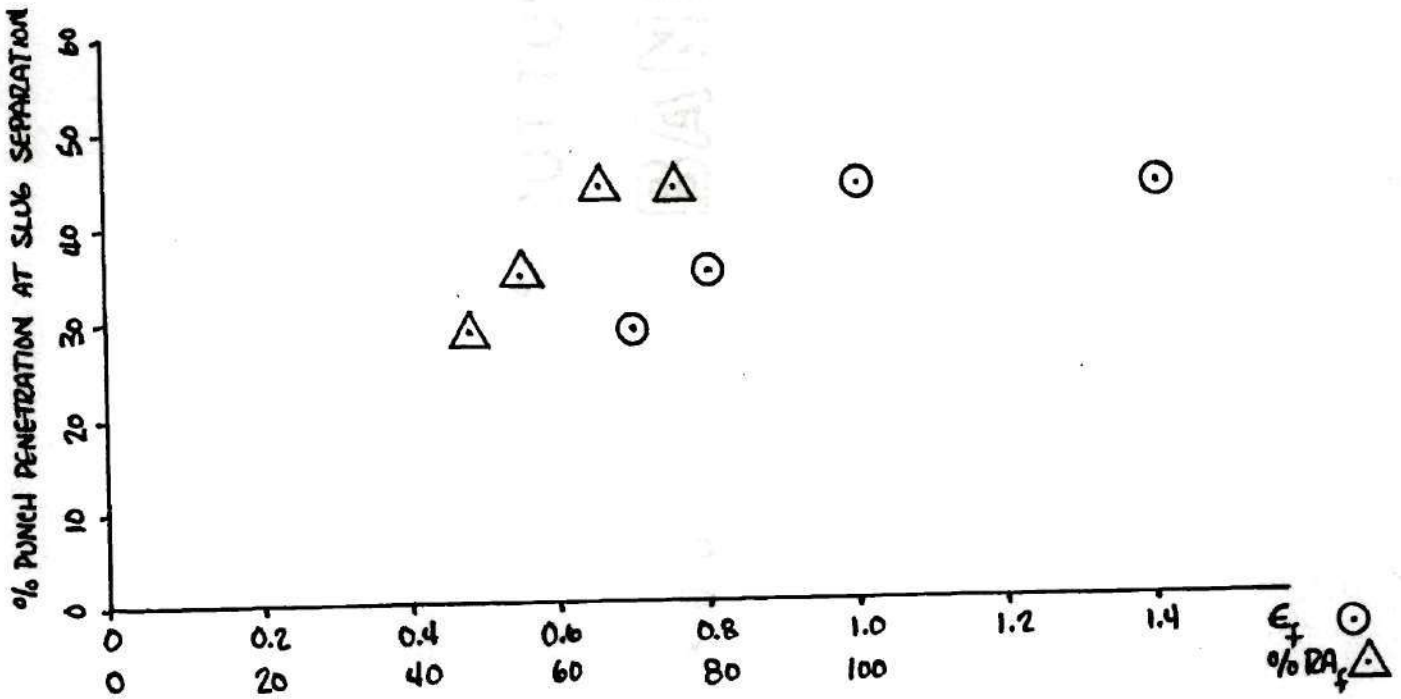

Fig. 141 Percent Punch Penetration at Slug Separation Versus Tensile Ductility Parameters

Table 4. Strain Rate Sensitivity Test Results*

Material	$\dot{\varepsilon}$	$\sigma_{0.2\%Y}$	σ_{UTS}	%RA	ε_f
HHPB	0.004	57.5±0.3	63.6±0.2	72.4±1.3	1.3±0.03
	0.4	57.2	63.2±0.4	75.9±2.3	1.4±0.10
	4.0	57.8	63.5	75.2	1.4
STPB	0.004	80.7±1.4	84.8±0.8	53.2±2.6	0.76±0.06
	0.4	80.2±2.8	88.6±0.3	49.7±6.8	0.69±0.13
	4.0	84.4	89.5	52.7	0.75
HCNS	0.004	76.2±0.8	78.9±0.4	65.5±1.1	1.06±0.03
	0.4	75.8±0.1	81.1±0.5	63.7±0.1	1.01±0
	4.0	79.4	82.1	63.3	1.00
STCNS	0.004	91.4±0.1	96.2±1.0	56.1±0.6	0.83±0.01
	0.4	97.0±1.2	99.0±0.7	53.4±3.0	0.76±0.06
	4.0	97.3	99.7	54.6	0.79

*$\dot{\varepsilon}$~[min^{-1}]; $\sigma_{0.2\%Y}$, σ_{UTS}~[10^3 psi]

corrected true stress at failure than any of the other materials, due to its high strain hardening exponent; it was 25 ksi higher than that of the STPB, 161 ksi versus 126 ksi. In the Cu-Ni-Sn alloy, however, the spring temper showed a slightly higher corrected fracture stress than the hard temper, 136 ksi versus 131 ksi.

In performing these tensile tests, sizeable voids were noticed on the fracture surfaces of tensile specimens of HHPB, HCNS, and STCNS. After sectioning samples of these materials, lamination cracks from the cold-rolling operation were discovered in these materials; these were attributed to improper treatment in the final annealing operation. The voids on the fracture surfaces were lamination cracks opened by the triaxial tensile stress state in the necks of the tensile samples as they strained to failure. As it was not feasible to reorder the materials at that point in the investigation, this defect had to be accepted throughout the study; however it was not considered to have a significant effect on the experimental results. The voids which appeared on the fracture areas as a result of these cold-rolling laminations were approximated as ellipses in measuring the fracture areas; the major and minor axes, a and b, of these elliptical voids were measured and the void areas were calculated as $A_{void} = \pi ab$ and subtracted from the gross fracture area measurements. The resultant net areas were used as the fracture areas, A_f, in all calculations.

Two difficulties were encountered in applying the Bridgman correction factor to obtain a corrected true stress at failure. From a theoretical viewpoint, the Bridgman analysis [22] assumes contractions only in the through-thickness direction of the necking tensile sample, ignoring width-wise strains. While this is a reasonable assumption for tensile samples with a high width, thickness ratio in the gage section, it is expected to give conservative correction factors for samples with large width reductions relative to thickness reductions, as is the case with the samples used in this investigation. A practical difficulty with application of this correction factor is the estimation of the radius of curvature in the neck of the tensile sample. This radius varies across the neck of a given sample and from the top of the sample to the bottom. Thus, at best, a rough estimate of the radius was made, using the 1/64-inch increment radius gages near the lateral center of the sample.

The largest Bridgman correction factors were calculated for HHPB; those for STCNS were slightly lower and the lowest factors were calculated for STPB and HCNS, which had similar correction factors. The application of the correction factor did not, in general, alter the scatter in the true stress at fracture values for any one material.

3.3. Discussion of Results: VHN Versus True Strain Correlations

The relative ductility and strain hardening behavior of these materials are apparent from the plots of micro-hardness versus true plastic tensile strain; also apparent is the inherent scatter in low-load hardness testing. Both the HHPB and the HCNS extend to true strains well over 1.0, indicating considerable ductility at these lower strength tempers. These two materials also showed similar strain-hardening rates which were markedly higher than that of the essentially non-strain-hardening STCNS.

From the experimental procedure used to generate these plots, a lower density of data points was obtained for the higher strain levels on the tensile samples. This is due to the high strain gradients along the tensile sample axes in the necked areas of the samples. The HHPB tensile samples exhibited considerable strain over the entire gage length, so that no data were obtained for this material at true strain levels of less than 0.2.

3.4. Discussion of Results: Stamping Tests

The stamping test data in Table 3 shows the percent penetration at slug separation decreases with increasing die clearance over the range of die clearances tested for both the HHPB and the HCNS, in agreement with accepted stamping technology. The ranges of slug separation penetrations

over this die clearance range is quite small, 43-49% for HHPB and 40-47% for HCNS, so that from a workpiece behavior standpoint, the difference between 3% and 9% die clearance is relatively minor. These percent penetration values each represent an average of two measurements; in no case was the spread in any such pair of measurements significant. Thus, the percent penetration at slug separation was found to be distinct for a given material and die clearance under these test conditions.

The percent penetration at slug separation is analogous to a percent-reduction-in-area-at-failure parameter for the stamping operation. A plot of the percent penetration at slug separation in stamping versus the tensile reduction in area at failure and versus the tensile true strain at failure in Figure 14 show nearly linear relationships. Only the HHPB, which has a very high tensile fracture ductility shows nearly the same percent penetration at slug separation as the less ductile HCNS. This suggests that possibly the relationship may level off for materials with a true tensile failure strain higher than about 1.

The maximum nominal shear stress data from the stamping tests, given in Table 3, show this parameter to be insensitive to die clearance, in agreement with the results of Biegel [17] and Masuda and Jimma [20], and in contrast to the results of Chang [14] and Tilsly and Howard [16].

Maximum nominal shear stress data are plotted against

ultimate tensile strength data and against zero-strain microhardness in Figure 13. The shear strength versus tensile strength data fall close to a straight line drawn through the origin; the effective ultimate stress in shear [24], is given by

$$\sigma_{eff} = \sqrt{3}\tau \qquad (6)$$

where τ is the shear stress, is slightly lower than the ultimate tensile strength. Ideally, these data should fall along a 45° line through the origin (see Appendix 4). Also noteworthy in Figure 13 is the apparent relationship between the VHN at zero plastic strain and the maximum nominal shear strength for these materials. The plots of Figure 13 thus give two material properties, the commonly available ultimate tensile strength and the easily obtainable VHN on the vertical/longitudinal plane at zero plastic strain, which can be related to the maximum nominal shear stress of the workpiece material in stamping.

3.5. Discussion of Results: Hardness Profiles on Stamping Samples

The profiles of Figures 9a through 9l reflect the inherent scatter in low load hardness testing. It would be expected in each case, however, that the extremities of the plots should vary about a mean hardness value corresponding

to the zero strain hardness for these two materials as given in Table 3; i.e. for HHPB the mean VHN should reach $148HV_{200}$ and for HCNS the mean should reach $177HV_{200}$ at the extremities of these profiles. This was not always the case; for HHPB this extreme mean ranges from the high 140's to the high 160's and for the HCNS plots, the mean at the extremities ranges from the mid 170's to the mid 190's. Thus, for any given plot, or row of hardness indentations, the increase in hardness near the center of the deformation zone must be related to the mean hardness at the extremities of the plot. These differences in mean hardness in the undisturbed regions of the different rows or samples are attributed to slight differences in sample preparation, such as differences in surface polish qualities.

Table 5 summarizes the plots of Figure 9 and Figure 10. The deformation zone widths and maximum VHN values given for HHPB and HCNS at 6% die clearance and all punch penetrations, are averages for five rows of the hardness test matrices on those samples. All other data in Table 5 are based on a single row of hardness tests (see Table 2). Deformation zone widths were determined by establishing the distance from the deformation line at which the hardness values were down to the apparent mean hardness value for that row.

Figures 9a through 9d show pronounced increases in the peak hardness at the centerline of the deformation zone

Table 5. Summary of Data from Hardness Profiles on Stamping Samples

Material	D.C.	Pen	Def. Width	Max VHN	Max* ε
HHPB	3%	25%	.042	221	0.5
		Sep	.038	266	2.0>1.4
	6%	11%	.046	182	0.06
		22	.052	197	0.15
		33	.052	228	0.66
		Sep	.052	243	1.07
	9%	22%	.056	212	0.31
		Sep	.052	255	1.39
STPB	6%	13%	0	215	0.52
		Sep	.024	234	5.7>0.7
HCNS	3%	23%	.028	214	0.81
		Sep	.038	246	4.6>1.1
	6%	11%	0	200	0.24
		22%	.018	208	0.53
		32%	.0	235	2.9>1.1
		Sep	.0	230	2.2>1.1
	9%	19.5%	.010	222	1.4>1.1
		Sep	.026	258	7.1>1.1
STCNS	6%	17%	.010	277	∞>0.8
		Sep	.019	236	∞>0.8

*These values obtained by inserting the max VHN value into Equation 5. Inequalities here indicate the predicted strain exceeds the average tensile fracture strain.

as the punch penetrates the HHPB workpiece with 6% die clearance. As summarized in Table 5, this peak hardness increase corresponds to a peak true strain increase from 0.06 at 11% punch penetration to 0.66 at 33% punch penetration. After slug separation the HHPB material at a distance of 0.0005 in from the fracture surface has been strained to a true strain of 1.07. The hardness increase in the deformation zone of HCNS workpiece samples with increasing punch penetration is also apparent in Figures 9e-9h, as summarized in Table 5. However at 32% punch penetration and in the separated slug, hardness values exceeded the hardness at which failure is predicted by the plot in Figure 8c. These peak hardness values, when related to the mean hardness values in their respective rows, are still above the predicted failure hardnesses. This may be attributed to the constraints imposed on the workpiece in stamping which differ from those imposed in the neck of a tensile sample or these high hardness values may be attributed to hardness test scatter. At 3% and 9% die clearances, HHPB and HCNS have the same deformation zone width at slug separation. At 3% die clearance, the deformation extends into the material approximately 0.20 inch, or about 15% of the material thickness, from the sheared edge. At 9% die clearance this deformation extends into the material about 0.26 inch or about 20% of the material thickness. At 6% die clearance, however, the deformation zone is nearly twice as wide in the HHPB as in the HCNS. The

HCNS slug separated at 6% die clearance showed deformation extending only about 0.012 inch in from the shear surface or about 10% of the material thickness. Three conclusions regarding deformation zone widths may be drawn from the summary in Table 5. First, it appears this width is related to die clearance: the HHPB shows an increased deformation zone width from 0.038 to 0.052 inch at slug separation with increased die clearance from 3% to 9%, as does the HCNS. Second, the HHPB exhibits a constant deformation zone width with increased punch penetration while the HCNS exhibits an increasing deformation zone width with increased punch penetration. These relationships hold true at all die clearances.

The third conclusion is that the tendency of the workpiece material to spread the stamping shear deformation over a wide deformation zone is apparently unrelated to the work hardening exponent of the material, given in Table 3. The HHPB and HCNS materials have similar work hardening exponents yet develop shear deformation zones quite differently. Although at 6% die clearance the STPB shows a much more narrow deformation zone than the HHPB which work hardens more, the STCNS, which work hardens very little, has the same deformation zone width at slug separation as the HCNS which work hardens much more than the STCNS.

Figures 11a through 11d indicate the hardness gradients along the deformation lines assume a "W" shape with peak hardness near the die edge and slightly lower hardness near

the punch edge as the punch approaches the separation penetration. A slight increase in hardness near the center of this line is also indicated. Only the HHPB sample failed to show these trends. The concentrated work hardening indicated at the punch and die edges is in agreement with the conclusions of PERA [15].

This evidence of maximum work hardening in the areas of the deformation zone nearest the punch and die corners is further substantiated in Figures 12a through 12c. Here, crack initiation is seen at the punch corner at 40% punch penetration with 6% die clearance on the HHPB sample, Figure 12a, and at 38% penetration with the same clearance on the HCNS sample, Figure 12b. By contrast, the crack formation on the STPB sample, Figure 12c, is at the die corner, with no apparent cracking at the punch corner of that sample; here the punch penetration is 23%. A sample of STCNS showing crack formation was not obtained among ten samples penetrated to near slug separation.

3.6. Discussion of Results: Strain Rate Sensitivity Tests

Two trends are apparent from the strain rate sensitivity data given in Table 4:

(a) All materials, except the HHPB, show slightly increased σ_{UTS} with increases strain rate over this range.

(b) The two spring temper materials show a dip in

ductility parameters (%RA and ε_f) at the middle strain rate, 0.007 sec^{-1}. However, both materials show a large spread in %RA and ε_f between the two samples, so that a conclusion cannot be drawn that tensile fracture ductility is strain rate dependent within this range of strain rates. The two lower temper materials do not reflect a ductility sensitivity to strain rate in this range.

The stamping tests were performed at a strain rate which varied somewhat, but approximated 0.007 sec^{-1} in shear. It may be concluded from these strain-rate sensitivity data that there is no change in the ductility of either the phosphor bronze or the Cu-Ni-Sn materials over a range of strain rates of three orders of magnitude covering the rate at which these stamping tests were performed. A typical strain rate for a production stamping operation might be of the order of 200 sec^{-1} or higher in shear. A test facility was not available for comparing ductility parameters for these alloys at strain rates of that order, so no conclusion can be drawn regarding the relative behavior of these alloys at production speeds.

CHAPTER IV

CONCLUSIONS AND RECOMMENDATIONS

Correlations were observed between ductility and strength properties of these copper alloy strip materials, as obtained from hardness and tensile tests, and ductility and strength performance characteristics in static shearing tests. Either the Vickers hardness number, measured as described here, or the ultimate tensile strength gives an indication of the ultimate nominal shear stress to be expected. The percent reduction in area, or true strain at fracture in tensile tests is related to the percent punch penetration at slug separation. Additional tests could reinforce these trends by extending the range of mechanical property values for these or similar copper alloys, investigating other tempers or compositions of these alloys. This would facilitate establishment of press load requirements and die clearance determination.

The peak load on the stamping punch was found to be insensitive to die clearance. The percent punch penetration at slug separation was found to be repeatable and distinct for a given workpiece material and die clearance, but was found to decrease over a fairly narrow range for increasing die clearances from 3% to 9% for the lower temper materials.

The microhardness surveys on sectioned stamping samples showed the shear deformation zone width increases with die clearance, but varies independent of the strain-hardening exponent of the material. In the Cu-Ni-Sn alloy the deformation zone widens with punch penetration but is constant with increased punch penetration in the CA510. As expected, the peak hardness in the deformation zone was found to increase with increasing punch penetration. Hardness surveys down deformation lines of sectioned stamping samples revealed maximum work hardening at the punch and die edges. Crack formation initiating slug separation was found to take place at the punch and die edges.

Microhardness test data from tensile test samples, when fitted to the generalized Holloman stress-strain relationship, showed a small drop in the strain-hardening exponent for the CA 510 between cold-rolling reductions of 20%, corresponding to the half hard temper, and 60%, corresponding to the spring temper. By contrast, the Cu-4Ni-4Sn alloy in the hard temper (37-1/2% cold-rolling reduction) had a strain-hardening exponent similar to the half hard CA 510, but in the spring temper the Cu-4Ni-4Sn had a strain-hardening exponent of zero, implying essentially no strain hardening capacity in this alloy in the higher temper. The spring temper CA 510 had a lower ultimate tensile strength than expected; it was only slightly higher than that of the hard temper Cu-Ni-Sn and was well below that of the spring temper

Cu-Ni-Sn. The fracture ductility in both alloys decreased in the higher tempers; in the spring temper the Cu-Ni-Sn showed a higher fracture ductility than the CA 510.

In order to extend these conclusions to production stamping, a press with suitable instrumentation for monitoring dynamic stamping loads would be necessary to check these results at speeds several orders of magnitude higher. However, neither the phosphor bronze nor the Cu-Ni-Sn alloy showed any significant strain rate sensitivity over three low strain rate orders of magnitude.

APPENDICES

APPENDIX 1

PRELIMINARY INVESTIGATIONS AND DETERMINATIONS

Partially penetrated stamping specimens of 0.020 in thick spring temper CA 510 phosphor bronze were metallographically sectioned for observation by light microscopy. The punch and die used were designed as shown in Figure A1-1, but were extremely dull when used for this exercise. Measurements of the width of the zone of observable grain structure deformation at 100X at different punch penetrations showed a linearly increasing deformation zone width with increased punch penetration, Figure A1-2. A photomicrograph of a sample shear deformation zone at 100X is shown in Figure A1-3.

Three conclusions were drawn from this exercise:

(a) The deformation zone width for spring temper CA 510 could be as wide as a third of the workpiece material thickness.

(b) With a dull punch and die, which condition would delay slug separation, the punch penetration at slug separation reached a maximum of 75% for the spring temper CA 510.

(c) The deformation zone apparently widens with increased punch penetration; this conclusion was not found to apply when a sharp punch and die were used in subsequent testing.

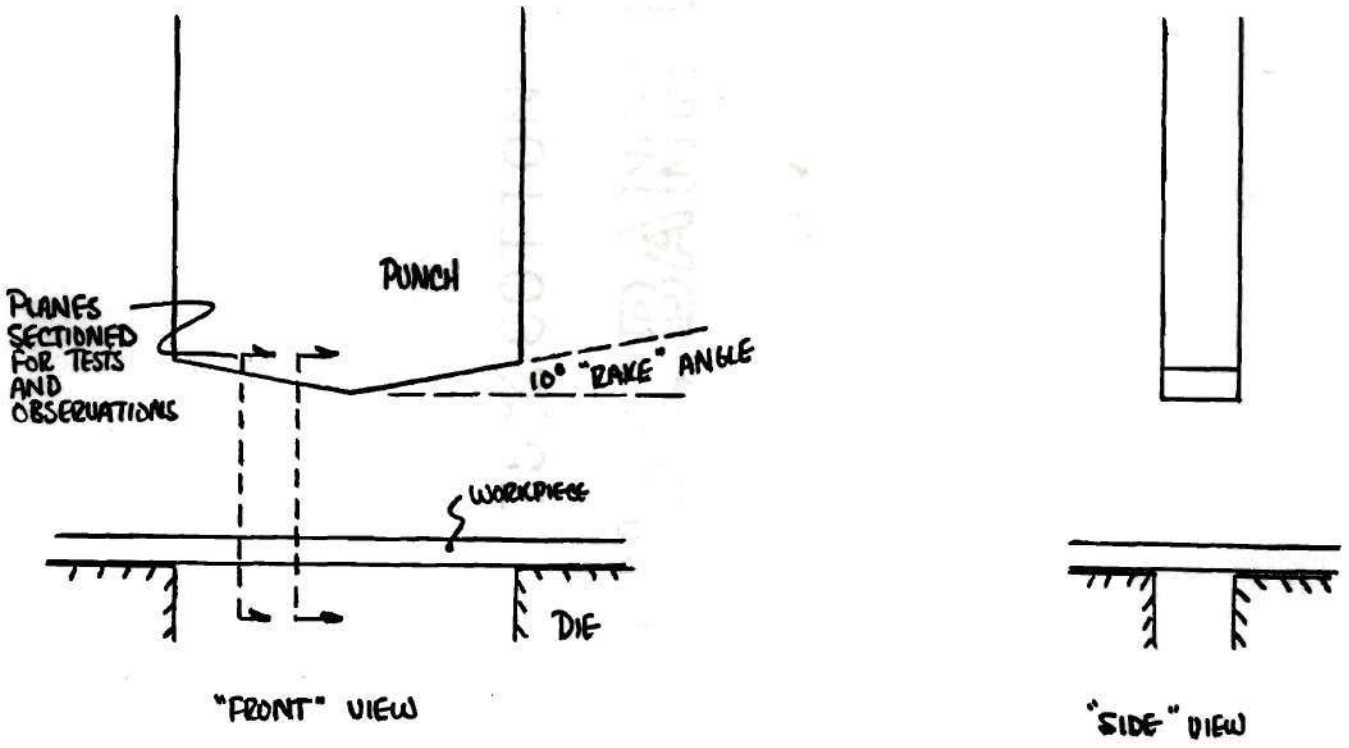

Fig. A1-1. Punch and Die Design Used for Preliminary Tests

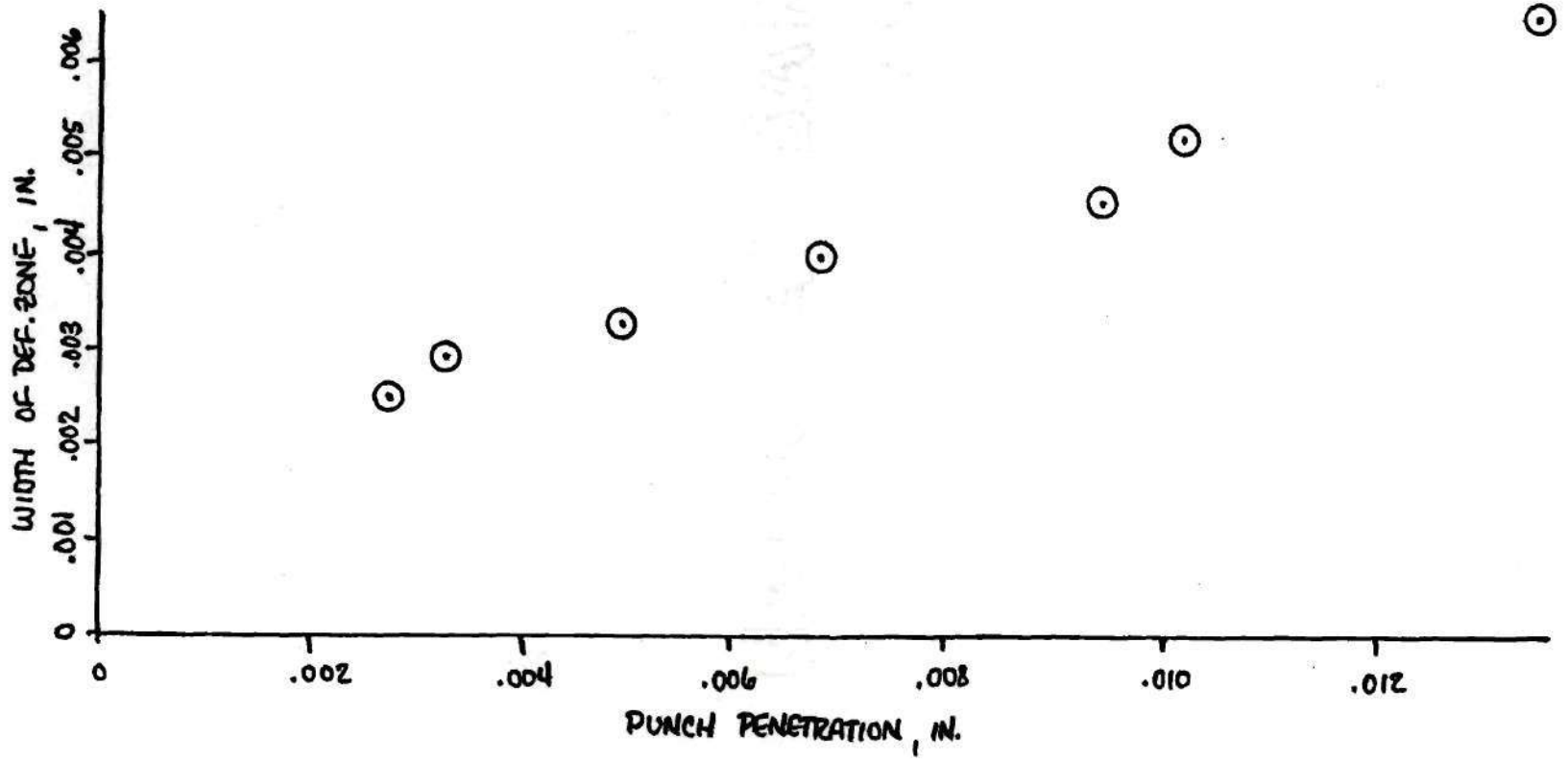

Fig. A1-2. Deformation Zone Width Versus Punch Penetration

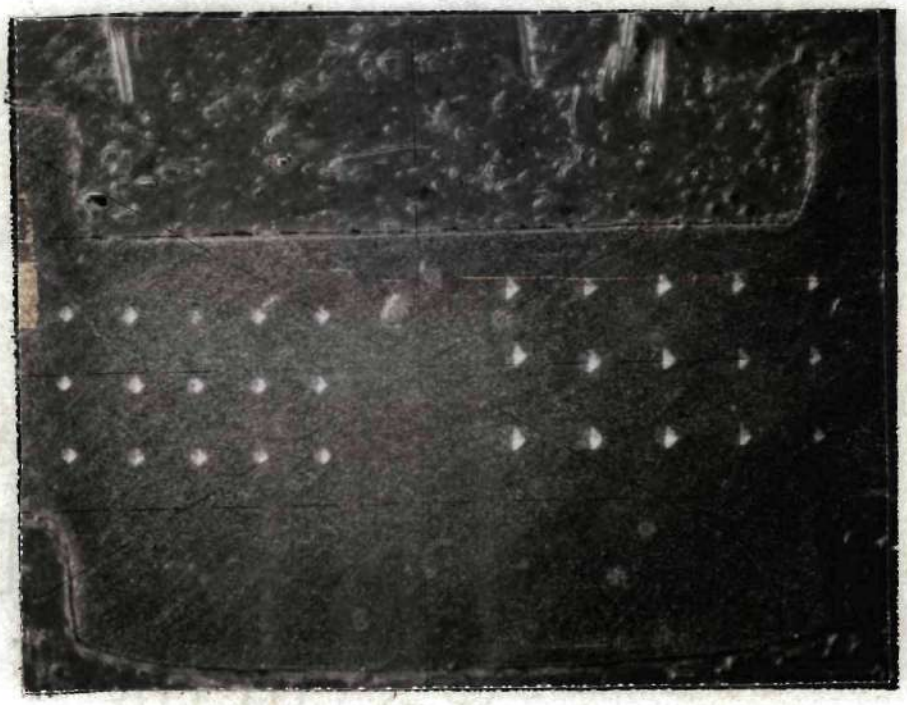

Fig. A1-3. STPB Shear Deformation, 0.020 In. Thick, 25% Punch Penetration (100X)

Next, microhardness tests were made in a 3X9 matrix array on each of the two exposed deformation zones of a metallographically prepared sample of 0.020 inch thick spring temper CA 510 penetrated about 37% with the punch and die described above. For these tests, the Vickers diamond pyramid indenter was used with a 50-gm load for one array and a 100-gm load for the other. The results are shown in Figure A1-4. The following conclusions were drawn from this exercise:

(a) Discrete patterns of work hardening under these conditions can be detected by such grids of microhardness tests.

(b) Hardness data from the row extremities of the arrays are useful for defining the base hardness of the undeformed material near the deformation zone for the particular sample being tested.

(c) The Vickers indentations made with the 50-gm load were not noticeably harder to measure than the larger indentations made with the 100-gm load; both gave similar work hardening profiles although those made with the 100-gm load had necessarily larger spacing.

Trial microhardness tests were also done using the Knoop indenter at loads of 25 and 50 gm on half hard CA 510 and at a 50-gm load on spring temper CA 510. Although the long axis of the indentation was easily measured at both loads and on both tempers, the test was found to be quite

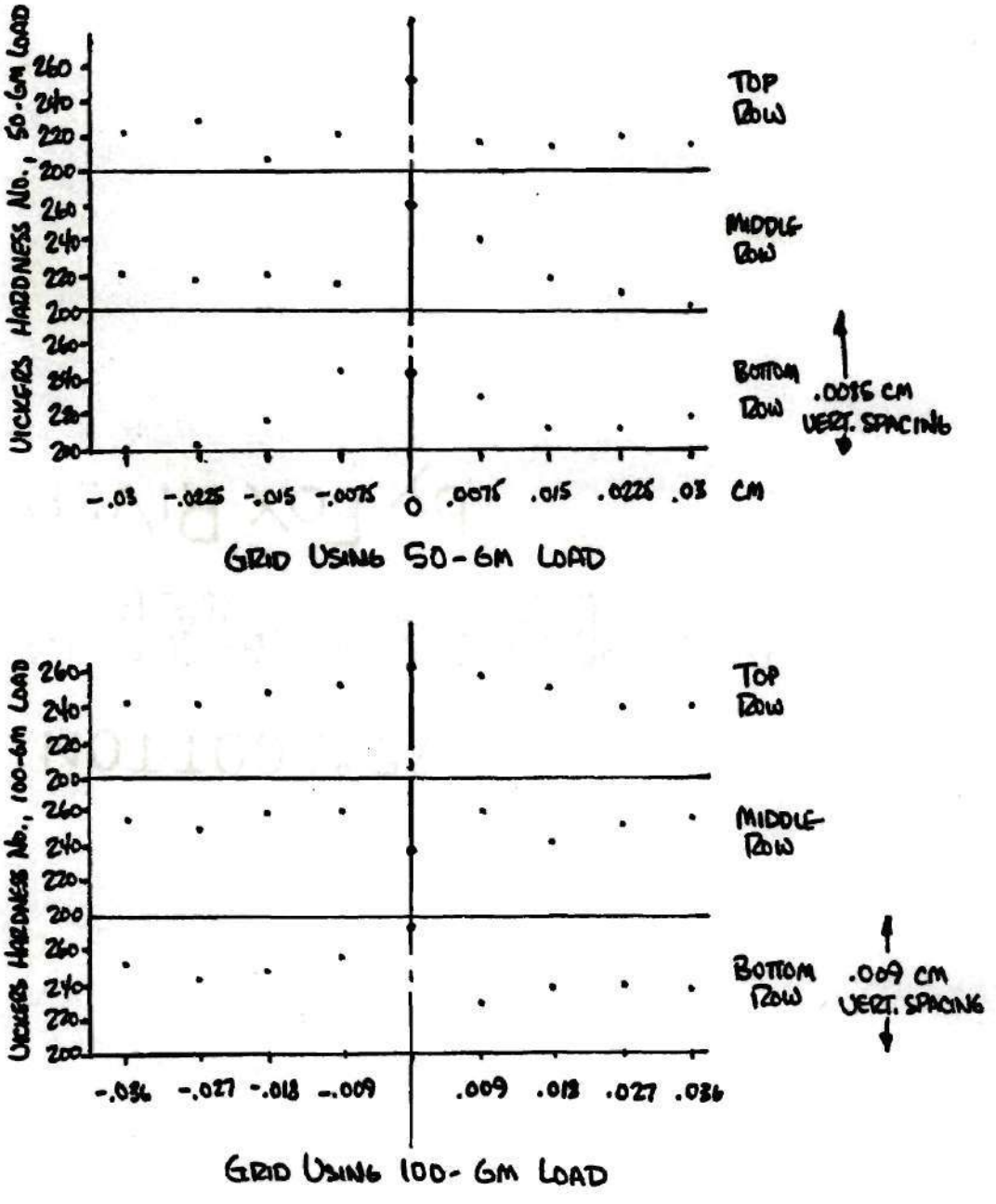

Fig. A1-4. Microhardness Profiles on STPB Shear Zones

sensitive to directional strength characteristics of the material: tests on the half hard temper in the plane of the strip showed an average of $202HK_{50}$ with the long axis of the indenter oriented with the strip rolling direction and $181HK_{50}$ with the indenter turned 90°. The corresponding Knoop hardness values for spring temper were $232HK_{50}$ and $214HK_{50}$, respectively. This orientation sensitivity made the Knoop test unsuitable for the present investigation since the complex strain patterns expected on the stamping samples would give unpredictable strength directionality.

The Vickers indenter was chosen instead for its relative insensitivity to the planar anisotropy of the test sample. A test load of 200 gm was chosen to overcome any grain size or other highly localized effects and help improve measurement repeatability.

Measurements were taken of the final cross-sectional areas of extra hard temper phosphor bronze tensile test specimens pulled to failure; the specimen thickness was 0.020 inch. Measurements were taken of both halves of each specimen to assess the accuracy and repeatability of the measurements. On three specimens measured, area measurements differed by 4.8%, 3.5%, and 2.1% from one half of a specimen to the other. It was concluded that fracture area measurements performed as these were would be reliable to within 5 percent accuracy.

Based in part on these preliminary exercises the

following judgements were made. The deepest punch penetration to be expected on any material before slug separation was conservatively estimated at 80 percent. In order to perform microhardness surveys arranged as shown in Figures 6a and 6b on samples at four evenly spaced increments of punch penetration from zero to and including slug separation, the height of the deformation zone could be a minimum of 20 percent of material thickness and must be nine times the maximum anticipated spacing requirements for the hardness indentations. The half hard CA 510 was assumed to have the lowest zero-strain hardness; preliminary tests on available HHPB samples suggested a zero plastic strain hardness of about $150HV_{200}$ in the vertical/longitudinal plane of the strip. Using a minimum center to center spacing between indentations of 3.4 times the indentation diagonal (a discussion of this spacing is given in Appendix 2), the requisite material thickness was suggested to be 0.24 inch by the following relationship given by McClintock and Argon [26] for the diagonal of the Vickers indentation:

$$VHN = 1.854\ P/d^2 \qquad \text{(A1-1)}$$

where P is the hardness test load and d is the average of the two indentation diagonals. Since this requisite sample thickness estimate had been arrived at by a series of grossly conservative estimates, the material thickness for the

experiment was selected at 0.125 inch. The lengths of the hardness survey matrix rows were chosen based on the assumptions that the deformation zone width might be a third of material thickness, about 0.040 inch or more; a row length of .240 inch with 35 evenly spaced indentations was chosen, again based on an assumed minimum hardness of $150HV_{200}$, to give sufficient hardness data from the row extremities to establish the hardness of the undisturbed material for that row.

Thus, standard 5X35 matrices of hardness tests were made with the Vickers indenter and a 200-gm load, for the initial series of tests on 0.125 inch thick HHPB and HCNS with 6% die clearance. Based on the results of this first series of tests in the experiment, it was concluded, in concurrence with PERA [15], that a single row of hardness tests would yield sufficient information about work-hardening levels and deformation zone widths for subsequent tests in the experiment. 1X15 indentation matrices were chosen for subsequent tests on STPB and STCNS at 6% die clearance and on HHPB and HCNS at 3% and 9% die clearance.

APPENDIX 2

HARDNESS INDENTATION SPACING

ASTM Standard E384-73, "Standard Method of Test for Microhardness of Materials," essentially recommends a minimum spacing between adjacent hardness indentations such that there is no overlapping of the deformed areas of the indentations.

O'Neil [26] recommends a center-to-center spacing between adjacent hardness indentations of 3 times the indentation diagonal, d, and a spacing from indentation center to any sample edge of 2.5d. Argon and McClintock [26], however, state that the linear dimensions of the deformed area around the Vickers indentation are 3.4d, which suggests a center-to-center spacing of 3.4d.

This last multiple, 3.4, was used for preliminary calculations and laying out hardness indentation matrices, however, in the experiment, the minimum actual center-to-center spacing between adjacent hardness indentations was over 3.6 times the diagonal of either indentation in the worst case, and in no case was an indentation closer than 3 times its diagonal to any edge of the test specimen.

APPENDIX 3

SAMPLE CALCULATIONS

The pages that follow include samples of data taken and written explanations of the calculations made to apply the Bridgman Correction Factor to the true tensile stress at failure data and to obtain the VHN Versus True Strain correlations. The procedures for these steps in the experiment are given in some detail in Section 2.4.

The reader should be able to follow the experimental procedure given in Chapter II for an understanding of other calculations made in the course of this experiment.

Sample Calculations for Application of the Bridgman Correction Factor to Tensile Fracture Stress Data

For tensile sample No. 1 (of HHPB), the mean thickness of the fracture surface was estimated to be 0.0555 inch. Thus, "a" in Equation (4) is estimated to be 0.02775 inch, or half the mean thickness. For this sample, radius gages of 3/64 inch and 1/16 inch radii most closely fit the contours of the two sides of the sample, so "R" in Equation (4) was estimated to be the average of these two radii, or 0.0547 inch. The ratio "a/R" in Equation (4) is 0.02775/0.0547, or 0.5073. Inserting these values into Equation 4, the Bridgman Correction Factor is calculated to be 1/1.153.

Table A3-1. Tensile Test Results

Sample No.	$\sigma_{0.2\%y}$*	UTS*	σ_f*	ε_f
01	58.46	65.54	192.21	1.43
02	57.45	65.65	201.32	1.46
03	59.69	65.54	166.67	1.28
HHPB AVE	58.53	65.58	186.73	1.39
04	77.29	85.80	120.75	0.53
05	86.16	88.36	169.77	0.85
06	85.85	87.11	116.48	0.61
STPB AVE	83.10	87.09	135.67	0.66
07	80.82	82.08	109.91	0.97
08	79.37	80.95	140.50	1.05
09	76.27	81.01	179.84	1.16
HCNS AVE	78.82	81.35	143.42	1.06
10	97.97	100.68	155.90	0.79
11	94.92	97.63	166.53	0.89
12	98.98	99.32	142.57	0.66
STCNS AVE	97.29	99.21	155.00	0.78

*ksi

The true fracture stress for this sample was calculated to be 192,210 psi by dividing the fracture load by the area of the fracture surface on this tensile sample. To account for the effect of the biaxial stress state in the necking tensile sample as described by Bridgman, the correction factor was multiplied by this true fracture stress to get (192,210 psi)(1/1.153) = 168,000 psi as the equivalent uniaxial tensile stress.

A Bridgman Correction Factor was calculated in this way for each tensile sample and applied to the calculated true fracture stress for that sample. Both the uncorrected and the corrected true fracture stresses from the three tensile samples of each material were averaged together. These results are given on the following page.

Sample Calculations for the Determination of the VHN Versus True Strain Relationships

A typical plot of tensile sample width versus distance from a preselected reference point on the fracture surface, as described on pages 20-21, follows. When this tensile sample was mounted and the first microhardness indentation was made at a distance of 0.13 mm from the fracture surface along the sample axis, the distance from the reference point to the first indentation, measured parallel to the sample axis, was -0.0196 inch. Since each successive hardness indentation was made at 0.18 mm, or 0.007 inch from the

"Corrected" Fracture Stress Data

Sample	σ_f, psi	Bridgman Corr. factor	Corrected σ_f, psi
1	192,210	1.153^{-1}	168,000
2	201,320	1.144^{-1}	176,000
3	166,670	1.197^{-1}	139,000
HHPB AVE	186,730		161,000
4	120,750	1.099^{-1}	110,000
5	169,770	1.063^{-1}	160,000
6	116,480	1.085^{-1}	107,000
STPB AVE	135,670		126,000
7	109,910	1.096^{-1}	100,000
8	140,500	1.079^{-1}	130,000
9	179,840	1.109^{-1}	162,000
HCNS AVE	143,420		131,000
10	155,900	1.161^{-1}	134,000
11	166,530	1.109^{-1}	150,000
12	142,570	1.158^{-1}	123,000
STCNS AVE	155,000		136,000

previous indentation, each indentation could be located on the plot of width versus distance from the reference point. For instance, the fifth indentation was four times 0.007 inch from the first, or -0.0196 inch + 4X0.007 inch = 0.0084 inch from the reference point. At this point on the width versus distance plot, the width is 0.1595 inch, which was entered in the table of data for sample no. 1 included here. The thickness at the fifth hardness indentation on this sample was measured on the sample as 0.0659 inch and recorded in the same table of data. The tensile sample width and thickness at the fifth microhardness indentation are now known, so that the sample cross-sectional area at the indentation can be calculated. This area was then divided into the original cross-sectional area of the tensile sample and the natural log of this ratio gives the true tensile plastic strain at the fifth hardness indentation. The cross-sectional area is thus A = (0.0659 inch)(0.1595 inch) = 0.0105 in^2. The original cross-sectional area of this tensile sample was measured to be 0.0325 in^2, so ε = ln (0.0325/0.0105) = 1.13. This datum point ($246HV_{200}$, 1.13) is encircled in Figure 8a, page 36.

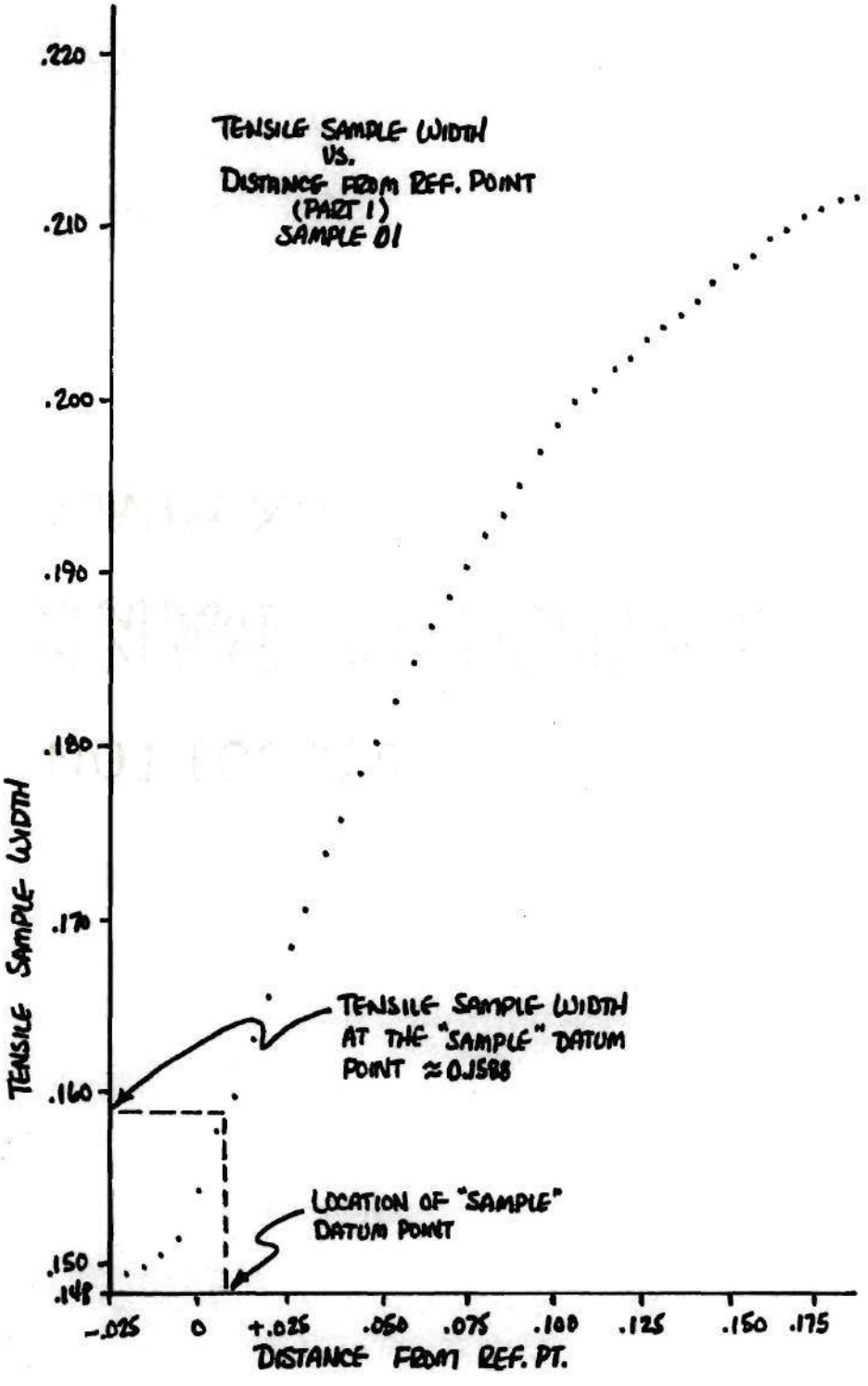
TENSILE SAMPLE WIDTH
VS.
DISTANCE FROM REF. POINT
(PART 1)
SAMPLE 01
.220
.210
.200
.190
.180
.170
.160
.150
.148
TENSILE SAMPLE WIDTH
TENSILE SAMPLE WIDTH AT THE "SAMPLE" DATUM POINT ≈ 0.1588
LOCATION OF "SAMPLE" DATUM POINT
-.025
0
+.025
.050
.075
.100
.125
.150
.175
DISTANCE FROM REF. PT.

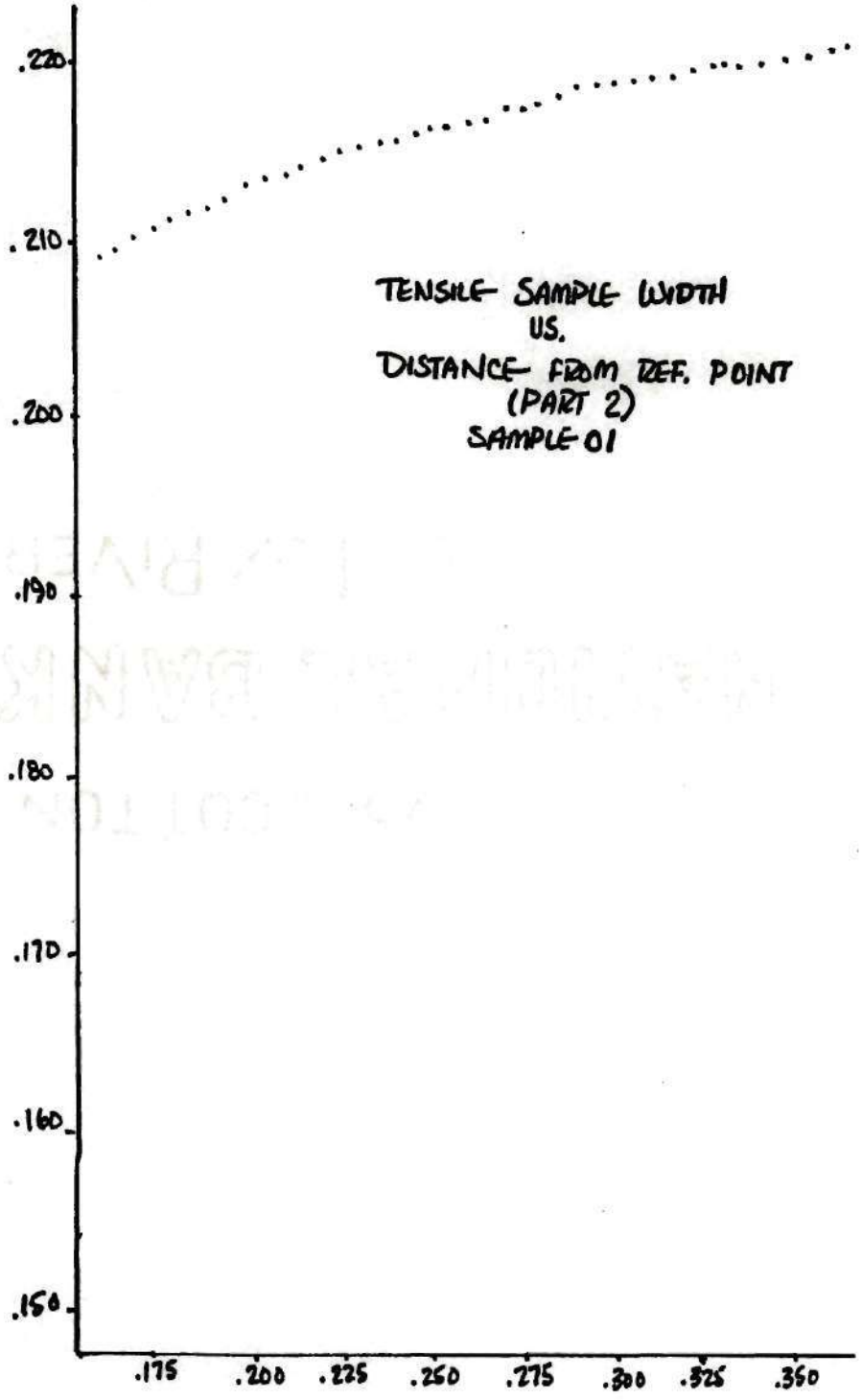
.220
.210
.200
.190
.180
.170
.160
.150
.175
.200
.225
.250
.275
.300
.325
.350
TENSILE SAMPLE WIDTH
US.
DISTANCE FROM REF. POINT
(PART 2)
SAMPLE 01

Tensile Sample 1: HHPB; VHN vs. ε Data

No.	VHN	t	Dist.	w	A	ln A_o/A
1.	256	.0496	-.0196	.1492	.0074	1.48
	268	.0525	-.0125	.1500	.0079	1.42
	270	.0563	-.0054	.1511	.0085	1.34
	269	.0607	.0016	.1554	.0094	1.24
5.	246	.0659	.0084	.1595	.0105	1.13*
	252	.0708	.0158	.1631	.0116	1.03
	234	.0760	.0229	.1673	.0127	.94
	238	.0798	.0300	.1704	.0136	.87
	238	.0835	.0371	.1743	.0146	.803
10.	219	.0965	.0725	.1896	.0183	.575
15.	210	.0982	.0796	.1922	.0189	.543
	228	.0992	.0866	.194	.0192	.524
	229	.1004	.0937	.1966	.0197	.499
	224	.1013	.1008	.1985	.0201	.480
	212	.1020	.1079	.2002	.0204	.465
20.	214	.1030	.1150	.2016	.0208	.448
	219	.1035	.1221	.2029	.0210	.437
	206	.1043	.1292	.2043	.0213	.422
	222	.1052	.1362	.2054	.0216	.408
	214	.1052	.1433	.2068	.0218	.401
25.	224	.1057	.1504	-.2076	.0219	.393
26.	208	.1063	.5175	.2090	.0222	.380
	222	.1068	.1646	.2097	.0224	.372
	224	.1069	.1717	.2107	.0225	.367
	205	.1073	.1787	.2114	.0227	.360
30.	226	.1074	.1858	.212	.0228	.356
	211	.1077	.1929	.2126	.0229	.350
	212	.1081	.2000	.2133	.0231	.343
	198	.1084	.2071	.2138	.0232	.338
	204	.1088	.2142	.2143	.0233	.332
35.	218	.1088	.2212	.2148	.0234	.330
	215	.1091	.2283	.2153	.0235	.325
	216	.1094	.2354	.2156	.0236	.321
	225	.1096	.2425	.2161	.0237	.316
	206	.1098	.2496	.2166	.0238	.312

*Datum point in sample calculation

No.	VHN	t	Dist.	w	A	ln A_o/A
40.	215	.1096	.2567	.2169	.0238	.313
	225	.1100	.2637	.2172	.0239	.308
	222	.1099	.2708	.2175	.0239	.307
	216	.1102	.2779	.2179	.0240	.303
	205	.1101	.2845	.2182	.0240	.302
45.	205	.1105	.2921	.2186	.0242	.297
	219	.1106	.2992	.2189	.0242	.294
	207	.1107	.3062	.2191	.0242	.293
	210	.1109	.3133	.2193	.0243	.29
	212	.1111	.3204	.2196	.0244	.287
50.	208	.1112	.3275	.2199	.0244	.284

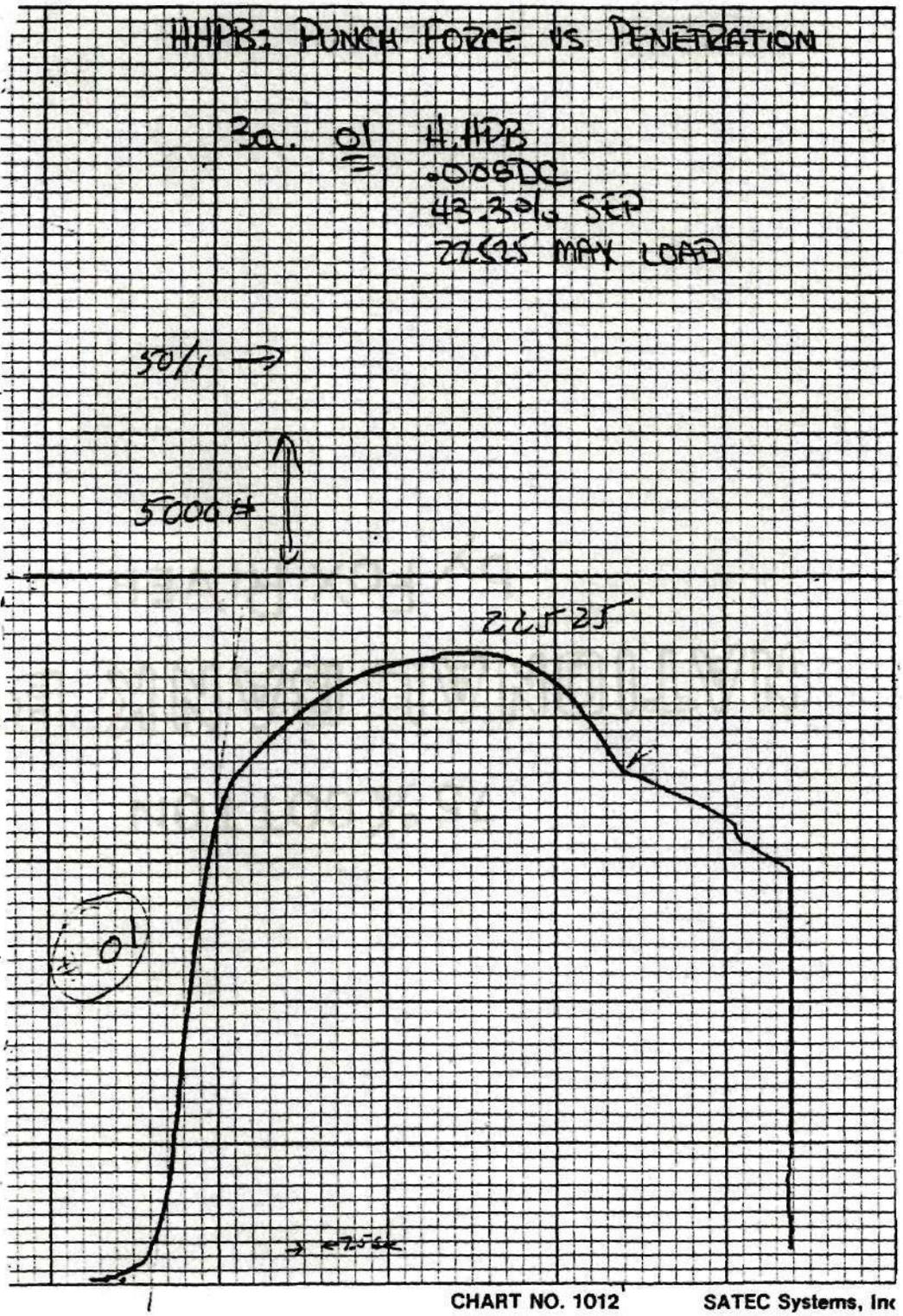
HHPB: PUNCH FORCE VS. PENETRATION
30a. 01
H.HPB
.008DC
43.3% SEP
22525 MAX LOAD
50/1 →
5000 #
22525
CHART NO. 1012
SATEC Systems, Inc

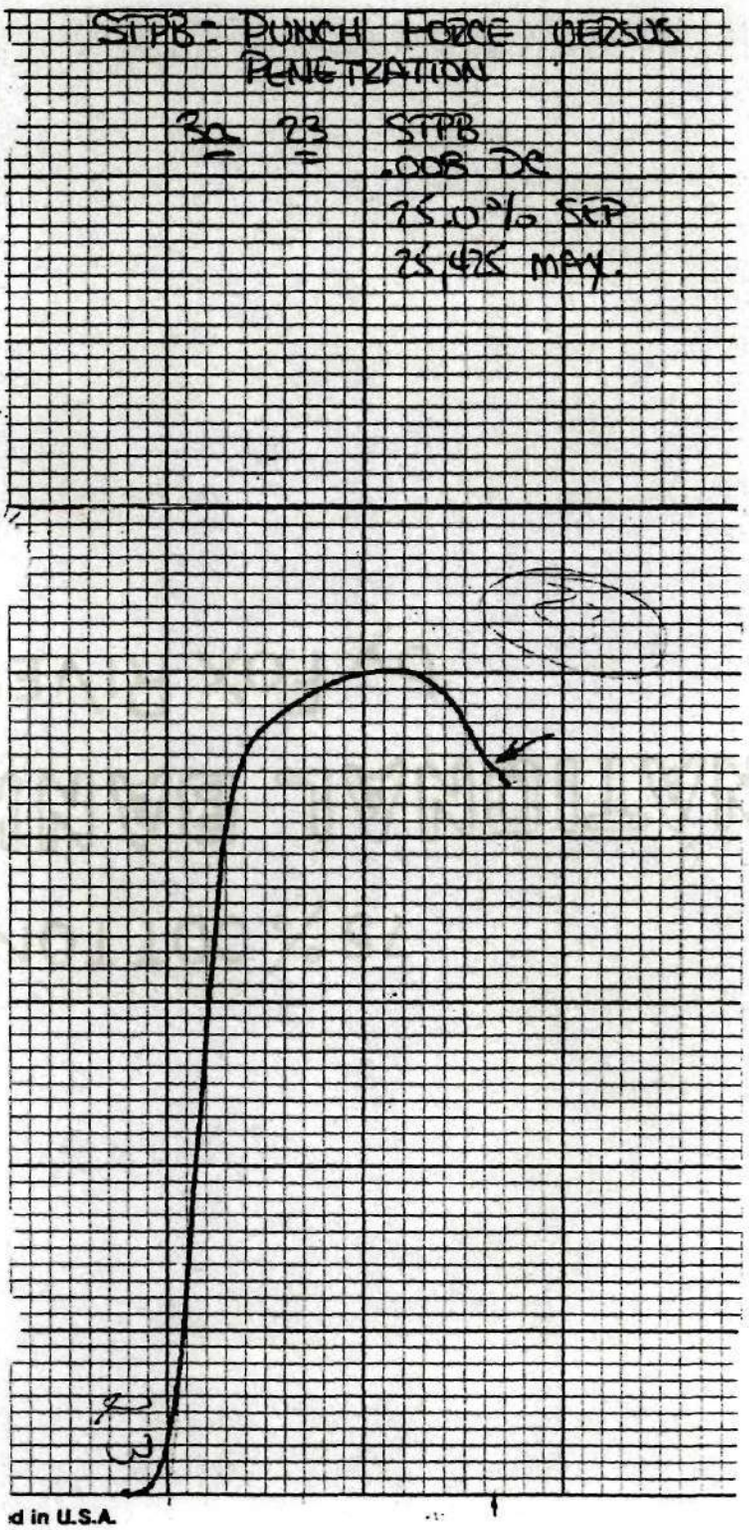
STPB - PUNCH FORCE VERSUS PENETRATION
STPB
.008 DC
25.0% SCP
25,475 MAX.

d in U.S.A.

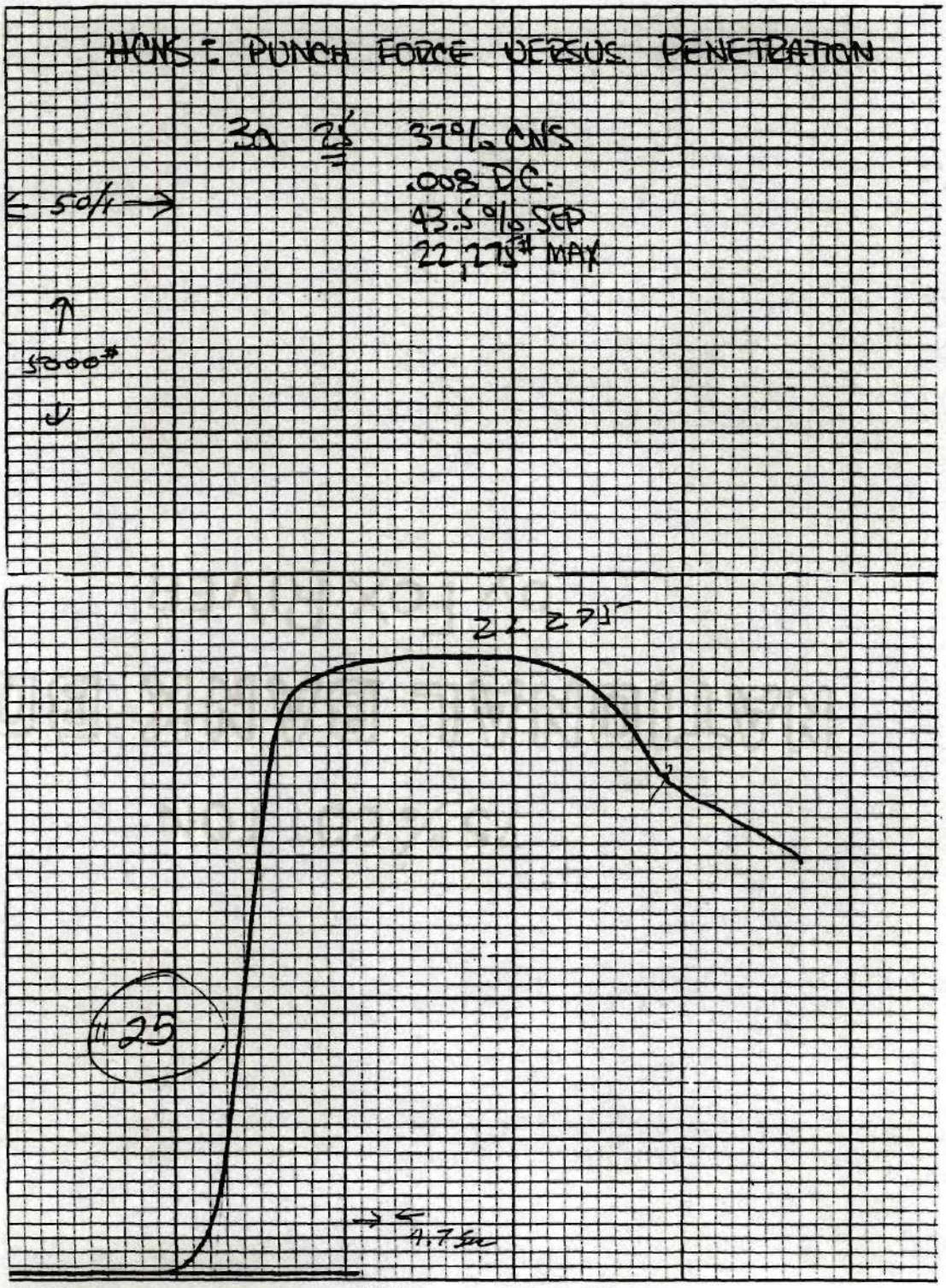

TEC Systems, Inc., Grove City, Pa. 16127 Printed in U.S.A.

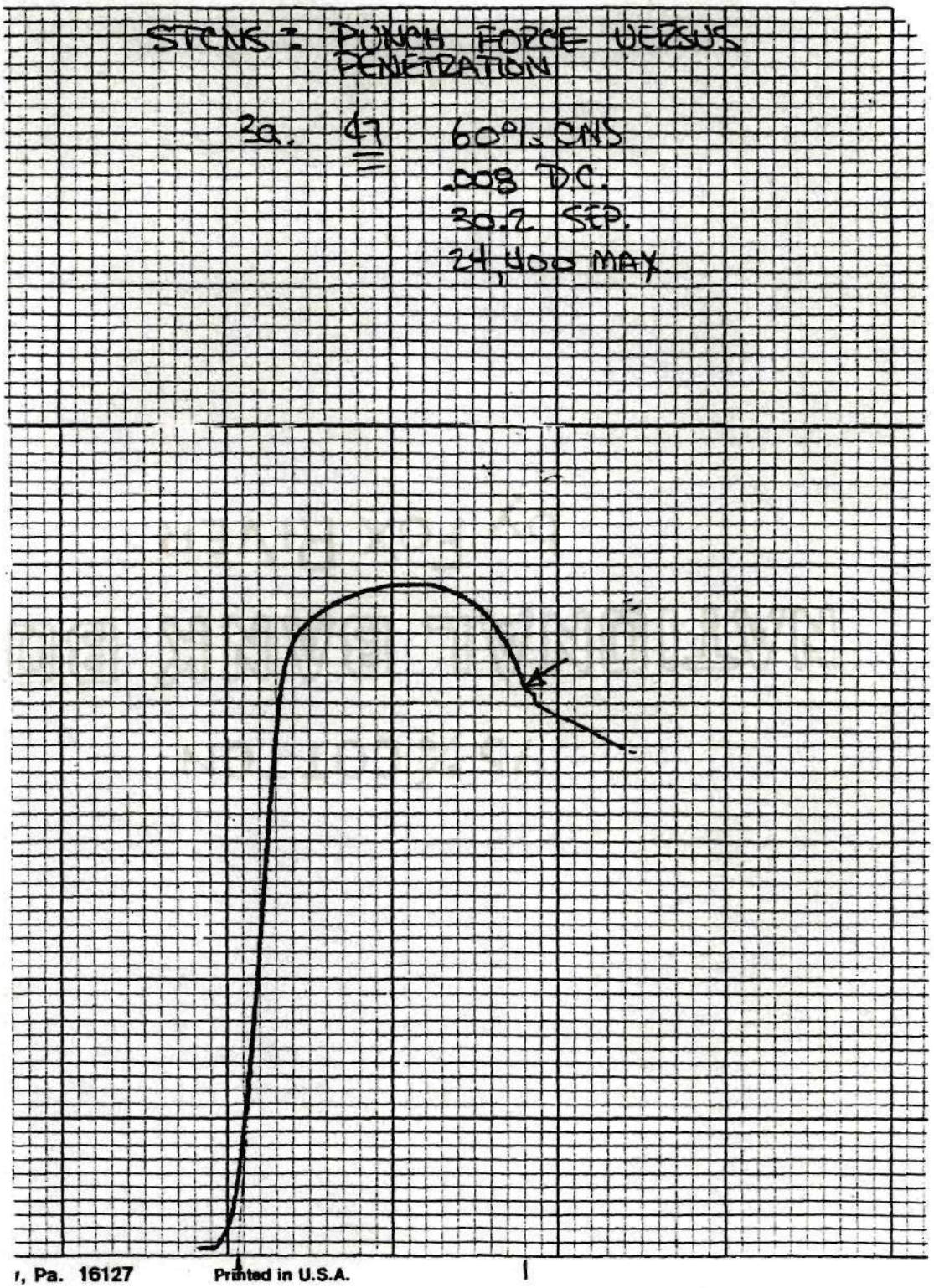

r, Pa. 16127 Printed in U.S.A.

APPENDIX 4

INITIAL WORKPIECE STRESS STATE

Consider the combination of shear and bending loads imposed on the workpiece by the punch and die in the die clearance zone at the instant of punch contact with the workpiece. Obviously the bending component will be much lower than the shear component on an element oriented with the die. Figure A4-1a shows the imposed stresses on an element of workpiece material in the die clearance zone near the top surface of the material and close to the punch edge. Figure A4-1b shows a Mohr's Circle representation of such a loading arrangement. Note that the maximum shear stress occurs on a plane inclined slightly counterclockwise from the vertical.

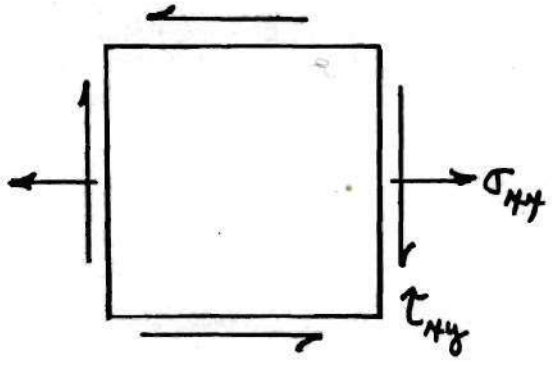

A. STRESSES ON AN ELEMENT

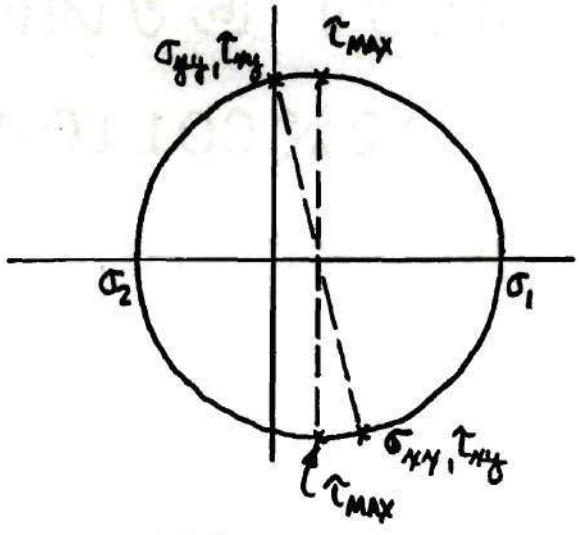

B. MOHR'S CIRCLE OF IMPOSED STRESS STATE

Fig. A4-1. Initial Workpiece Stress State

BIBLIOGRAPHY

1. Patent Numbers 3,234,498; 3,798,587; and 3,858,158; Western Electric Co. ,Inc., assignee.

2. Gohn, G. R., Guerard, J. P., and Freynik, H. S., "The Mechanical Properties of Wrought Phosphor Bronze Alloys," American Society for Testing and Materials, Philadelphia, Pa., 1956.

3. Plewes, J. T., "Spinodal Cu-Ni-Sn Alloys are Strong and Superductile," Metal Progress, July, 1974, p. 46-50.

4. Metals Handbook, 8th Ed., Vol. 8: Metallography, Structures, and Phase Diagrams; Pub. by the American Society for Metals, Metals Park, Ohio; 1973; p. 184.

5. Schwartz, L. H., Mahajan, S., and Plewes, J. T., "Spinodal Decomposition in a Cu-9wt% Ni-6wt% Sn Alloy," Acta Metallurgica, Vol. 22, May, 1974; p. 601-609.

6. Schwartz, L. H. and Plewes, J. T., "Spinodal Decomposition in Cu-9wt% Ni-6wt% Sn--II. A Critical Examination of Mechanical Strength of Spinodal Alloys," Acta Metallurgica, Vol. 22, July, 1974; p. 911-921.

7. Metals Handbook, 8th Ed., Vol. 1: Properties and Selection of Metals; Pub. by the American Society for Metals, Metals Park, Ohio, 1961; p. 1006.

8. Jones, F. D., Die Design and Die Making Practice, Industrial Press, New York, N. Y., 1951.

9. Vezzani, A. A., Die Design and Construction; ASTME, Prakken Publishers, Ann Arbor, Mich., 1974.

10. Vezzani, A. A., Manual of Instruction for Die Design; ASTME, Prakken Publishers, Ann Arbor, Mich., 1964.

11. Wilson, F. W., Die Design Handbook, 2nd Ed.; McGraw-Hill Book Co., 1965.

12. Condensed Practical Aids for the Experienced Die Engineer, Die Designer, and Die Maker, "Die Techniques" Publishers, Box 632, Medinah, Ill. 60157; 1972.

13. Chang, T. M. and Swift, H. W., "Shearing of Metal Bars," Journal of the Institute of Metals, October, 1950; p. 119-146.

14. Chang, T. M., "Shearing of Metals Blanks," Journal of the Institute of Metals, December, 1950; p. 393-414.

15. "Blanking and Piercing: A Metallographic Study of the Mechanism of Constrained Shear," Pub. by the Production Engineering Research Association, Melton Mowbray, Leicestershire, England; December, 1961.

16. Tilsly, R. and Howard, F., "Recent Investigations into Blanking and Piercing of Sheet Metals," Machinery (London), July 16, 1958; p. 151-158.

17. Biegel, J. E., "Punch-Die Clearances--Their Effects on Stamping Forces," Tool and Manufacturing Engineering, July, 1962; p. 89-92.

18. Allingham, J. W., "Importance of Clearance in Manufacturing of Blanking Dies," ASTME 32nd Annual Meeting--Collected Papers, Vol. 64, Book 4, Paper No. 622, 1964.

19. Holiga, L. A., "Punch-to-Die Clearance--Its Effect on Punched Hole Characteristics in Cold Rolled Steel," ASTME Paper No. 713, 1965.

20. Masuda, M. and Jimma, T., "Theoretical Research on the Blanking of Sheet Material," Japan Society of Mechanical Engineers--Transactions; December, 1962; p. 1638-1654.

21. Maeda, T., Nakagawa, T., Murakami, I., and Chino, S., "On the Accuracy of Sheared Blanks," Japan Society of Mechanical Engineers--Bulletin, Vol. 7, No. 28, November, 1964; p. 843-851.

22. Bridgman, P. W., Studies in Large Plastic Flow and Fracture; McGraw-Hill Book Co., Inc., 1952; p. 32-37.

23. Holloman, J. H., "Tensile Deformation," Metals Technology, Vol. 12, No. 4, June, 1945; Technical Paper No. 1879.

24. Backofen, W. A., Deformation Processing, Addison-Wesley Publishing Co., 1972; p. 35-36.

25. McClintock, F. A., and Argon, A. S., Mechanical Behavior of Materials, Addison-Wesley Publishing Co., 1966; Ch. 13.

26. O'Neil, H., Hardness Measurement of Metals and Alloys, Chapman and Hall Publishing Co., London, 1967.